



THE HONG KONG
POLYTECHNIC UNIVERSITY

香港理工大學

Pao Yue-kong Library

包玉剛圖書館

Copyright Undertaking

This thesis is protected by copyright, with all rights reserved.

By reading and using the thesis, the reader understands and agrees to the following terms:

1. The reader will abide by the rules and legal ordinances governing copyright regarding the use of the thesis.
2. The reader will use the thesis for the purpose of research or private study only and not for distribution or further reproduction or any other purpose.
3. The reader agrees to indemnify and hold the University harmless from and against any loss, damage, cost, liability or expenses arising from copyright infringement or unauthorized usage.

IMPORTANT

If you have reasons to believe that any materials in this thesis are deemed not suitable to be distributed in this form, or a copyright owner having difficulty with the material being included in our database, please contact lbsys@polyu.edu.hk providing details. The Library will look into your claim and consider taking remedial action upon receipt of the written requests.

**CHARACTERIZATION OF NOVEL
FLAVONOID DIMERS AS BREAST
CANCER RESISTANCE PROTEIN
(BCRP)-MODULATORS**

CHONG TSZ CHEUNG

PhD

**The Hong Kong Polytechnic
University**

2018

**The Hong Kong Polytechnic
University**

**Department of Applied Biology and
Chemical Technology**

**Characterization of Novel Flavonoid
Dimers as Breast Cancer Resistance
Protein (BCRP)-modulators**

Chong Tsz Cheung

**A thesis submitted in partial fulfillment of the requirements for
the degree of Doctor of Philosophy**

March 2018

CERTIFICATE OF ORIGINALITY

I hereby declare that this thesis is my own work and that, to the best of my knowledge and belief, it reproduces no material previously published or written, nor material that has been accepted for the award of any other degree or diploma, except where due acknowledgement has been made in the text.

_____ (Signed)

Chong Tsz Cheung (Name of student)

ABSTRACT

Cancer causes many deaths each year. A lot of anticancer drugs have been developed and some of them give promising results. Nevertheless, some patients become unresponsive to chemotherapy after prolonged treatment and develop multidrug resistance (MDR). Some MDR cases are caused by overexpression of ATP Binding Cassette (ABC) transporter ABCG2/BCRP. Inhibition of BCRP-mediated drug efflux could be one of the possible solutions to tackle MDR. Previously, flavonoid dimers have been shown to reverse ABCB1-mediated drug resistance. In view of the promising reversal potential of flavonoid dimers, a click chemistry approach was developed to generate a library of novel flavonoid dimers to discover new BCRP modulators. Click chemistry allowed rapid synthesis of a large combinations of triazole-containing homodimers and heterodimers of flavonoids. Screening resulted in the identification of **FD 15_8** as a potent BCRP modulator. Its EC₅₀s were 1.3±0.7nM in reversing topotecan resistance in BCRP-overexpressing MCF7/MX100 cells and 70.4±17.1nM in S1M180 cells. **FD 15_8** increased intracellular level of topotecan and doxorubicin in BCRP-expressing cells. It did not affect BCRP protein expression level, nor cellular localization of BCRP. Instead **FD15_8** inhibited BCRP-ATPase activity. Lineweaver-Burk and Dixon analysis suggested that **FD 15_8** was a non-competitive inhibitor for BCRP in a mixed mode of inhibition.

Intraperitoneal administration of **FD 15_8** resulted in the best pharmacokinetics profile in mice with plasma level maintained above its EC₅₀ level for more than 10 hours. Co-administration of **FD 15_8** at 45 mg/kg with topotecan at 2 mg/kg can suppress the S1M180 tumor volume by 40.3% after 24 times of treatment for once every two days. Administration **FD 15_8** alone or topotecan did not result in severe

toxicity. No death incidence recorded during the combination of 45 mg/kg **FD 15_8** and 2mg/kg topotecan combination group. In conclusion, **FD 15_8** is a safe and potent BCRP modulator.

ACKNOWLEDGEMENTS

First, I would like to thank my supervisor Prof. Larry Ming-Cheung Chow. He provided valuable comments on the project. We have plenty of time to discuss the project and I expanded my scope of knowledge during his guidance. I learned that stay curious and persistent are not only crucial for doing research, but also in life.

I would like to thank Prof. Tak-Hang Chan for his advice on the project. His comments were inspiring and helped to improve the progress a lot. I am also grateful to Dr. Iris Lai-King Wong for her contribution in the *in vitro* studies. I would also like to thank Dr. Kin-Fai Chan, Dr. Man-Chun Law, Dr. Jia-Hua Cui, Mr. Xue-Zhen Zhu, Mr. Zhen Liu for the synthesis of compounds. A special gratitude goes to Dr. Jason Wing-Yiu Kan and Dr. Clare Sau-Woon Yan for teaching me the animal works. And I would also thank Mr. Xin-Qing Yang and Xiao-Chun Su for assisting of the animal works.

I would like to acknowledge Dr. Pui-Kin SO for assisting the mass spectrometry works.

I would also like to thank Dr. Kit-Ying Choi and Mr. Kalvin Tsun-Sing Chow for the helping of protein related works.

I would like to thank the peer support from Miss Aya Man-Ying Lo, Miss Teng Chen, Mr. Terry Chin-Fung Chan, Dr. Xue-sen Hu and other lab members.

Last but not the least, I would like to thank my family. I could not pursuit my dream without their support.

LIST OF PUBLICATIONS AND CONFERENCE PRESENTATION

List of Publication

Clare S. W. Yan, Iris L. K. Wong, Kin-Fai Chan, Jason W. Y. Kan, **Tsz Cheung Chong**, Man Chun Law, Yunzhe Zhao, Shun Wan Chan, Tak Hang Chan, and Larry M. C. Chow

A New Class of Safe, Potent, and Specific P-gp Modulator: Flavonoid Dimer FD18 Reverses P-gp-Mediated Multidrug Resistance in Human Breast Xenograft *in Vivo*. *Molecular pharmaceutics* **12**, 3507-3517 (2015).

Conference Presentation

Tsz-Cheung Chong, Xue-zhen Zhu, Iris L.K. Wong, Man-Ying Lo, Kin-Fai Chan, Man-Chun Law, Larry M. C. Chow, Tak-Hang Chan

“Novel flavonoid homodimer FD15_8 reverses BCRP-mediated topotecan resistance *in vitro* and *in vivo*”. Multi-Drug Efflux Systems, Gordon Research Conference, Renaissance Tuscany Il Ciocco Resort, Lucca Barga, Italy, April 26-May 1st (2015)

TABLE OF CONTENTS

ABSTRACT.....	I
ACKNOWLEDGEMENTS	III
LIST OF PUBLICATIONS AND CONFERENCE PRESENTATION.....	IV
TABLE OF CONTENTS.....	V
LIST OF FIGURES	VII
LIST OF TABLES.....	VIII
LIST OF ABBREVIATIONS	IX
1. INTRODUCTION.....	1
1.1 Cancer and multidrug resistance.....	1
1.1.1 Cancer	1
1.1.2 Multidrug resistance.....	3
1.1.3 Identification of ABC transporters as a mediator of MDR	6
1.2 Characteristics of breast cancer resistance protein	7
1.2.1 Breast cancer resistance protein.....	7
1.2.2 BCRP substrates.....	10
1.2.3 Physiological role of BCRP	11
1.2.4 Regulation of BCRP expression.....	13
1.2.5 Single nucleotide polymorphism (SNP) of <i>BCRP</i>	13
1.2.6 Cancer MDR and BCRP	15
1.3 BCRP modulators/inhibitors.....	16
1.3.1 Development of ABC transporter inhibitor.....	16
1.3.2 Design, synthesis and characterization of flavonoids compounds	17
1.3.3 Flavonoid dimers as BCRP modulators	18
1.4 Topotecan	21
1.5 Objectives.....	22
2. MATERIALS AND METHODS.....	23
2.1 Mammalian cell lines	23
2.1.1 Maintenance of cell lines	23
2.1.2 Cell proliferation assay	24
2.2 Drug accumulation and efflux assays.....	25
2.2.1 Topotecan accumulation assay	25
2.2.2 Doxorubicin accumulation assay	25
2.2.3 FD 15_8 accumulation assay	26
2.2.4 FD 15_8 efflux assay	26
2.3 Vanadate-inhibitable ATPase assay.....	27
2.4 Molecular docking for prediction of FD 15_8 binding site.....	28
2.5 Cell treatment for assessing BCRP level	28
2.6 Immunofluorescence staining	28
2.7 Protein sample preparation.....	29
2.8 SDS-PAGE and Western blot analysis	31
2.9 Mass spectrometry	32
2.9.1 Materials	32
2.9.2 Identification of parent and daughter ion of FD 15_8 for analysis	32

2.9.3 Identification of parent and daughter ion of internal standard Ac15Az5	35
2.9.4 Identification of parent and daughter ion of topotecan	38
2.9.5 Identification of parent ion and daughter ion of internal standard tetracycline	41
2.9.6 Conditions of LC-MSMS for FD 15_8 analysis	44
2.9.7 Conditions of LC-MSMS for topotecan analysis.....	45
2.9.8 Sample preparation	46
2.10 Animal studies	47
2.10.1 Pharmacokinetic study	47
2.10.2 Toxicity study of FD 15_8 and topotecan.....	47
2.10.3 <i>In vivo</i> efficacy study of FD 15_8.....	48
2.10.4 Topotecan accumulation in tumor xenograft.....	49
2.11 Drug formulations.....	50
3. SCREENING OF FLAVONOID DIMERS FOR REVERSING BCRP-MEDIATED MDR	51
3.1 Introduction.....	51
3.2 Confirmation of BCRP expression by immunoblotting assay.....	52
3.3 Expression of BCRP monitored by confocal microscopy	53
3.4 Topotecan and doxorubicin resistance of S1 and S1M180	55
3.5 Screening for BCRP modulators.....	56
3.5.1 Screening of BCRP modulators at high topotecan concentration	56
3.5.2 Screening of BCRP modulator on the basis of potency (EC ₅₀).....	58
3.5.3 FD 15_8 as a potent BCRP modulator	61
3.5.4 Summary	62
4. MECHANISM OF FD 15_8 for REVERSING BCRP-MEDIATED MDR	63
4.1 Introduction.....	63
4.2 FD 15_8 accumulation and efflux assay	63
4.3 Effect of FD 15_8 on BCRP protein expression level.....	66
4.4 Effect of FD 15_8 on BCRP intracellular localization	67
4.5 Effect of FD 15_8 on intracellular topotecan and doxorubicin accumulation... 	69
4.6 Relationship between FD 15_8 and BCRP substrate doxorubicin	71
4.7 Effect of FD 15_8 on doxorubicin accumulation as demonstrated by confocal microscopy	74
4.8 Effect of FD 15_8 on vanadate-inhibitable ATPase activity of BCRP.....	76
4.9 Evaluation of FD 15_8 binding to nucleotide binding site through docking	78
4.10 Summary.....	82
5. PHARMACOKINETIC STUDIES AND TOXICITY STUDIES OF FD 15_8 ...	83
5.1 Introduction.....	83
5.2 Pharmacokinetic study of FD 15_8.....	84
5.3 Pharmacokinetic study of topotecan	88
5.4 Toxicity studies for FD 15_8 and topotecan in combination	91
6. <i>IN VIVO</i> EFFICACY OF FD 15_8 IN REVERSING BCRP-MEDIATED DRUG RESISTANCE	93
6.1 Introduction.....	93
6.2 <i>In vivo</i> efficacy of FD 15_8 in modulating BCRP-mediated drug resistance.....	93
6.3 Effect of FD 15_8 on topotecan accumulation in S1M180 xenograft	101
7. GENERAL DISCUSSION.....	103
8. FURTHER STUDIES	107

9. APPENDIX: SUPPLEMENTARY FIGURES.....	108
10. LIST OF REFERENCES	111

LIST OF FIGURES

Figure 1.1. Proposed transport mechanism of BCRP.....	9
Figure 1.2. Localization and function of BCRP in different organ.....	12
Figure 1.3. SNP variants and mutants of BCRP.....	14
Figure 1.4. Schematic diagram of click dimer formation	19
Figure 1.5. Structure of Ac15.....	19
Figure 1.6. Structure of Az8.....	19
Figure 1.7. Structure of FD 15_8 free base.....	20
Figure 1.8. Structure of topotecan.....	21
Figure 2.1. Full scan mass spectrum of FD 15_8.....	33
Figure 2.2. MSMS scan for identifying daughter ion of 608m/z from FD 15_8.....	34
Figure 2.3. Structure of Ac15Az5, the internal standard of FD 15_8.....	35
Figure 2.4. Full scan mass spectrum of Ac15Az5.....	36
Figure 2.5. MSMS scan for identifying daughter ion of 594m/z from Ac15Az5.....	37
Figure 2.6. Full scan mass spectrum of topotecan.....	39
Figure 2.7. MSMS scan for identifying daughter ion of 422m/z from topotecan....	40
Figure 2.8. Structure of tetracycline, the internal standard of topotecan.....	41
Figure 2.9. Full scan mass spectrum of tetracycline.....	42
Figure 2.10. MSMS scan for identifying daughter ion of 445m/z from tetracycline.	43
Figure 3.1. BCRP expression level in different cell lines.....	52
Figure 3.2 BCRP expression level in MCF7 and MCF7/MX100	53
Figure 3.3. Confocal images of BCRP.....	54
Figure 3.4. Primary screening of BCRP modulators using S1M180.....	57
Figure 3.5. EC ₅₀ s of BCRP modulators in revering topotecan resistance in S1M180.	59
Figure 3.6. Dose dependence of FD15_8 in reversing topotecan and doxorubicin resistance in S1M180 cells.....	61
Figure 4.1. FD 15_8 accumulation and efflux assays.....	65
Figure 4.2. Effect of FD 15_8 on BCRP expression.....	66
Figure 4.3. Effect of FD 15_8 on BCRP localization.....	68
Figure 4.4. Effect of FD 15_8 on topotecan (A) and doxorubicin (B) accumulation.	70
Figure 4.5. Lineweaver-Burk plot for FD 15_8 at different concentrations with doxorubicin.....	72
Figure 4.6. Dixon plot for FD 15_8 with at different concentrations with doxorubicin.....	73
Figure 4.7. Doxorubicin accumulation in S1 and S1M180 cell lines as observed by confocal microscopy.....	75
Figure 4.8. Effect of FD 15_8 on vanadate-inhibitable BCRP ATPase activity.....	77
Figure 4.9. BCRP cryo-EM structure with grid box at the nucleotide binding domain.....	79
Figure 4.10. BCRP cryo-EM structure and walker A and walker B highlighted green.....	79
Figure 4.11. Ko143 docked to nucleotide binding domain of BCRP model.....	80
Figure 4.12. FD 15_8 docked to nucleotide binding domain of BCRP model.....	80

Figure 4.13. ATP docked to nucleotide binding domain of BCRP model.....	81
Figure 5.1. Pharmacokinetics of FD 15_8 in rat.....	85
Figure 5.2. Pharmacokinetic study of FD 15_8 at mice.....	86
Figure 5.3. Effect of FD 15_8 on pharmacokinetics of topotecan in mice.....	89
Figure 5.4. Body weight change of BALB/c mice after receiving FD 15_8 and or topotecan.....	92
Figure 6.1. Effect of topotecan with or without FD 15_8 on S1 and S1M180 xenograft.....	95
Figure 6.2. Effect of topotecan with or without FD 15_8 on the body weight of S1 or S1M180-bearing BALB/c nude mice.....	96
Figure 6.3. Effect of topotecan with or without FD 15_8 on tumor weight of S1M180 xenograft.....	98
Figure 6.4. Effect of FD 15_8 on tumor volume of S1M180 xenograft and its body weight.....	99
Figure 6.5. Effect of 15mg/kg topotecan on body weight of S1M180 bearing BALB/c nude mice.....	100
Figure 6.6. Effect of FD 15_8 on the accumulation of topotecan in plasma and S1M180 xenograft.....	102
Figure 9.1. Structures of Az monomers.....	108
Figure 9.2. Structures of Ac monomers.....	109
Figure 9.3 ABCB1 expression level in different cell lines.....	110
Figure 9.4 ABCC1 expression level in different cell lines.....	110

LIST OF TABLES

Table 1. Characteristics of mammalian cells used in the study.....	23
Table 2. Ultra Performance Liquid Chromatography conditions for FD 15_8.....	44
Table 3. Ultra Performance Liquid Chromatography conditions for topotecan.....	45
Table 4. S1 and S1M180 sensitivity to topotecan and doxorubicin.....	55
Table 5. EC ₅₀ of BCRP modulators in reversing topotecan resistance in S1M180 and MCF7/MX100.....	60
Table 6. Cytotoxicity of BCRP modulators to L929 fibroblast and cross reactivity with P-gp and MRP1 mediated drug resistant cell lines.....	60
Table 7. Pharmacokinetic parameters of FD 15_8 in rats.....	85
Table 8. Pharmacokinetic parameters of FD 15_8 in mice.....	87
Table 9. Effect of FD 15_8 on pharmacokinetic parameters of in mice.....	90
Table 10. Effect of topotecan with or without FD 15_8 on tumor volume and tumor doubling time of BCRP-overexpressing S1M180 xenograft.....	97

LIST OF ABBREVIATIONS

ABC	ATP binding cassette
ATP	Adenosine triphosphate
BCRP	Breast cancer resistance protein
CYP	Cytochrome P450
DAPI	4',6-diamidino-2-phenylindole
DNA	Deoxyribonucleic acid
GSTs	Glutathione S-transferases
IC ₅₀	half maximal inhibitory concentration
LC-MSMS	Liquid chromatography–tandem mass spectrometry
MDR	Multidrug resistance
MRP1	Multidrug resistance-associated protein 1
MTX	Mitoxantrone
NBD	Nucleotide binding domain
NMP	N-Methyl-2-pyrrolidone
P-gp	Permeability glycoprotein
SDS-PAGE	Sodium dodecyl sulfate polyacrylamide gel electrophoresis
TKI	Tyrosine kinase inhibitors
TMD	Transmembrane domain
TPT	topotecan

1. INTRODUCTION

1.1 Cancer and multidrug resistance

1.1.1 Cancer

Cancer is one of the toughest challenges to public health. According to CancerResearchUK.org, there were 14.1 million new cases and 8.2 million deaths worldwide in 2012 (CancerResearchUK). The number of new cases is growing and is estimated to reach 23.6 million by 2030 worldwide. Among the new cases, lung cancer is the most common one, followed by breast cancer and colorectal cancer. In Hong Kong, the top three cancers were colorectal cancer, lung cancer and breast cancer according to the 2015 Hong Kong Cancer Registry. There were 5036, 4748 and 3920 cases of colorectal, lung and breast cancer respectively. Colorectal cancer is the top killer and it occurs more frequently in the elderly. About 40% of patients are diagnosed at advanced stages with symptoms including constipation, diarrhea and vomiting which are not prominent at early stages. Treatment of early stage colorectal cancers includes colectomy, whereas those diagnosed in late stages receive chemotherapy (Miller et al., 2016).

Cancer is the uncontrolled cell growth and these cells are invasive to other parts of the body. Gene mutations could lead to uncontrolled cell proliferation. In normal cells, cell proliferation is under regulation. Mutation of tumor suppressor genes disrupts their anti-proliferation function, meanwhile, proto-oncogene mutation or amplification triggers cell proliferation. For example, p53, a well-known tumor suppressor gene, is found in more than 50% of human cancers with loss of function mutation (Ozaki and Nakagawara, 2011). P53 is a nuclear transcription factor which regulates genes involving cell cycle arrest and apoptosis (Levine, 1997). Upon stress such as DNA

damage, p53 is activated and causes transcription of p21, which stops cell cycle by binding to some cyclins and Cdk complexes to inhibit kinase activity. P53 could also activate proapoptotic Bcl-2 protein Bax to trigger apoptosis (Chipuk et al., 2004). The frequent mutations of p53 are within the DNA-binding domain (Ozaki and Nakagawara, 2011) thus disabled p53 to activate its downstream protein for cell cycle arrest or apoptosis. Mutation or amplification of proto-oncogene resulted oncogene activation. Many proto-oncogenes produce proteins involved in signaling pathway (Sever and Brugge, 2015). Mutation of oncogene causes dysregulated cell growing signaling, for example, G12V Ras mutation, resulted Ras to be insensitive to inactivation (Scheffzek et al., 1997) and become always in active form.

Metastasis is a characteristic of malignant cancer. Cancer cells leave primary tumor where they originate and invade other parts of the body. The metastatic cancer cells destroy the functions of organs which they invaded. Cancer cells is first dissociated from the primary tumor, and then spreading through the circulatory system or lymphatic system (Alizadeh et al., 2014). They adhere or infiltrate into different parts of the body. Dissociation of cancer cells from primary tumors and adhesion of cancer cells could be mediated by cadherin. E-cadherin is responsible for cell adhesion while expression of N-cadherin could downregulate E-cadherin (Alizadeh et al., 2014).

The metastatic cancer cells trigger angiogenesis which help the cancer cells to acquire nutrients. Angiogenesis can be mediated by many regulators, for examples, vascular endothelial growth factor, angiogenin and epidermal growth factor (Nishida et al., 2006). Blocking these proteins could possibly inhibit tumor growth.

Cancer stem cell is suggested to cause relapse and metastasis (Jordan et al., 2006). Cancer stem cells could arise from mutated progenitor cells and they are resistant to chemo drugs. Anticancer drugs target active dividing cells, quiescence property of

some cancer stem cells such as leukemia cancer stem cell, help them to escape from the chemotherapy. Expression of drug efflux proteins could also contribute to drug resistant of cancer stem cells. Allowing them to survive chemotherapy. The survived cancer stem cells develop tumors at distal sites from the original tumor resulting in metastasis and relapse.

Chemotherapy represents one of the most important treatment methods for cancers. Chemo drugs work in various mechanisms, such as inhibiting cell division, targeting cell signaling proteins, inhibiting cell cycle progression, inducing proteasome and inducing apoptosis. Many of them give promising results. For example, paclitaxel and carboplatin are two first-line anticancer drugs. Breast cancer patients who received trastuzumab with paclitaxel and carboplatin treatment had a total response rate of 52% in a phase III study (Robert et al., 2004). However, drug resistance could occur resulting cancer relapses. There is an urgent need to tackle drug resistance to restore the potencies of anticancer drugs.

1.1.2 Multidrug resistance

Multidrug resistance (MDR) in cancer is a phenomenon that results when cancer cells become resistant to multiple structurally-diverse anticancer drugs simultaneously. MDR can be mediated by several mechanisms, including drug inactivation by overexpression of detoxification enzymes, alteration of targets, partitioning of drugs to different intracellular compartments and drug efflux by overexpression of transporter proteins. The followings are some examples of mechanisms that cause MDR in cancers.

1.1.2.1 Drug inactivation

Cytochrome P450 (CYP) system is involved in detoxification of drugs. Both Class I and Class II CYP participate in drug metabolism. Class I CYP enzymes (CYP1A1, CYP1A2, CYP2E1, and CYP3A4) are well conserved whereas Class II CYP enzymes

(CYP2B6, CYP2C9, CYP2C19, and CYP2D6) are highly polymorphic (Housman et al., 2014). Class II CYP enzymes can recognize a wide spectrum of compounds and therefore is more likely to be involved in MDR.

Glutathione S-transferase (GST) is a major group of detoxification enzymes highly expressed in cancer. They can catalyze glutathione conjugation to drugs. After modification, anticancer drugs are inactivated, become more water soluble and excretable. Anticancer drugs are eliminated more readily after conjugation of glutathione. It has been shown that transfection of GST to Chinese hamster ovary cells could increase cisplatin and carboplatin resistance by two to three fold (Tew, 2016).

1.1.2.2 Reduced drug activation

To become effective, some drugs need activation in a cell, including phosphorylation and cleavage. Reduced phosphorylation or cleavage could lead to drug resistance. For examples, cytarabine is an anticancer drug which requires deoxycytidine kinase (dCK)-mediated phosphorylation for activation. Cell lines which were resistant to nucleoside analogues were found to have lower deoxycytidine kinase activity. Sensitivity to cytarabine found in dCK-deficient cells can be restored when dCK gene was added back (Galmarini et al., 2001). In addition, myeloid leukemia cell line U937 was found to be resistant to an aminopeptidase inhibitor prodrug CHR2863 (Verbrugge et al., 2016) and have low carboxylesterase expression. Carboxylesterase is responsible for converting CHR2863 to its active form CHR6768. Reduced activity of carboxylesterase reduced CHR2863 activation, resulting in drug resistance.

1.1.2.3 Alteration of drug targets

Alteration of drug targets is another mechanism that causes drug resistance (Housman et al., 2014). For example, kinase inhibitors target signaling kinase, which triggers downstream signaling pathway and results in cell proliferation. Once the kinase has

mutated, the kinase inhibitors could no longer stop the proliferation signaling. Hence the cancer cells grow without control. For example, T790M mutation of EGFR could interfere with the binding of gefitinib and finally lead to gefitinib resistance (Ma et al., 2011).

1.1.2.4 Alteration of DNA repairing activity

Cells either repair DNA or undergo apoptosis when there is DNA damage. Anticancer drug DNA topoisomerase inhibitors such as mitoxantrone induce DNA double strand breaks causing apoptosis. However, in drug resistant cancer cells, the drug-induced DNA damage is compensated by the high DNA repair activity. A combination of DNA damaging drug with DNA repair inhibitor could be a solution for this type of resistance (Holohan et al., 2013).

1.1.2.5 Overexpression of drug efflux transporters in drug resistant cancers

There are three main drug transporters in the ATP binding cassette (ABC) family which contribute to MDR. They are ABCB1/P-glycoprotein (P-gp), ABCC1/Multidrug resistance protein 1 (MRP1) and ABCG2/Breast Cancer Resistance Protein (BCRP). These ABC transporters have large cavities for drug binding so that structurally different drugs could be pumped out. These proteins hydrolyze ATP to generate energy for mediating drug efflux. Thus, intracellular drug level is reduced to a level insufficient to kill the cancer cells resulting in drug resistance

1.1.3 Identification of ABC transporters as a mediator of MDR

Among the three ABC transporters, ABCB1 was first discovered to be overexpressed in colchicine resistant Chinese hamster ovary cells (Gottesman and Ling, 2006). The colchicine-resistant cells were also found to be cross-resistant to other drugs such as daunomycin. A comparison between colchicine-resistant and sensitive cells using gel electrophoresis resulted in the identification of a 170 kDa band being overexpressed in the resistant cells. Such protein was later identified and named as ABCB1/P-gp. There was a correlation between ABCB1 overexpression and MDR. It was suggested that inhibition of ABCB1 could reverse MDR and restore drug sensitivity. Many ABCB1 modulators/inhibitors have been investigated in the past decades. These experiences help the development of other drug transporter inhibitors.

After the identification of ABCB1, another transporter BCRP that mediates MDR was also found. In 1998, L. A. Doyle *et al* studied a doxorubicin resistant breast carcinoma cell line of MCF-7, MCF7/AdrVp which was selected in the presence of a P-gp modulator verapamil.

The resistant cell line MCF-7/AdrVp cell line also showed a reduced intracellular accumulation of doxorubicin, which was similar to other cells overexpressing P-gp or MRP (Doyle et al., 1998). Interestingly, P-gp and MRP were not upregulated in this cell line, suggesting that another membrane protein transporter was overexpressed in such cell line. A new protein was identified as ABCG2/BCRP by RNA fingerprinting and it was found to be responsible for reducing intracellular accumulation of daunorubicin. By depleting ATP in BCRP-overexpressing cell line, intracellular level of rhodamine 123 was restored (Doyle et al., 1998), which suggested that the BCRP may belong to the ATP binding cassette family.

1.2 Characteristics of breast cancer resistance protein

1.2.1 Breast cancer resistance protein

Breast cancer resistance protein (BCRP) is also called ABCG2. It belongs to the ATP binding cassette (ABC) superfamily subgroup G. There are 49 ABC genes in the human genome (Vasiliou et al., 2009). Many ABC proteins are ATP-dependent membrane proteins that can transport substances across membrane.

Human *ABCG2* gene is located on chromosome 4q22 (Mao and Unadkat, 2015). The gene product BCRP protein is made of 655 amino acids with an expected molecular weight of 72 kDa (Litman et al., 2002). Its functional form is suggested to be a 144kDa homodimer, consisting of 2 BCRP protein linked at cysteine 603 located at an extracellular loop. A disulphide bond between cysteine 603 of two BCRP monomers resulting a homodimer (Basseville et al., 2016). Dimerization is suggested to occur in endoplasmic reticulum and the dimer is then transported to Golgi apparatus for posttranslational modification (Basseville et al., 2016). It is glycosylated at asparagine 596 (Basseville et al., 2016). However, the glycosylation does not affect the protein expression or substrates transportation (Diop and Hrycyna, 2005). Higher oligomeric forms of BCRP have also been reported (Dezi et al., 2010). The variation of oligomeric states depends on the overexpression systems and purification procedures (Dezi et al., 2010). For monomer, it contains a nucleotide binding domain (NBD) and a transmembrane domain (TMD) with 6 hydrophobic segments (Basseville et al., 2016). *ABCG2* gene is distinct from *ABCB1* and *ABCC1* genes. *ABCG2* gene only codes for half transporter, while the *ABCB1* and *ABCC1* genes code for a full transporter with 2 NBDs and two TMDs. Therefore, monomeric BCRP is a half-transporter. In addition, the NBD of BCRP is near the N-terminus while the NBD of P-gp and MRP1 is near the

C-terminus (McDevitt et al., 2009).

Before the crystal structure of human BCRP was revealed, the crystal structures of *C. elegans* ABCB1 and murine ABCB1 were used as a template to perform molecular modeling for BCRP (Kathawala et al., 2014; (Sodani et al., 2014). The crystal structure of human BCRP has been recently revealed by cryo-electron microscopy. The crystal structure formed was a BCRP homodimer bound by a 5D3-Fab (Taylor et al., 2017a). The overall resolution is 3.8Å whereas the resolution at the transmembrane domain is 3Å. However, the resolution of NBD was low because of its flexibility. This cryo-EM structure may facilitate the development of BCRP inhibitors. It provides a more accurate template for *in silico* docking.

The proposed mechanism of how BCRP work was shown in **Figure 1.1**. BCRP is suggested to have two cavities, named as cavity 1 and cavity 2. Cavity 1 is hydrophobic whereas cavity 2 is less hydrophobic. Leucine residues separates the two cavities. When there is no ATP bound to NBD, BCRP is inward facing. Cavity 1 could be reached by substrate. The binding of substrate might stabilize the TMD and bring the 2 NBD closer, which might increase ATPase activity. When BCRP is bound by both substrate and ATP, BCRP becomes outward facing. Substrate moves from cavity 1 to cavity 2 as the conformation changes. The substrate is expelled because of hydrophobic mismatch in cavity 2. ATP is hydrolyzed and inorganic phosphate is released. BCRP conformation is then restored to original state allowing another substrate to bind.

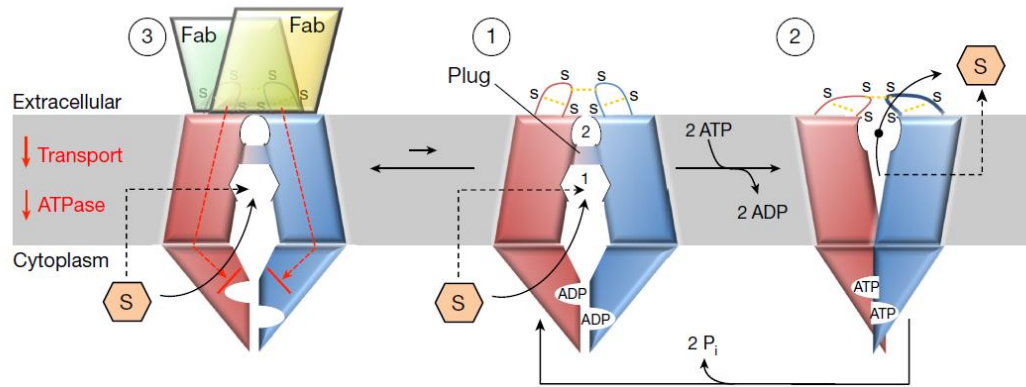


Figure 1.1. Proposed transport mechanism of BCRP.

Substrate binds to hydrophobic cavity 1, the 2 NBDs become closer and activate its ATPase activity. Binding of substrate and ATP to the BCRP causes conformation change, allows the substrate to move to less hydrophobic cavity 2. Substrate is expelled because of hydrophobic mismatch. ATP is hydrolyzed and the 2 NBDs separates. Cavity 1 restores to its original conformation. Fab antibody may be added to the BCRP to stabilize the inward facing conformation. The binding of Fab allosterically inhibits ATP hydrolysis and transport. This figure is reproduced from Taylor et al.(2017b).

1.2.2 BCRP substrates

BCRP mediates efflux of many compounds from intracellular space to extracellular space. It has a broad range of specificity for substrates with diverse structures. They include anticancer drugs such as mitoxantrone, topotecan, doxorubicin (Mao and Unadkat, 2015) and tyrosine kinase inhibitors such as imatinib and erlotinib (Lemos et al., 2008; Marchetti et al., 2008). BCRP could lower the efficacy of chemotherapy when drugs are BCRP substrates. In addition, there are endogenous BCRP substrates such as sulphated estrogens, but not the free one (Imai et al., 2003).

Pheophorbide a is also a BCRP substrate. It is the product from the breakdown of chlorophyll. BCRP limits the uptake of pheophorbide a from dietary plants. It was found that *Bcrp1*^{-/-} mice show protoporphyria suggesting that BCRP prevents protoporphyria by reducing the uptake of pheophorbide a (Jonker et al., 2002).

Drugs conjugated with sulphate, glutathione and glucuronide could also be BCRP substrates (Mao and Unadkat, 2015). Phosphorylated nucleosides and nucleotides could also be pumped by BCRP. BCRP prefers conjugated organic anions as substrates. Many nucleoside analogues can inhibit reverse transcriptase and can be used to treat HIV. They were found to be BCRP substrates. For example, the levels of zidovudine and abacavir were found to be lower in *Abcg2/Bcrp1* transfected cells compared to wild type (Alam et al., 2016). Inhibition of BCRP could therefore be beneficial to HIV chemotherapy.

1.2.3 Physiological role of BCRP

BCRP is expressed in liver, kidney, intestine, blood brain barrier, blood testis barrier, placenta and mammary gland (**Figure 1.2**). BCRP expressed in intestinal epithelial cells is involved in limiting oral bioavailability of many food substances and drugs. BCRP is also expressed at bile canalicular membrane of hepatocytes. Substances absorbed from GI tract are first transported to liver through hepatic portal vein; some are metabolized by liver and eliminated by BCRP into bile. BCRP is therefore involved in first pass elimination. In general, BCRP present in the blood-organ barriers prevent xenobiotics from entering these organs. Because of this, BCRP also limits drugs from reaching certain organs, rendering these organs to be difficult to treat in cases of diseases. For example, BCRP and P-gp present in the blood brain barrier work synergistically to prevent anticancer drugs from entering into the brain, making brain cancer difficult to treat.

High level of BCRP was also found in the mammary gland and placenta. It was found that BCRP substrates can be secreted through mammary gland (Jonker et al., 2005) and may be harmful to breastfed babies. It was found that wild type mice had higher concentration of topotecan secretion in milk than *abcg2* knockout mice (Jonker et al., 2005).

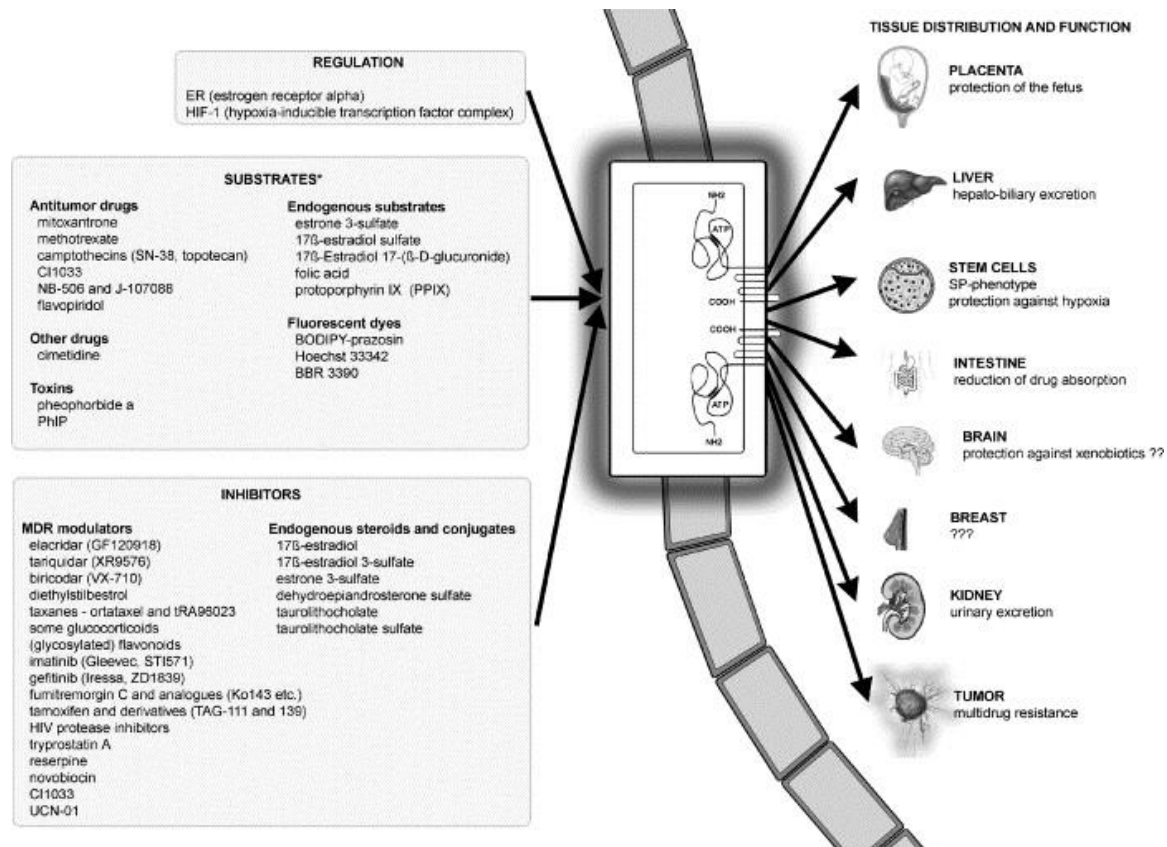


Figure 1.2. Localization and function of BCRP in different organ.

This figure describes BCRP distribution in different organs, including the placenta, liver, intestine, brain and kidney. BCRP is also found in tumor and stem cells. The figure also lists different BCRP substrates and inhibitors. Substrates of “wild-type” BCRP are shown. This figure is reproduced from Staud and Pavék (2005).

1.2.4 Regulation of BCRP expression

Estradiol (17 β -estradiol) can down-regulate BCRP expression in rat brain capillaries (Mahringer and Fricker, 2010) and human placental cell line BeWo (Wang et al., 2006). However, an estrogen response element was found in the promoter region of the *ABCG2* gene and estrogen upregulated the expression of BCRP in the ER positive cell lines T47D:A18 and PA-1 (Ee et al., 2004). The effect of estradiol on BCRP expression may be cell line-dependent.

BCRP mRNA level and Hoechst dye efflux are also stimulated by hypoxia (Krishnamurthy et al., 2004). Hypoxia-inducible factor HIF-2 α response element is found in *ABCG2* promoter. Under hypoxia, HIF-2 α binds to HIF-2 α response element in *ABCG2* gene promoter region, leading to a higher transcription rate of *ABCG2* (Martin et al., 2008).

1.2.5 Single nucleotide polymorphism (SNP) of *BCRP*

Seven *BCRP* SNPs were identified in a study of 100 Japanese volunteers (Kondo et al., 2004). They were G34A(V12M), C376T(Q376Stop), C421A(Q141K), G1098A(E366E), G1322A(S441N), T1465C (F489L), and C1515- (AFFVM505-509ASSL Stop) (**Figure 1.3**). G34A and C421A represent 22% and 29% in such population respectively. In an *in vitro* study, C421A-transfected cells showed only 30%-40% BCRP expression compared to wild type. The lower protein expression level of BCRP might be due to ubiquitination and subsequent proteasomal degradation of the SNP variant. It was also found that C421A mutation can lower BCRP ATPase activity (Woodward et al., 2013). Clinically, Q141K mutation is correlated with higher blood uric acid level and gout (Woodward et al., 2013). Uric acid is a BCRP substrate and this mutation may reduce activity of BCRP, resulting in a reduced clearance of uric acid and

elevated blood level. The G34A-mutant of BCRP had lower activity and was ten-fold more sensitive to topoisomerase inhibitor I when compared with the wild type (Mizuarai et al., 2004). Another SNP was identified in the S1M180 cell line which was selected with mitoxantrone and overexpressing BCRP. R482 was changed to R482G or R482T (Honjo et al., 2001). The mutation affects substrate specificities. BCRP with R482G mutation pumps rhodamine 123 and doxorubicin, whereas the wild type BCRP pumps methotrexate, but not the doxorubicin or rhodamine 123 (Sarkadi et al., 2004). Nonsense mutations Q126X, Q246X, and R236X were identified in the *BCRP* gene. They are found among the Japanese and Asian populations. People with these nonsense mutations have Jr(a-) blood type (Basseville et al., 2016) as Jr(a) antigen was not present. When Jr(a-) people receive blood transfusion from a Jr(a) donor, anti-Jr(a) may appear and cause hemolytic transfusion reaction (Saison et al., 2012).

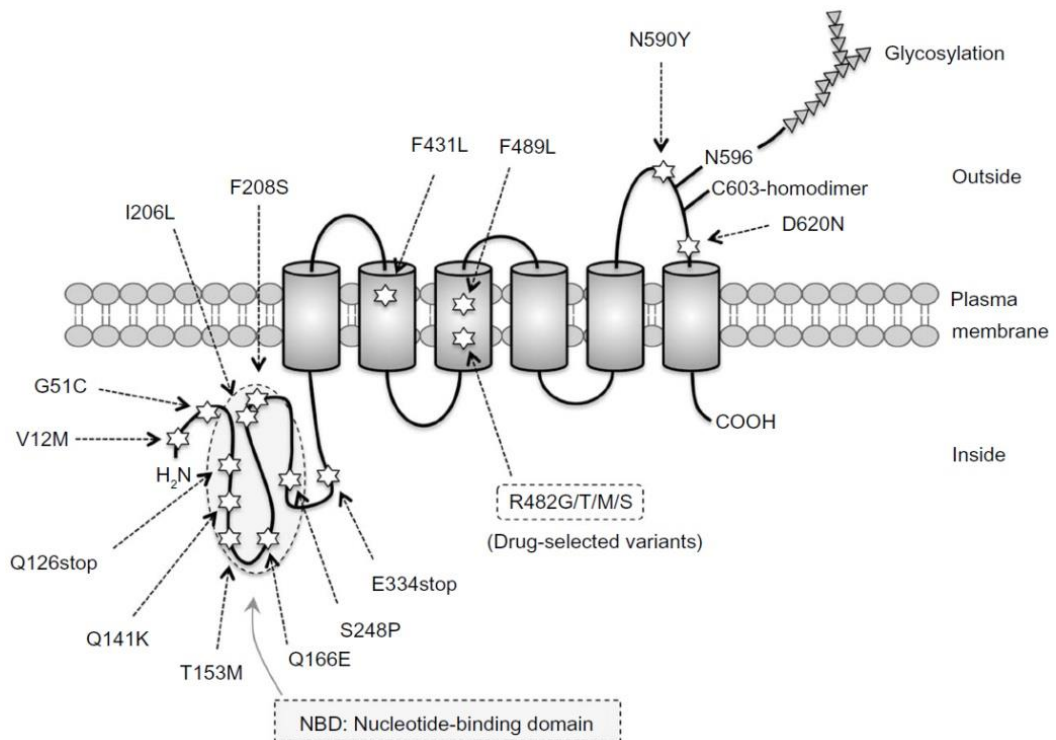


Figure 1.3. SNP variants and mutants of BCRP.

The diagram illustrates the BCRP amino acids with frequent mutations. The SNPs were labeled with stars. The figure was reproduced from (Noguchi et al., 2014)

1.2.6 Cancer MDR and BCRP

Cancer cells acquire BCRP-mediated MDR when selected with anticancer drugs; for example, in breast cancer cell line (MCF-7/AdrVp (Doyle et al., 1998)), esophageal cancer cells (Eca109/ADM (Liu et al., 2014)) and colon cancer cell line (S1M180 (Honjo et al., 2001)). Drug-selected cell lines overexpress BCRP protein and develop MDR.

A similar phenomenon was observed clinically. BCRP level was found to be higher in patients of relapsed or refractory acute myeloid leukemia (AML) than at the initial stage. These patients were initially treated with cytosine-arabioside, daunorubicin, adriamycin, idarubicin and etoposide (Van den Heuvel-Eibrink et al., 2002). The *BCRP* mRNA level in relapsed or refractory state patients was 1.7 fold higher after treatment (Van den Heuvel-Eibrink et al., 2002). This suggested that BCRP might contribute to drug resistance in AML. Inhibiting BCRP could possibly reverse AML drug resistance. High expression level of BCRP can also be observed in side population of stem cells/cancer stem cells (Patrawala et al., 2005). However, there are no significant differences in tumorigenicity between non-BCRP overexpressing and high BCRP expressing cell (Patrawala et al., 2005).

1.3 BCRP modulators/inhibitors

1.3.1 Development of ABC transporter inhibitor

There are three generations of P-gp inhibitors (Dash et al., 2017). The first-generation inhibitors are the verapamil and cyclosporin A. They need a high concentration to achieve the inhibitory effect, but the high concentration brings toxicity. The second-generation inhibitors are the derivatives of the first-generation inhibitors. For example, PSC833 is derived from cyclosporin A. These inhibitors have reduced toxicity, however, they interact with the cytochrome P450 enzyme. The third-generation inhibitors include elacridar and tariquidar. Toxicity is further reduced and there is less interaction with cytochrome P450 enzymes. However, they are not perfect. Some of them are not specific and can also inhibit BCRP. Some of the third-generation inhibitors have entered clinical trials, such as Zosuquidar.

In view of the possibility of reversing P-gp mediated multidrug resistance, BCRP modulators were investigated. Soon after BCRP was discovered, fumitremorgin C (FTC), a fungal toxin, was found to reverse resistance to mitoxantrone and topotecan in BCRP overexpressing cell line in which ABCB1 was not overexpressed (Rabindran et al., 2000). However, the use of FTC is limited because it is neurotoxic. A more potent but less toxic FTC analog, ko143, was developed. However, it has been reported that ko143 is not specific to BCRP. It also interacts with ABCB1 and ABCC1 (Weidner et al., 2015). EC₅₀ of ko143 for reversing ABCB1 paclitaxel resistance is 1 μ M while reversing ABCC1-mediated etoposide resistance is 2 μ M (Weidner et al., 2015). Tyrosine kinase inhibitors (TKIs) are another class of BCRP modulators. For example, lapatinib (Dai et al., 2008), imatinib, nilotinib and dasatinib (Eadie et al., 2014) are BCRP inhibitors. Some TKIs are both BCRP substrates and BCRP inhibitors.

1.3.2 Design, synthesis and characterization of flavonoids compounds

Flavonoids are polyphenols commonly found in vegetables and fruit. Flavonoids have a lot of health benefits including prevention of coronary heart disease (Hertog et al., 1995) and anticancer (Lin et al., 2008). This could be due to different properties of flavonoids. For example, some flavonoids act as antioxidant and prevent DNA strand break (Ohshima et al., 1998). Some flavonoids are phytoestrogens, which can help to regulate the ERs signaling pathways (Lin et al., 2008). Flavonoids can also modulate ABCB1-mediated resistance in MCF7 breast cancer cells (Scambia et al., 1994).

Because flavonoids are generally considered to be safe to consume and they have low P-gp modulating activity, our research group has previously investigated the use of apigenin dimer to reverse MDR mediated by ABCB1 and BCRP.

ABCB1 is a pseudodimeric protein containing two transmembrane domains (TMD) and two nucleotide binding domains (NBD). It was hypothesized that dimeric small molecules could have better P-gp inhibitory activity than monomer. Our research group has used synthetic chemistry to link two apigenins using polyethylene glycol to form a flavonoid dimer (Chan et al., 2006). After further modification of apigenin with defined length spacer, P-gp modulating activity has been greatly improved when compared with the monomer (Chan et al., 2006). FD18, one of the flavonoid dimers, was shown to reverse P-gp mediated drug resistance in breast xenograft *in vivo* (Yan et al., 2015). Similarly, ABCC1 is also a pseudodimer. Some of the synthetic apigenin homodimers were also shown to reverse ABCC1-mediated doxorubicin resistance *in vitro* (Wong et al., 2009).

To further increase the structural diversity of the flavonoid dimer library, our research group has developed a rapid and efficient method to generate a library of triazole-

containing flavonoid dimers.

1.3.3 Flavonoid dimers as BCRP modulators

A novel class of flavonoid dimers were synthesized by adopting click chemistry approach which can join an azide-containing flavonoid monomer with an alkyne-containing flavonoid monomer. It allows a library of flavonoid dimers with structural diversity to be synthesized rapidly. In the presence of azide monomer, alkyne monomer, copper-(I) catalyst, triazole ring is formed (Kolb and Sharpless, 2003) which acts as the bridge between the two flavonoid monomers. This reaction takes place at a relatively mild temperature (90°C). Click chemistry greatly simplifies synthesis steps and can rapidly generate dimer library for high throughput screening for MDR modulators. Briefly, the clicked dimers were made by refluxing 1mM Ac monomer (compounds with alkyne group), 1mM Az monomer (compounds with azide group) and 1mM Cu(I) as catalyst at 90 °C overnight as shown in **Figure 1.4**. The reaction mixtures were allowed to dry. The compounds were then dissolved in DMSO for testing modulating activity. After the high throughput screening, the active compounds were chosen for scale up synthesis and purification. The pure compounds were used to perform cell proliferation assay again to confirm their potency.

FD 15_8 was found to be a potent BCRP inhibitor after the screening of the flavonoid dimer library. Therefore, this compound was further investigated for its mechanism of action and its *in vivo* efficacy. **FD 15_8** was a homodimer where Ac15 with 2 alkyne groups (**Figure 1.5**) was used to form 2 triazole bridges with an azide-containing monomer Az8 (**Figure 1.6**). Structure of FD 15_8 is shown in **Figure 1.7**.

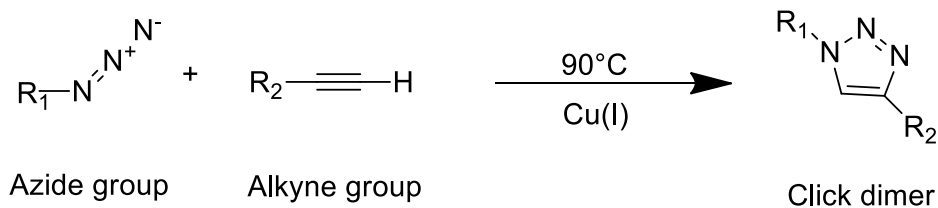
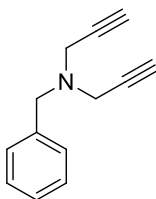


Figure 1.4. Schematic diagram of click dimer formation

Clicked dimers were made by refluxing 1mM Ac monomer (compounds with alkyne group), 1mM Az monomer (compounds with azide group) and 1mM Cu(I) as catalyst at 90 °C overnight. The reaction mixtures were allowed to dry. The compounds were then dissolved in DMSO for testing modulating activity.

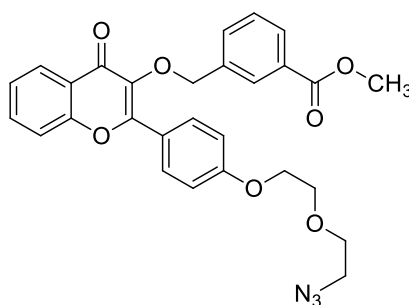


Chemical Formula: C₁₃H₁₃N
 Exact Mass: 183.10480
 Molecular Weight: 183.24902
 Elemental Analysis: C, 85.21; H, 7.15; N, 7.64

Ac15

Figure 1.5. Structure of Ac15.

The two alkyne groups of Ac15 can react with two azide-containing monomers to form two triazole rings.

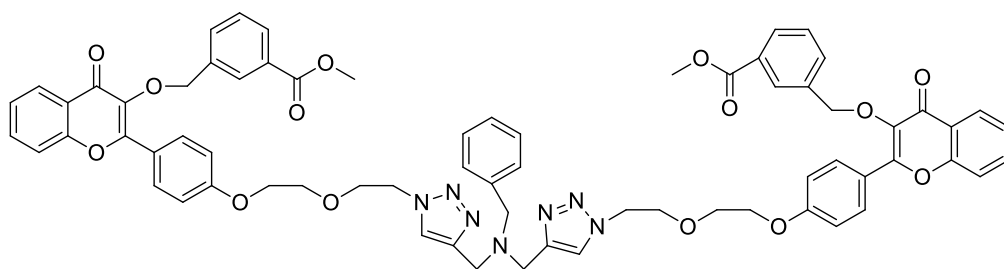


Chemical Formula: C₂₈H₂₅N₃O₇
 Exact Mass: 515.17
 Molecular Weight: 515.51
 Elemental Analysis: C, 65.24; H, 4.89; N, 8.15; O, 21.73

Az8

Figure 1.6. Structure of Az8.

Az8 is the major component of **FD 15_8**. Its azide group can react with alkyne groups in Ac15 to form triazole ring. Homodimer thus produced is named **FD 15_8**.



Chemical Formula: $C_{69}H_{63}N_7O_{14}$

Exact Mass: 1213.44330

Molecular Weight: 1214.27702

Elemental Analysis: C, 68.25; H, 5.23; N, 8.07; O, 18.45

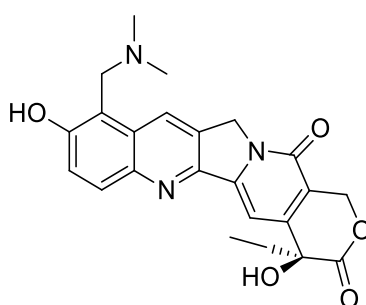
FD 15_8

Figure 1.7. Structure of FD 15_8 free base.

Structure of **FD 15_8** free base. It is a homodimer formed by one Ac15 linking two Az8 flavonoid monomers.

1.4 Topotecan

Topotecan (**Figure 1.8**) is an anticancer drug also called Hycamtin. It is derived from camptothecin, which is found in *Camptotheca acuminata*. Topotecan is a DNA topoisomerase I inhibitor. DNA topoisomerase I relieves DNA torsion strain by binding to DNA and making a nick on DNA (Takimoto and Arbuck, 1997). Such DNA nick is needed for the formation of a cleavable complex, which is needed for DNA replication. Topotecan binds to the topoisomerase I and stabilizes the cleavable complex. DNA replication thus stops and causes DNA double strand breaks and apoptosis. Topotecan is active when it is in the lactone form. Lactone form dominates in acidic condition, while carboxylic form dominates in neutral or basic condition. Topotecan has been used for the treatment of ovarian cancer, small cell lung cancer and cervical cancer (Creemers et al., 1996). The main toxicities caused by topotecan are leukocytopenia and neutropenia. Because topotecan is a well-known BCRP substrate, overexpression of BCRP is known to be associated with topotecan resistance. Inhibition of BCRP can potentially reverse topotecan resistance.



Chemical Formula: C₂₃H₂₃N₃O₅

Exact Mass: 421.16377

Molecular Weight: 421.44582

Elemental Analysis: C, 65.55; H, 5.50; N, 9.97; O, 18.98

Topotecan

Figure 1.8. Structure of topotecan.

Topotecan is an anticancer drug which act as a topoisomerase inhibitor. Topotecan binds to topoisomerase I and stabilizes cleavable complex. This results in double strand DNA break and apoptosis.

1.5 Objectives

The aims of this study were to develop a potent and safe BCRP modulator which can reverse BCRP-mediated topotecan resistance in cancer.

In this project, there were 4 objectives:

1. To identify potent and safe BCRP modulators *in vitro*.
2. To investigate the mechanism of action of how flavonoid dimer reverse BCRP-mediated MDR.
3. To investigate the pharmacokinetics of flavonoid dimer and
4. To test the efficacy of the flavonoid dimer in reversing BCRP-mediated MDR *in vivo*.

2. MATERIALS AND METHODS

2.1 Mammalian cell lines

Cell lines used in this project (S1, S1M180, MCF7, MCF7/MX100, HEK293/pcDNA3 and HEK293/BCRP) are listed in **Table 1**. They were obtained from Dr. Susan Bates's lab.

Table 1. Characteristics of mammalian cells used in the study.

	Cell type	Resistance obtained by
Sensitive cell lines		
S1	Human colon carcinoma	-
MCF7	Human breast adenocarcinoma	-
HEK293/pcDNA3	Human embryonic kidney	-
Resistant cell lines		
S1M180	Human colon carcinoma	Mitoxantrone selection
MCF7/MX100	Human breast adenocarcinoma	Mitoxantrone selection
HEK293/BCRP	Human embryonic kidney	Transfection of BCRP gene

S1, MCF7, HEK293/pcDNA3 were sensitive cell lines while S1M180, MCF7/MX100 and HEK293/BCRP were resistant cell lines. MCF7/MX100 and S1M180 were selected by mitoxantrone. HEK293/BCRP was transfected with plasmid containing *BCRP* gene.

2.1.1 Maintenance of cell lines

S1 and S1M180 cell lines were maintained in Minimum Essential Media (Gibco) supplemented with 26.2 mM sodium bicarbonate (Sigma-Aldrich), 10 mM HEPES(Sigma-Aldrich), 1 mM sodium pyruvate(Sigma-Aldrich), supplemented with 10% (v/v) Fetal Bovine Serum (Gibco) and 100 U/ml penicillin, 100 µg/ml streptomycin.

MCF7 and MCF7/MX100 were maintained in Roswell Park Memorial Institute (RPMI) 1640 Medium with 4.0 mM glutamine, 23.8 mM sodium bicarbonate(Sigma-Aldrich),

100 U/ml penicillin, 100ug/ml streptomycin and 10% (v/v) Fetal Bovine Serum (Gibco). HEK293/pcDNA3 and HEK293/BCRP were maintained in Dulbecco's Modified Eagle's medium (Gibco), 100 U/ml penicillin, 100ug/ml streptomycin and 10% (v/v) Fetal Bovine Serum (Gibco). G418 at a final concentration of 0.75 mg/ml was added to the medium to maintain the transfected clones. HEK293/pcDNA3 and HEK293/BCRP were grown in collagen coated plates. All of the above cell lines were kept in 5% CO₂ of humidified atmosphere at 37°C.

2.1.2 Cell proliferation assay

For S1 and S1M180 cells, 7 x 10³ cells were used in cell proliferation assays. For MCF7, MCF7/MX100, HEK293/pcDNA3 and HEK293/BCRP, 1 x 10⁴ cells were used. Cells without topotecan acted as control. Cells were incubated with 2 nM to 1000 nM of click dimers and 0.015 µM to 100 µM topotecan (Sigma-Aldrich) to a final volume of 100 µl. Cells were incubated for 72 hours at 37°C with 5% CO₂. After incubation, the drug containing medium was removed and replaced by 50 µl of drug-free MEM medium. Ten microliters of MTS (2 mg/ml, Promega): PMS (0.92 mg/ml, Promega) in 1:20 mixture was added to each well. The plates were protected from light and incubated at 37°C for 1 hour. Absorbance at 490 nm was measured by a CLARIOstar[®] microplate reader (BMG). IC₅₀ values were determined by sigmoidal dose-response (variable slope) method using GraphPad Prism5.

2.2 Drug accumulation and efflux assays

2.2.1 Topotecan accumulation assay

S1 and S1M180 cells were used in topotecan accumulation assay. One million cells were placed in 0.98 ml MEM. Ten microliters of modulator at 10 μ M and 100 μ M were added to the 0.98 ml MEM and incubated at 37°C with shaking at 180 rpm for 2 hours. After that, 10 μ l of topotecan at 5 mM were added. After one hour, the cells were chilled on ice for 1 minute and centrifuged at 14,000 rpm. The supernatant was removed and the cells were washed with ice-cold PBS thrice. The cells were then lysed by 100 μ l absolute ethanol. The lysates were centrifuged at 14000 rpm for 1 minute and supernatant was transferred to a 96-well tissue culture test plate (black, SPL). Fluorescence (excitation: 394 nm, emission: 536 nm) was measured by CLARIOstar® microplate reader (BMG).

2.2.2 Doxorubicin accumulation assay

S1 and S1M180 cells were used in doxorubicin accumulation assay. One million cells were placed in 0.98 ml MEM. Ten microliters modulator at 10 μ M and 100 μ M were added to the 0.98 ml MEM and incubated at 37°C with shaking at 180 rpm for 2 hours. After that, 10 μ l of doxorubicin at 2 mM were added. After one hour, the cells were chilled on ice for 1 minute and centrifuged at 14000 rpm. The supernatant was removed and the cells were washed with ice-cold PBS thrice. The cells were then lysed by lysis buffer (0.75 M hydrochloric acid, 0.2% triton X-100 in isopropanol). Lysate was centrifuged at 14,000 rpm for 1 minute and supernatant was transferred to a 96-well tissue culture testplate (black, SPL). Fluorescence (excitation: 488 nm, emission: 556 nm) was measured by CLARIOstar® microplate reader (BMG).

2.2.3 FD 15_8 accumulation assay

S1 and S1M180 cells were used in **FD 15_8** accumulation assay. One million cells were placed in 0.99 ml MEM. Ten microliters of **FD 15_8** at 100 μ M were added and incubated at 37°C with shaking at 180rpm. At 10, 30, 60 and 120 minutes, cells were chilled on ice for 1 minute and centrifuged at 14,000 rpm. Supernatant was removed and the cells were washed with ice-cold PBS thrice. Cells were lysed by adding 90 μ l acetonitrile. Ten μ l of 5ug/ml Ac15Az5 was added as an internal standard. Supernatant was filtered by a 0.22 μ m filter. Supernatant was analyzed by UPLC-MSMS (Acquity Waters UPLC, and triple quadrupole mass analyzer Quattro Ultra with an electrospray ionization source in positive mode). Parent and daughter ion of **FD 15_8** was 608 m/z and 149 m/z respectively. Collision energy was 20 eV. Parent and daughter ion of Ac15Az5 was 594 m/z and 1097 m/z respectively. Collision energy was also 20 eV.

2.2.4 FD 15_8 efflux assay

S1 and S1M180 cells were used in **FD 15_8** efflux assay. One million cells were placed in 0.99 ml MEM. Ten microliters of **FD 15_8** at 1,000 μ M were added and incubated at 37°C with shaking at 180 rpm for 2 hours. Cells were then chilled on ice for 1 minute and centrifuged at 4,000 rpm for 5 minutes. Cells were then washed with PBS. After washing, cells were pelleted by centrifugation for 1 minutes at 4,000 rpm. Cells were re-suspended in **FD 15_8** free MEM medium. At 0, 30, 60, 120 minutes, cells were collected and chilled on ice for 1 minute and centrifuged at 14000 rpm. Supernatant was removed and the cells were washed with ice-cold PBS thrice. Cells were lysed by adding 90 μ l of acetonitrile. Ten μ l of 5 ug/ml Ac15Az5 was added as an internal standard. Supernatant was filtered by a 0.22 μ m filter and analyzed by UPLC-MSMS

(Acquity Waters UPLC, and triple quadrupole mass analyzer Quattro Ultrima with an electrospray ionization source in positive mode).

2.3 Vanadate-inhibitable ATPase assay

Reagents include homogenization buffer: 0.33 M sucrose, 300 mM Tris (pH7.4), 1 mM EDTA, 1 mM EGTA, 2 mM DTT, 100mM 6-aminocaproic acid, 1 mM PMSF and 1x protease inhibitor (cOmplete™ Protease Inhibitor Cocktail Tablets, Roche); ATPase assay buffer: 50mM Tris at pH7.5, 2 mM EGTA at pH 7.0, 2 mM DTT, 50 mM KCl, 10 mM MgCl₂, 5 mM Sodium azide, and 1 mM Ouabain; and stopping buffer: 0.2% ammonium molybdate, 1.4% sulphuric acid, 0.9% SDS and 1% ascorbic acid.

S1 and S1M180 cells were re-suspended in homogenization buffer and lysed by sonication using Q700 sonicator (QSONICA) at 10KHz for 10 minutes (30 seconds operation with 30 seconds resting time). Lysate was centrifuged at 3,500 g for 40 minutes at 4°C. Supernatant was centrifuged at 45,000 rpm by Himac CP70G (Hitachi) for 1.5 hours. Pellet was re-suspended in assay buffer to form microsomes. Five micrograms of microsome was used in each reaction. Compounds at 1.1 nM to 500 nM and 0.3mM sodium orthovanadate were added to the microsomes and pre-incubated at 37°C for 30 minutes. ATP was added to each reaction to a final concentration of 2.5mM and further incubated for 1 hour. Reactions were stopped by adding 200 µl freshly prepared cold stopping buffer and incubated at room temperature for 15 minutes. Absorbance of 655nm was measured by CLARIOstar® microplate reader (BMG).

2.4 Molecular docking for prediction of FD 15_8 binding site

Molecular docking was performed to predict the binding sites of **FD 15_8** on BCRP. BCRP structure (PDB ID: 5nj3) was used as the receptor. Water molecules were removed and hydrogen atoms were added to the 5nj3. Three dimensional structures of **FD 15_8** and ATP were generated by ChemDraw Ultra 12.0. Pdbqt files were generated by AutoDock Tools (Morris et al., 2009) version 1.5.6. Autodock vina version 1.1.2 (Trott and Olson, 2010) was used for docking.

FD 15_8 and ATP were docked with 5nj3 at the nucleotide binding site. The xyz dimensions were 21.84 x 25.88 x 23.53 Å³ and the grid box parameters were x center: 117.628, y center: 114.075 and z center: 169.667 and spacing 1Å. The exhaustiveness was 15. Other parameters were set as default.

2.5 Cell treatment for assessing BCRP level

One million cells of HEK293/pcDNA3 or HEK293/ABCG2 were treated with 1µM of **FD 15_8** for 24 hours. The cells were washed with PBS before lysis.

2.6 Immunofluorescence staining

Reagents used in the experiment include immunofluorescence staining blocking solution: 3% bovine serum albumin and 0.1% triton X-100 in PBS. One hundred thousand cells were seeded on a sterilized glass coverslip in a 24-well plate overnight at 37°C with 5% CO₂. For the doxorubicin accumulation assay, 1 µM of doxorubicin was added in the presence or absence of 1 µM **FD 15_8** when the cells were seeded and incubated overnight. After that, media was removed and cells were washed with 1x PBS. Cells were fixed with 4% paraformaldehyde for 15 minutes at room temperature.

Cells were washed thrice with 1x PBS. staining Blocking solution was added to block non-specific binding and incubated at room temperature for 30 minutes. Cells were further incubated with primary antibody for 1 hour at room temperature. BCRP antibody BXP21 (Santa Cruz) diluted in 1:1,000 was used. The antibody was diluted in the blocking solution. After that, cells were washed thrice with 1x PBS, each time for 5 minutes. Secondary antibody of donkey anti-mouse IgG(H+L) secondary antibody conjugated with Alexa Fluor 594 (invitrogen) diluted at 1:500 was added and incubated for 1 hour at room temperature with the coverslips protected from light. After that, the coverslips were washed thrice with 1x PBS. Hoechst 33342 (10mg/ml) was added in 1:1,500 and incubated for 10 minutes at room temperature. Coverslip was washed with 1x PBS thrice and washed with distilled water before adding FluorSave™ Reagent (Milipore). After that, the glass slides were kept at 4°C until use. The slides were analyzed by Leica TCS SP8 confocal laser scanning microscopy platform. Alexa Fluor 594 excitation wavelength used was 561nm and emission wavelength collected was 600nm-630nm. Excitation wavelength for Hoechst 33342 was 410nm and emission wavelength collected was 475 nm-510 nm. Excitation wavelength for doxorubicin was 488 nm and emission wavelength collected was 549 nm-591 nm.

2.7 Protein sample preparation

Lysis buffer (150 mM NaCl, 1% v/v NP-40 and 50mM Tris-Cl at pH 8.0. 1x cOmplete™, EDTA-free Protease Inhibitor Cocktail (Roche) and 1mM PMSF) was added to protein sample before use. Sample buffer (6x): 7ml of stacking gel buffer, 3ml glycerol, 1 g SDS, 0.93g dithiothreitol, 1.2 mg bromophenol blue and water was added to top up 10 ml. Sample buffer was stored at -20°C until use.

Mammalian cells were lysed by lysis buffer at 4°C for 15 minutes. Lysate was centrifuged at 14,000 rpm for 15 minutes at 4°C. Supernatant was collected and stored

at -20°C until use. Protein concentration of lysate was measured by Bradford protein assay. Lysate was diluted 100-fold and 1000-fold with 10 mM HEPES buffer at pH 7.6 while bovine serum albumin was diluted to 1 to 20 µg/ml. Protein was mixed with 1:1 Bio-Rad Protein Assay Dye Reagent Concentrate (Bio-rad) in transparent 96-well plate. Absorbance at 595 nm was recorded by CLARIOstar® microplate reader(BMG).

2.8 SDS-PAGE and Western blot analysis

Reagents used include ammonium persulfate (Bio-rad): 10% (v/v) ammonium persulfate in water; tetramethylethylenediamine (TEMED) (Bio-rad); separating gel buffer: 1.5M Tris-Cl, 0.4% SDS, pH 8.8; stacking gel buffer: 0.5M Tris-Cl, 0.4% SDS, pH6.8; acrylamide/bisacrylamide: 30% acrylamide, 0.8% bisacrylamide; SDS-PAGE running buffer (1x): 25 mM Tris base, 192 mM glycine, 0.1% SDS; transfer buffer (1x): 25 mM Tris base, 192 mM glycine, 10% methanol and TBS buffer (1x): 20 mM Tris base, 140 mM sodium chloride, 0.1%(v/v) Tween 20 at pH7.6.

To set a 9% acrylamide separating gel, 1.5ml of 30% acrylamide/0.8% bisacrylamide buffer, 1.25 ml of 4xTris-Cl/SDS pH 8.8 separating gel buffer, 2.25 ml of H₂O, 25 µl of 10% ammonium persulfate and 12.5 µl TEMED was mixed together. For stacking gel, 0.217 ml of 30% acrylamide/0.8% bisacrylamide, 0.417 ml of stacking gel buffer, 1.02 of ml H₂O, 25 µl of 10% ammonium persulfate and 5 µl of TEMED was added.

For the analysis of BCRP, 10ug of protein lysate was loaded on a 9% SDS-PAGE. Proteins gel was resolved at 120 V for 1.5 hours and then transferred to PVDF membrane at 130 V for 1 hour. PVDF membrane was blocked in 5% skim milk with shaking for 1 hour at room temperature. Primary antibody BCRP antibody BXP-21 (Santa Cruz) diluted in 1:3000 or β-Actin Antibody (C4) sc-47778 (Santa Cruz) diluted in 1:3000 were added to the membrane and incubated at 4°C overnight. The membrane was washed 3 times with TBST, with 10 minutes each. Secondary antibody HRP-conjugated anti-mouse antibody in 1:3000 was incubated with the membrane at room temperature for 1 hour. Membrane was washed 3 times with TBST, each time 10 minutes. Pierce™ ECL Western Blotting Substrate (Thermo Fisher) was added according to the protocol and incubated for 2 minutes at room temperature. The chemiluminescence of protein on membrane was detected by c600 Azure Biosystems.

2.9 Mass spectrometry

2.9.1 Materials

All solvents used were of analytical grade and purchased from Tedia. To all solvents, 0.1% formic acid (v/v) (Sigma-Aldrich) was added. Acquity UPLC BEH C8 column (1.7 μm 2.1 x50mm) and Acquity UPLC BEH C18 column (1.7 μm 2.1x50mm) were purchased from Waters. UPLC (Acquity Waters) and triple quadrupole mass analyzer (Quattro Ultra) with an electrospray ionization source in positive mode were used for analysis.

2.9.2 Identification of parent and daughter ion of FD 15_8 for analysis

In positive ionization mode, full scanning of mass to charge ratio m/z from 100 to 1500 was performed. A stable and abundant peak at 608 m/z was identified as shown in **Figure 2.1**. It was used to select for daughter ion scan. By varying the collision energy from 15eV to 30eV, 149 m/z was identified as the stable and abundant daughter ion as shown in **Figure 2.2**.

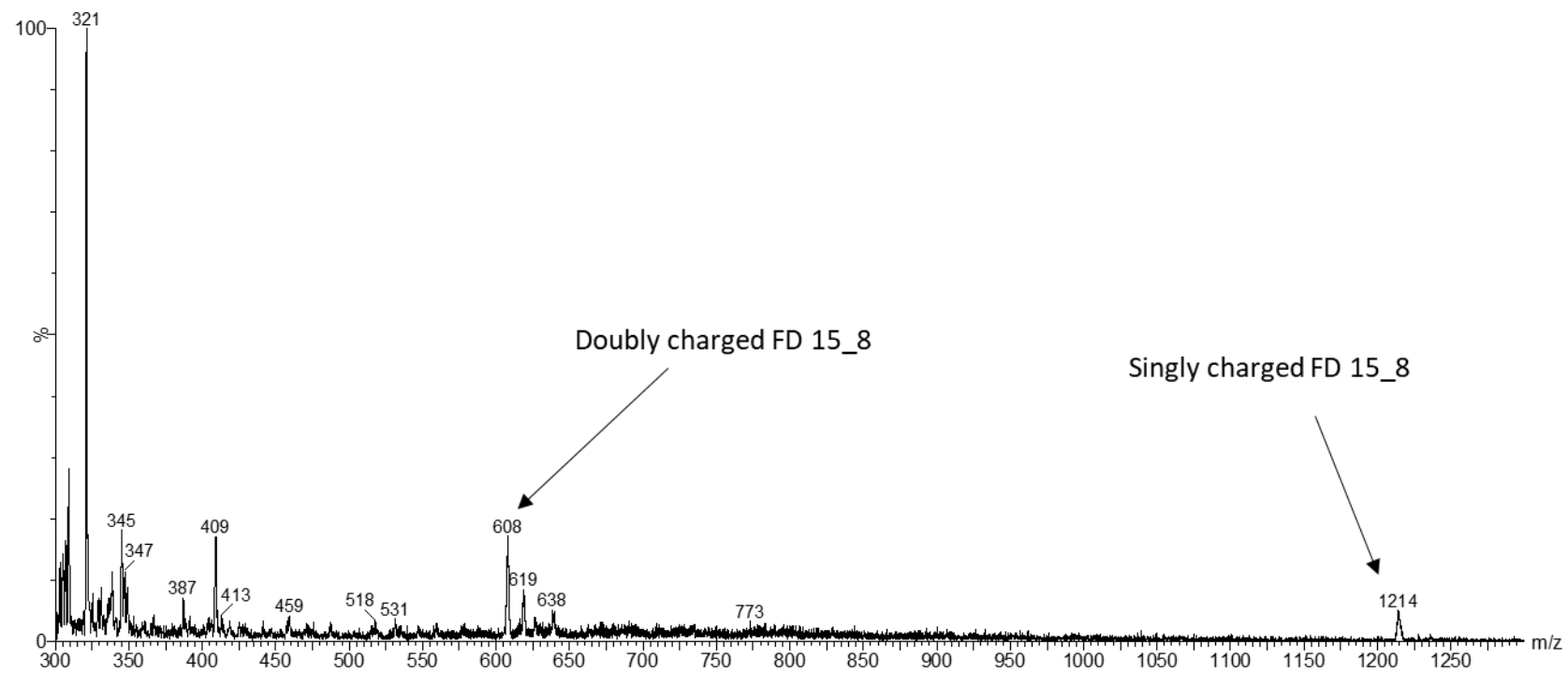


Figure 2.1. Full scan mass spectrum of FD 15_8.

In positive charge ionization mode, 608 m/z was identified as the stable and abundant peak. It is predicted to be the doubly charged **FD 15_8**, **FD 15_8** has an exact mass of 1213.4 g/mol. 1214 m/z could be the singly charged **FD 15_8**.

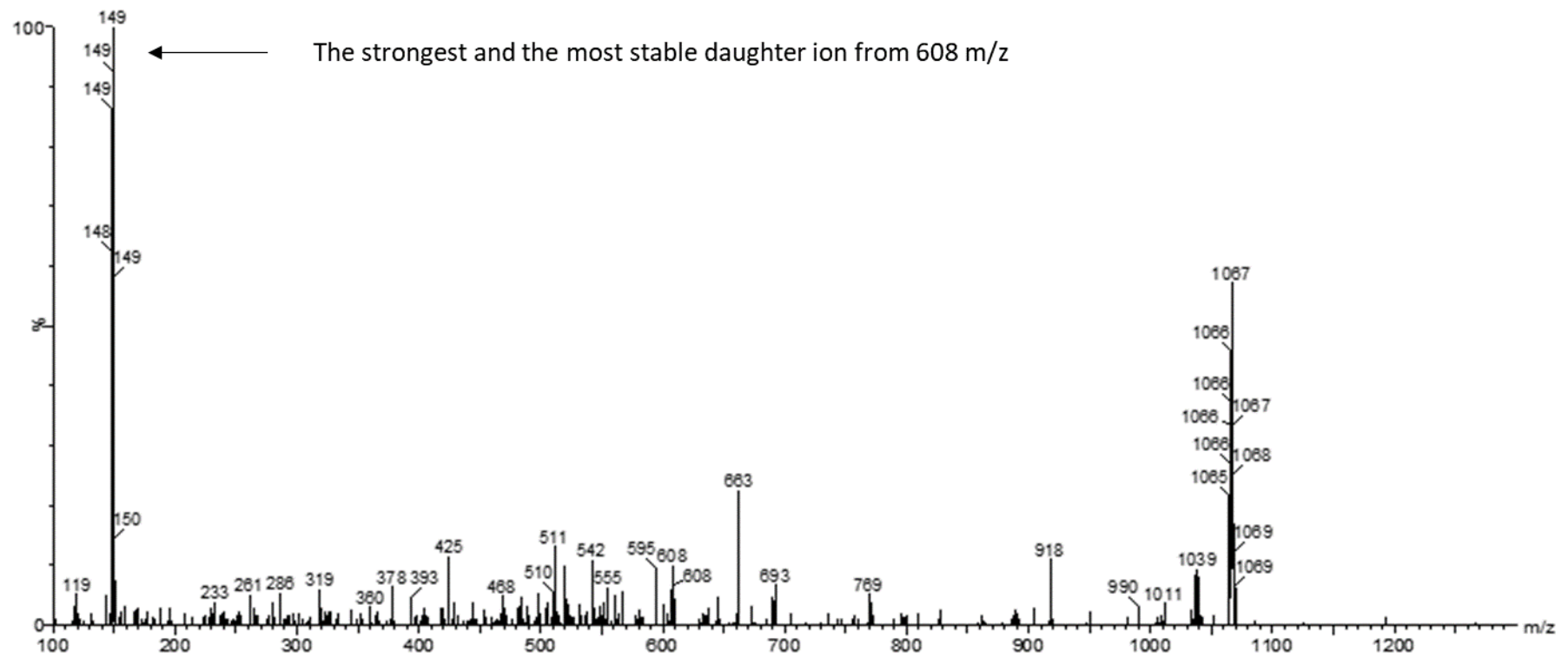
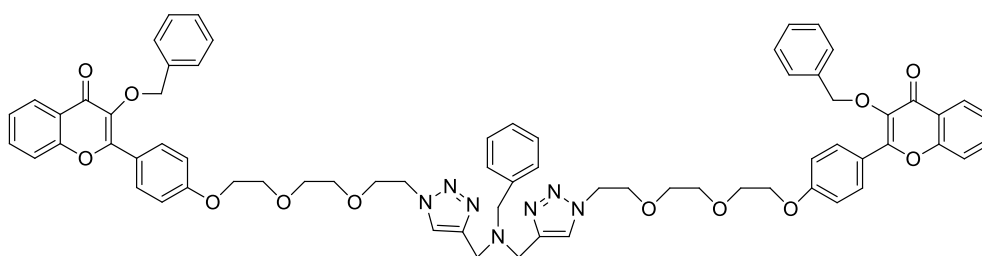


Figure 2.2. MS/MS scan for identifying daughter ion of 608m/z from FD 15_8.
 By selecting 608 m/z as the parent ion for MS/MS scan, 149m/z was identified as the stable, abundant daughter ion peak.

2.9.3 Identification of parent and daughter ion of internal standard Ac15Az5

Ac15Az5 was selected as the internal stand for **FD 15_8**. In positive ionization mode, full scanning of mass to charge ratio m/z from 200 to 1500 was performed. A stable and abundant peak at 594 m/z was identified. It was used to select for daughter ion. By varying the collision energy from 15 eV to 30 eV, 1097 m/z was identified as the stable and abundant daughter ion.



Chemical Formula: $C_{69}H_{67}N_7O_{12}$
Exact Mass: 1185.48477
Molecular Weight: 1186.30998
Elemental Analysis: C, 69.86; H, 5.69; N, 8.26; O, 16.18

Ac15Az5

Figure 2.3. Structure of Ac15Az5, the internal standard of FD 15_8.

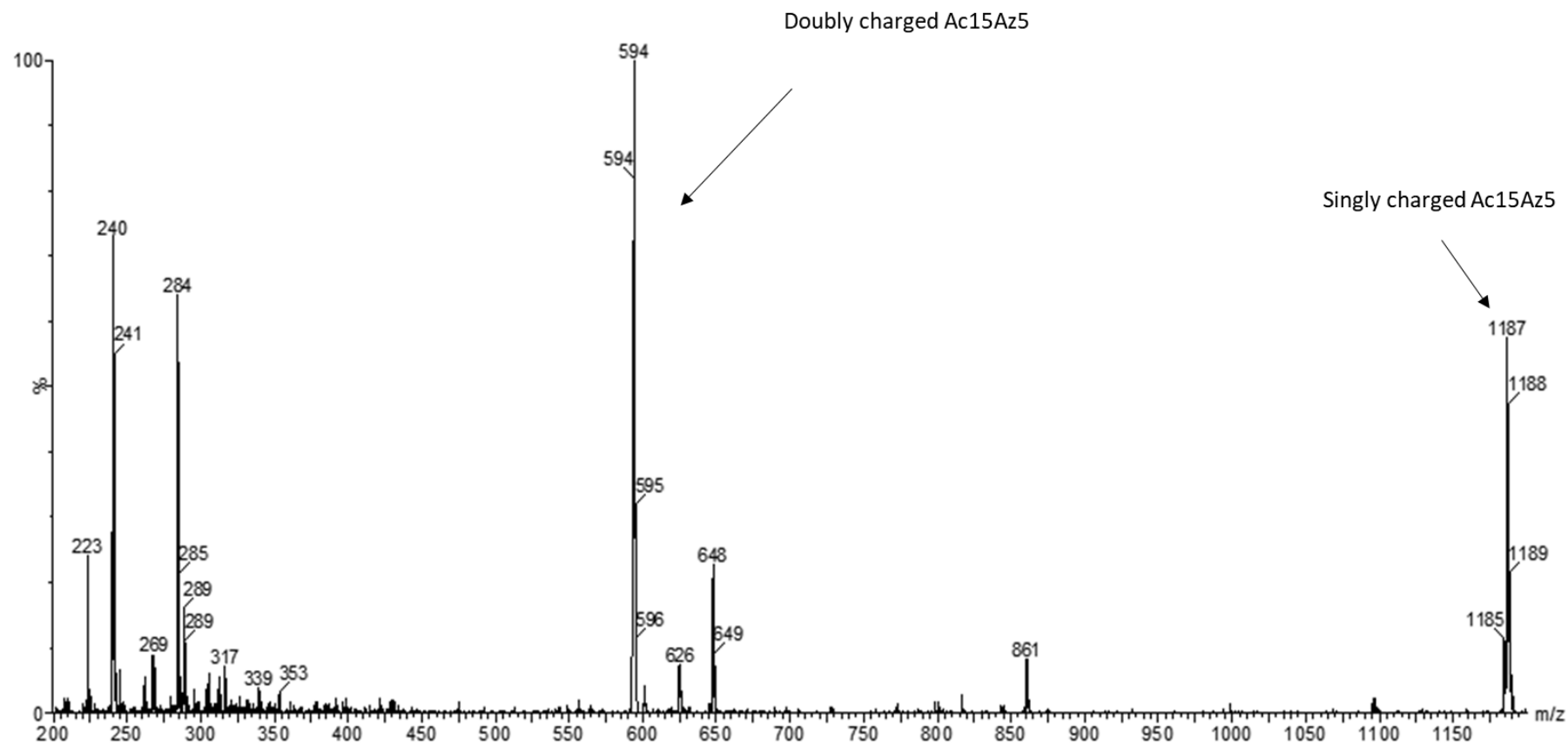


Figure 2.4. Full scan mass spectrum of Ac15Az5.

In positive charge ionization mode, 594 m/z was identified as the stable and abundant peak. It is predicted to be the doubly charged Ac15Az5, which with the exact mass 1185.5 g/mol. 1187 m/z could be the singly charged Ac15Az5.

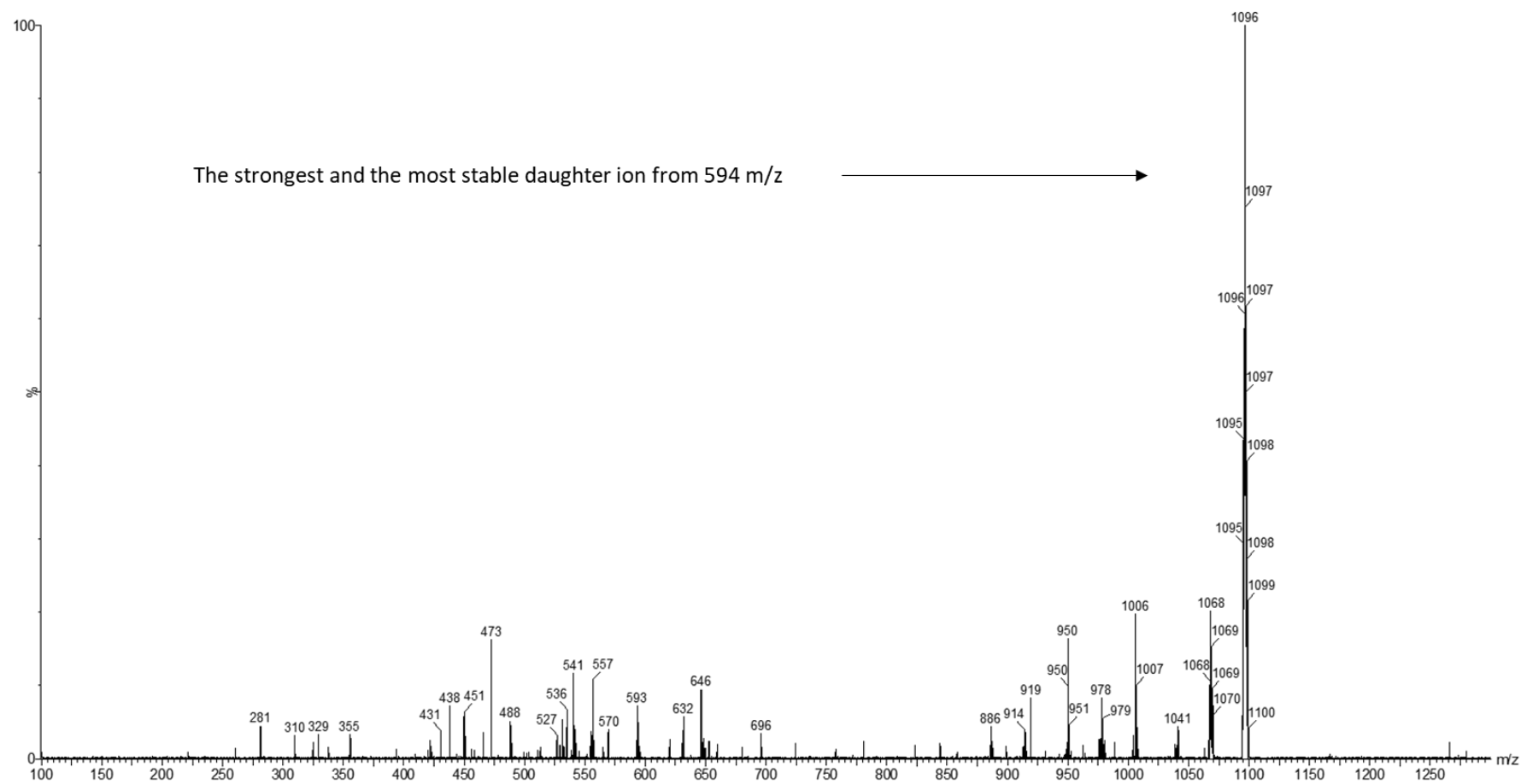


Figure 2.5. MSMS scan for identifying daughter ion of 594m/z from Ac15Az5.

By selecting 594 m/z as the parent ion for MS/MS scan, 1097m/z was identified as the stable, abundant daughter ion peak.

2.9.4 Identification of parent and daughter ion of topotecan

In positive ionization mode, full scanning of mass to charge ratio m/z from 200 to 1500 was performed. A stable and abundant peak at 422 m/z was identified (**Figure 2.6**). It was used to select for daughter ion. By varying the collision energy from 15eV to 30eV, 377 m/z was identified as the stable and abundant daughter ion (**Figure 2.7**).

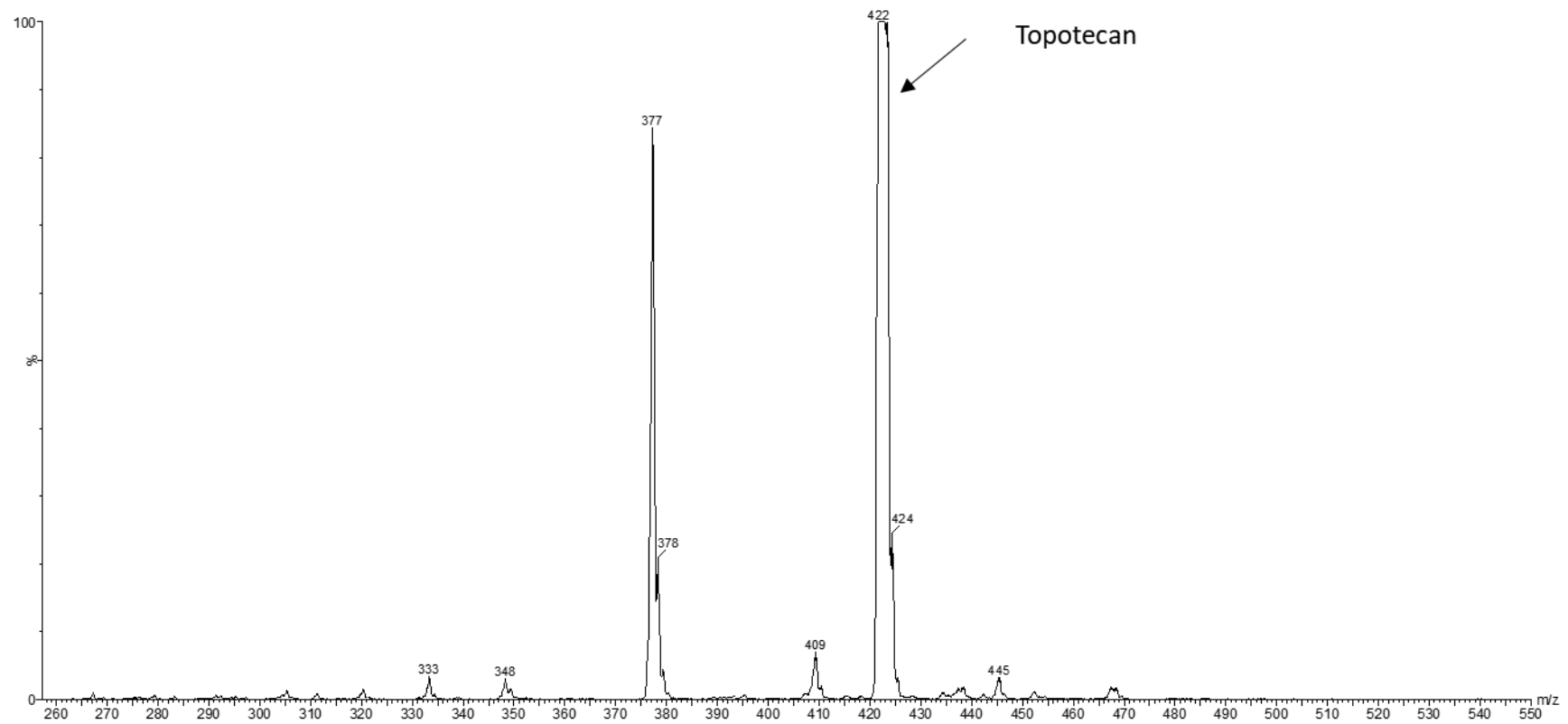


Figure 2.6. Full scan mass spectrum of topotecan

The full scan mass spectrum of topotecan showed the stable and abundant peak at 422m/z. Topotecan has an exact mass of 421.2 g/mol. 422 m/z could be the singly charged topotecan.

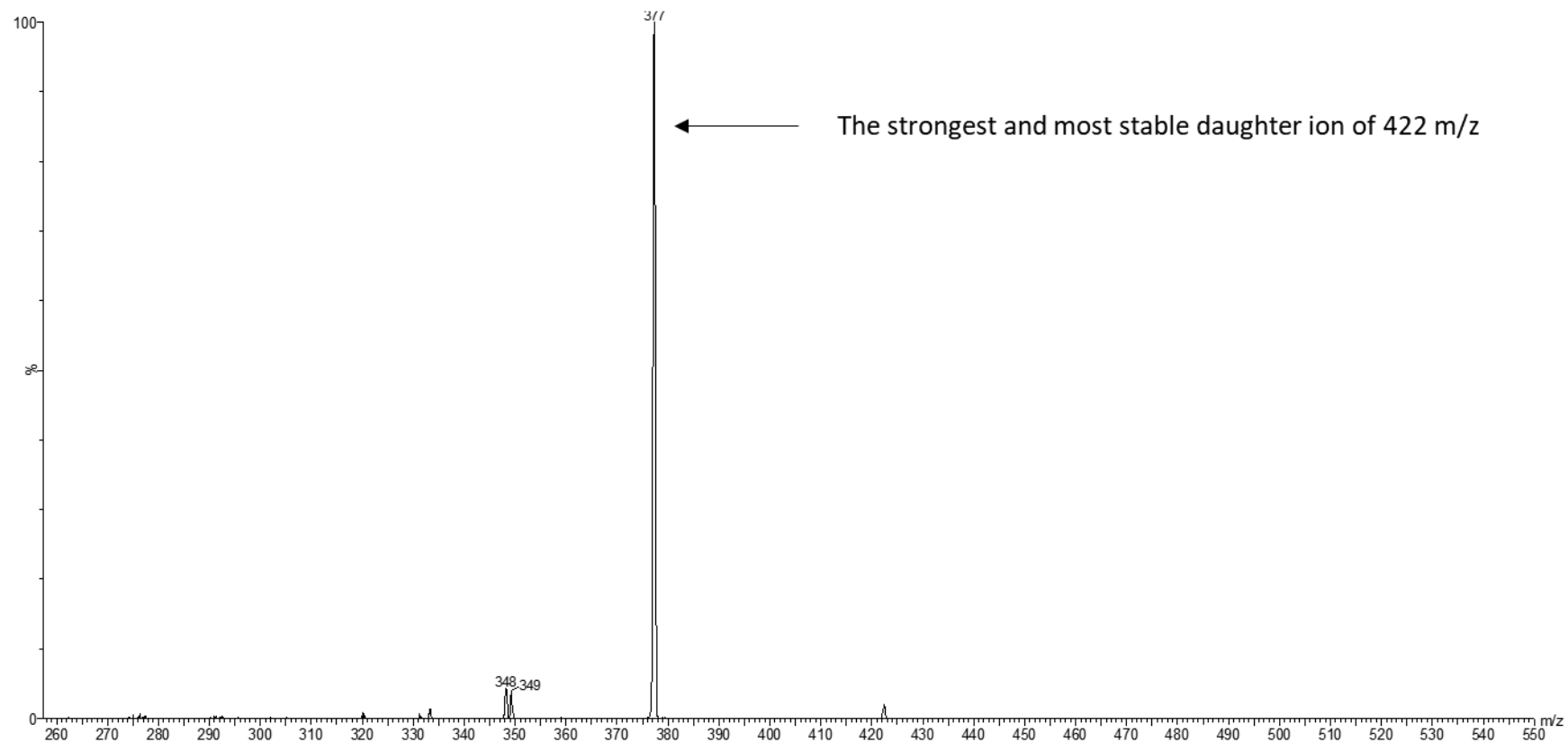
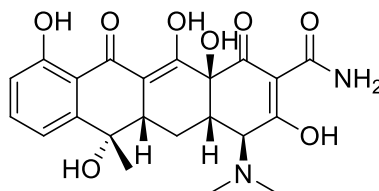


Figure 2.7. MS/MS scan for identifying daughter ion of 422m/z from topotecan.

By selecting 422m/z as the parent ion for MS/MS scan, 377m/z was identified as the stable, abundant daughter ion peak.

2.9.5 Identification of parent ion and daughter ion of internal standard tetracycline

In positive ionization mode, full scanning of mass to charge ratio m/z from 200 to 1500 was performed. A stable and abundant peak at 445 m/z was identified (**Figure 2.9**). It was used to select for daughter ion scan. By varying the collision energy, from 15eV to 30eV, 410 m/z was identified as the stable and abundant daughter ion (**Figure 2.10**).



Chemical Formula: $C_{22}H_{24}N_2O_8$

Exact Mass: 444.15327

Molecular Weight: 444.43456

Elemental Analysis: C, 59.45; H, 5.44; N, 6.30; O, 28.80

Tetracycline

Figure 2.8. Structure of tetracycline, the internal standard of topotecan.

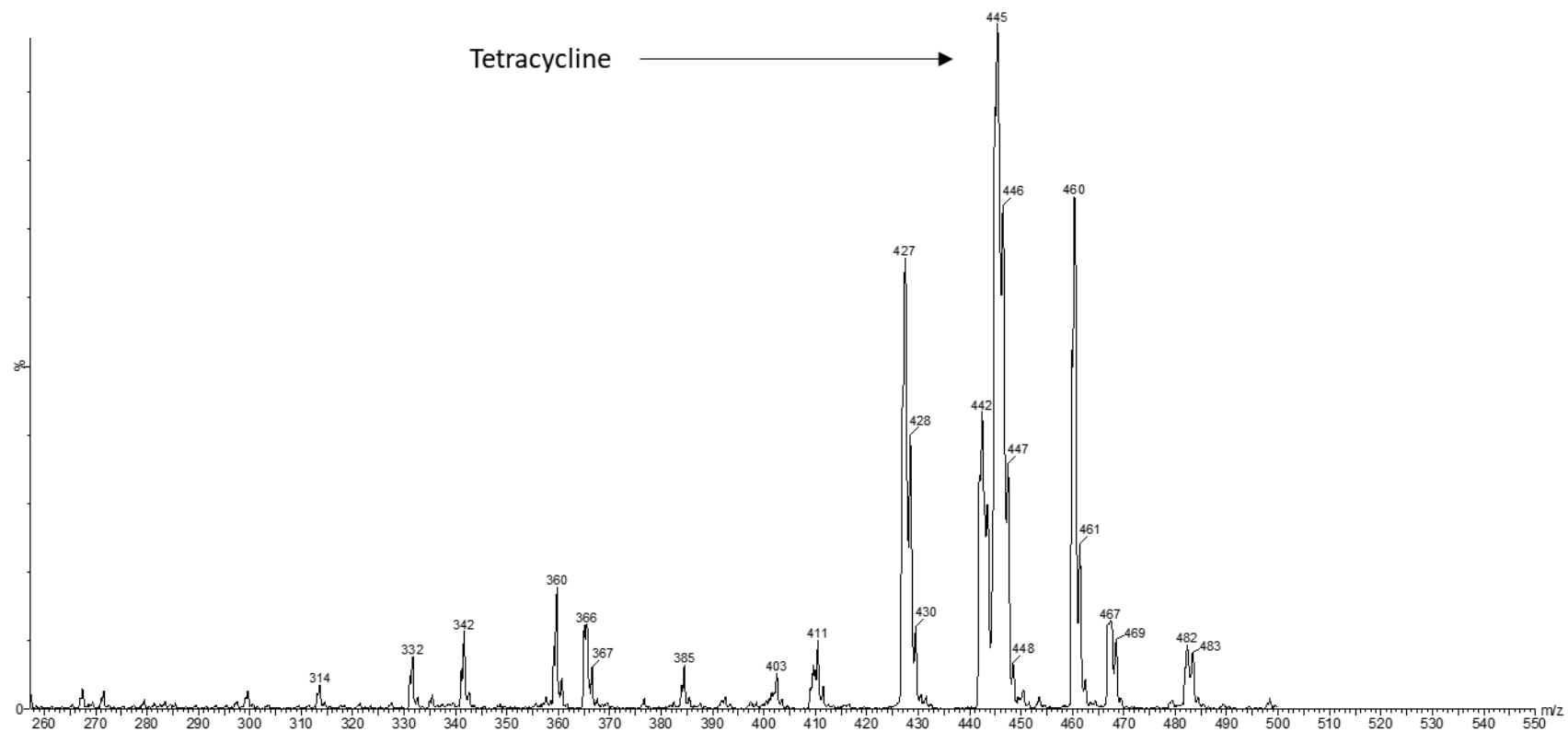


Figure 2.9. Full scan mass spectrum of tetracycline.

The full scan mass spectrum of tetracycline showed the stable and abundant peak at 445m/z. Tetracycline has an exact mass of 444.2 g/mol. The 445 m/z could be the singly charged tetracycline.

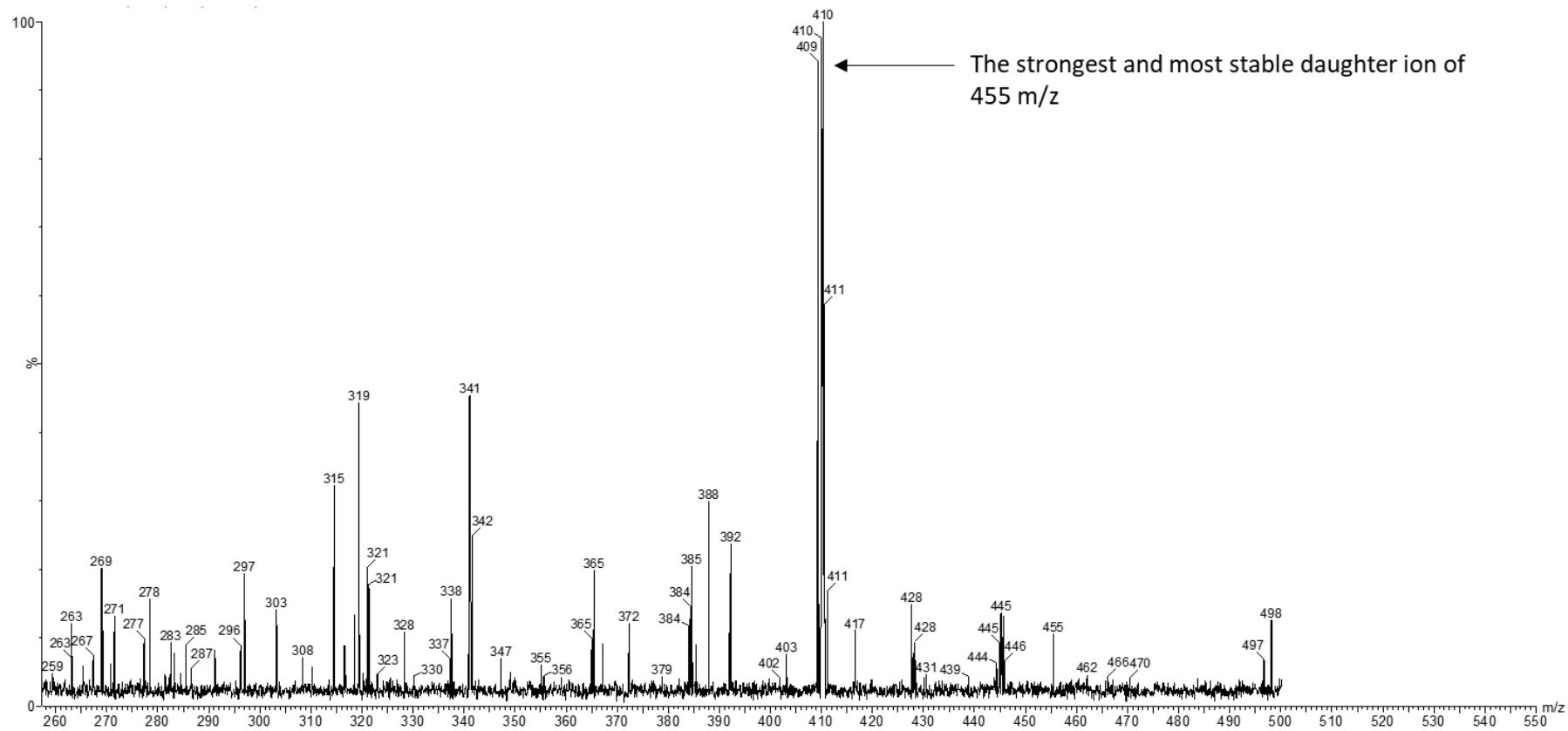


Figure 2.10. MSMS scan for identifying daughter ion of 445m/z from tetracycline.
 By selecting 445m/z as the parent ion for ms/ms scan, 410 was identified as the stable, abundant daughter ion peak.

2.9.6 Conditions of LC-MSMS for FD 15_8 analysis

For liquid chromatography, C8 column was used. Solvents were H₂O with 0.1% FA and acetonitrile(ACN) with 0.1%FA. Gradient elution was adopted and shown as follows:

Table 2. Ultra Performance Liquid Chromatography conditions for FD 15_8.

Time(min)	Flow(mL/min)	% (Water)	% (Acetonitrile)
Initial	0.4	80	20
1.0	0.4	80	20
5.0	0.4	28	72
7.0	0.4	0	100
9.0	0.4	0	100
10.0	0.4	80	20
14.0	0.4	80	20

The gradient elution condition was shown with the use of water and acetonitrile as the elution solvents.

The mass spectrometry conditions were 608->149 for **FD 15_8** and 594->1097 for internal standard Ac15Az5. The collision energy was 20eV for both compounds.

2.9.7 Conditions of LC-MSMS for topotecan analysis

For liquid chromatography, C18 column was used. Solvents were H₂O with 0.1% FA and methanol with 0.1%FA. Gradient elution was adopted and shown as follows:

Table 3. Ultra Performance Liquid Chromatography conditions for topotecan.

Time(min)	Flow(mL/min)	% (Water)	% (Methanol)
Initial	0.4	90	10
3.0	0.4	70	30
3.4	0.4	70	30
3.6	0.4	60	40
4.0	0.4	60	40
5.0	0.4	10	90
9.0	0.4	90	10
10.0	0.4	90	10

The gradient elution condition was shown with the use of water and methanol as the elution solvents.

The mass spectrometry conditions were 422->377 for topotecan, 445->410 for internal standard tetracycline. The collision energy was 20eV for both compounds.

2.9.8 Sample preparation

For analysis of **FD 15_8** in plasma, 80 μ l of plasma sample was added to 10 μ l of internal standard Ac15Az5. Another 210 μ l acetonitrile was added to precipitate protein. The mixture was centrifuged for 5 minutes at 14000rpm. The supernatant was passed through a 0.22 μ m filter before LC-MSMS.

For analysis of topotecan in plasma, 10 μ l of internal standard tetracycline was added to 80 μ l of collected plasma sample. Another 210 μ l methanol was added to precipitate protein. The mixture was centrifuged for 5 minutes at 14000rpm. The supernatant was passed through a 0.22 μ m filter before LC-MSMS analysis was carried out.

For analysis of topotecan in tumor, the tumors were dehydrated by liquid nitrogen, weighed and homogenized in PBS. The volume of PBS added was 2:1 to tumor weight. The mixture was then precipitated by adding 3 times of the volume of methanol. The supernatant was then used for LCMSMS analysis.

2.10 Animal studies

The animal study protocols were reviewed by the research ethics committee of The Hong Kong Polytechnic University (ASESC No.:13/32) and Department of Health of The Hong Kong Special Administrative Region. The compounds to be tested were administrated either through oral, intraperitoneal or tail vein administration.

2.10.1 Pharmacokinetic study

For pharmacokinetic study performed in SD rats, the rats received surgery under anesthesia for the jugular vein cannulation. Blood was sampled at 10, 30, 60, 120, 240, 420, 540, 720, 870, and 1440 minutes post administration through cannula. Blood was transferred to heparinized micro-centrifuge tube and precipitated by centrifugation at 14,000rpm for 5 minutes. The supernatant/ plasma was stored at -20°C until analysis. The rats were terminated by cervical dislocation under anesthesia at the end of the experiment.

For pharmacokinetic study performed on BALB/c mice, blood was collected by cardiac puncture under anesthesia at 10, 30, 60, 120, 240, 480, 720, and 1440 minutes. Blood was transferred to heparinized micro-centrifuge tubes and by centrifugated at 14,000rpm for 5 minutes. The supernatant/ plasma was stored at -20°C until analysis. The mice were sacrificed by cervical dislocation under anesthesia at the end of the experiment.

2.10.2 Toxicity study of FD 15_8 and topotecan

BALB/c mice were used in the toxicity experiment. Topotecan was used at 3mg/kg, 6, 9, 12 or 15mg/kg in combination with 15mg/kg **FD 15_8**, or 45mg/kg **FD 15_8** with topotecan at 15mg/kg. Both topotecan and **FD 15_8** were administrated intraperitoneally. **FD 15_8** was administrated 1 hour prior to topotecan administration. The mice received treatment every four days. A total four rounds of treatments were given. During the treatments, body weight and behavior of the mice were monitored.

At the end of the experiments, the mice were sacrificed by cervical dislocation under anesthesia.

2.10.3 *In vivo* efficacy study of FD 15_8

For *in vivo* efficacy experiment, female BALB/c nu/nu mice were used. Ten million S1 or S1M180 cells were injected subcutaneously to each mouse. When the tumor grew to 500mm³, the mouse was sacrificed under anesthesia. The tumor was cut into pieces and transplanted to other mice subcutaneously. This method results a more regular shape of tumour formation, thereby allowing more accurate determination of tumour volume. In addition, the tumour volume variation between groups will be reduced, as tumour xenograft is from same source. The mice were under anesthesia during the xenograft process. When the tumor grew up to 100mm³, the mice were randomized into three groups and received different treatments for the efficacy experiment. By either administration of solvent control, 45mg/kg **FD 15_8**, 2mg/kg topotecan or a combination of 45mg/kg **FD 15_8** and 2mg/kg topotecan. Both **FD 15_8** and topotecan were injected through intraperitoneal administration. **FD 15_8** was administrated one hour prior to topotecan administration. The mice received treatment once every two days, with a total of 6 rounds of treatments. The mice were allowed to rest for a week. The mice received another 6 rounds of treatments and rest for a week again. Total four cycles of 6 rounds of treatment. Tumor size and body weights of the mice were monitored. The tumor size was calculated by the length times square of width and then divided by 2. At the end of the experiments, the mice were sacrificed by cervical dislocation under anesthesia.

The tumor size was calculated by **Equation 1**:

$$Tumor\ volume(mm^3) = \frac{l \times w^2}{2}$$

Where l is the longest diameter of the tumor and w is diameter perpendicular to l .

Equation 1. Mathematical equation for the calculation of tumor volume.

The tumor volume (%) was calculated by **Equation 2**:

$$\text{Tumor volume (\%)} = \frac{\text{tumor volume 2} - \text{tumor volume 1}}{\text{tumor volume 1}} \times 100\%$$

Where tumor volume 2 is the tumor volume at day of measurement, tumor volume 1 is the tumor volume of initial day of treatment.

Equation 2. Mathematical equation for the calculation of tumor volume (%).

Tumor doubling time was calculated by **Equation 3**.

$$\begin{aligned} \text{Tumor doubling time (Td)} \\ = (t_2 - t_1) \frac{\log(2)}{\log(\text{tumor volume 2}) - \log(\text{tumor volume 1})} \end{aligned}$$

Where, t_2 is final day; t_1 is initial day of treatment; *tumor volume 2* = tumor volume at t_2 ;

tumor volume 1 = tumor volume at t_1

Equation 3. Mathematical equations for the calculation of tumor doubling time (Td)

2.10.4 Topotecan accumulation in tumor xenograft

For topotecan accumulation in tumor, the S1M180 tumor-bearing mice were injected with 45mg/kg **FD 15_8** intraperitoneally. Six mg/kg of topotecan was administrated intraperitoneally 1 hour later. Mice were sacrificed five hours after topotecan injection by cervical dislocation under anesthesia. Plasma and tumor were collected and stored at -20°C until analysis.

2.11 Drug formulations

Formulation for dissolving drugs or modulators need to be optimized as follows. The compounds have to be dissolved in solvent first. A co-solvent was then added. The purpose was to stabilize the compounds. After that, the compounds were diluted to designated concentrations for use. The color change in each step should be monitored. A milky solution suggests that the compound has precipitated. Besides, after addition of co-solvent or dilution, the solutions were centrifuged at high speed for a minute to check if the compound has precipitated. Mild heating was occasionally needed to get the compounds dissolved. As the compounds were synthesized at 90°C, mild heating (<60°C) is not likely to affect their stability. A change in concentrations might be needed. The compounds may precipitate when the concentrations were too high. The amounts of compounds dissolved in formulation were compared before and after passing through filters. The precipitated compounds trapped in the filters and resulted in a lower amount. The quantities of compounds could be analyzed by LC-MSMS.

After formulation optimization, the following formulation were chosen for animal studies. For topotecan, it was dissolved in sterile H₂O in 1mg/ml. For **FD 15_8**, it was first dissolved in N-Methyl-2-pyrrolidone (NMP), then Cremophor-EL and finally diluted in sterile H₂O. The solvent ratio of NMP: Cremophor-EL: H₂O was 1:1:8. The final concentration was 3mg/ml. N-Methyl-2-pyrrolidone is an acceptable pharmaceutical solvent (Jouyban et al., 2010). It was also used as vehicle in dissolving nilotinib which was tested if it was able to reverse drug resistance mediated by P-gp, and BCRP (Tiwari et al., 2013).

3. SCREENING OF FLAVONOID DIMERS FOR REVERSING BCRP-MEDIATED MDR

3.1 Introduction

Cancer MDR is one of the most challenging problems in chemotherapy. Overexpression of drug efflux transporters is one of the mechanisms causing multidrug resistance. BCRP is one of the transporters of the ATP-binding cassette family overexpressed in some cancers. Under stepwise drug selection, BCRP protein expression level is found to be increased in various cancer cell lines. MCF7/MX100 is one example. This breast cancer cell line overexpresses BCRP when cultured by prolonged incubation of the MCF7 cell line with the anticancer drug, mitoxantrone. Similarly, a colon cancer cell line S1M180 overexpressed BCRP after its parental cell line S1 was selected with mitoxantrone. These two cell lines have high BCRP expression and are resistant to many anticancer drugs. In view of these properties, they were used for screening of modulators that can reverse BCRP-mediated MDR.

3.2 Confirmation of BCRP expression by immunoblotting assay

BCRP expression in the cell lines contributes to the level of resistance to different kinds of anticancer drugs, including topotecan. S1M180 highly expressed BCRP while low level BCRP was detected in its parental cell line S1 (**Figure 3.1**). MCF7/MX100 also expressed higher level of BCRP compared to its parental cell line MCF7. S1M180 has much higher BCRP expression than MCF7/MX100. S1M180 was more suitable for screening BCRP modulators. MCF7/MX100 also expressed BCRP. However, the S1M180 expressed much higher level of BCRP. The dynamic range of detector may not be able to detect BCRP in MCF7/MX100. In another western blot, BCRP was shown to be expressed in MCF7/MX100 (**Figure 3.2**). S1M180 and MCF7/MX100 expressed ABCB1 too, but at a slightly lower level than that of S1. MRP1 was expressed in both S1 and S1M180 at an equally low level. The two figures were shown in appendix (**Figure 9.3** and **Figure 9.4**).

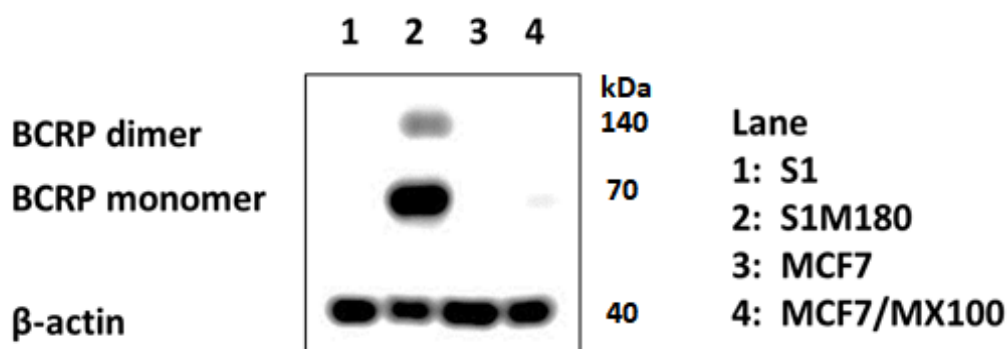
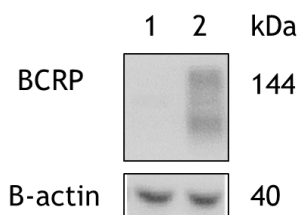


Figure 3.1. BCRP expression level in different cell lines.

Ten micrograms protein was loaded in each lane. Lane 1: S1, lane 2: S1M180, lane 3: MCF7 and lane 4: MCF7/MX100 cell lysates were separated by SDS-PAGE, transferred to PVDF membrane and BCRP was detected by BXP21 antibody (mouse anti-BCRP/ABCG2). Beta-actin acted as loading control and was detected by mouse anti- β -actin antibody C4. BCRP monomer and dimer were expected to have 72 and 140 kDa respectively.



Lane
 1:MCF7
 2:MCF7/MX100

Figure 3.2 BCRP expression level in MCF7 and MCF7/MX100

Ten micrograms protein was loaded in each lane. Lane 1: MCF7 and lane 2: MCF7/MX100 cell lysates were separated by SDS-PAGE, transferred to PVDF membrane and BCRP was detected by BXP21 antibody (mouse anti-BCRP/ABCG2). Beta-actin acted as loading control and was detected by mouse anti β -actin antibody C4.

3.3 Expression of BCRP monitored by confocal microscopy

To further confirm BCRP expression in the cell lines, immunostaining was used and the cells were observed through confocal microscopy.

BCRP was not detected in S1 and MCF7, but strongly stained in S1M180 and MCF7/MX100. BCRP signals was localized in the cell membrane. The results were consistent with the literatures which described that S1M180 and MCF7/MX100 high level of BCRP expression and that BCRP is localized in the cell membrane.

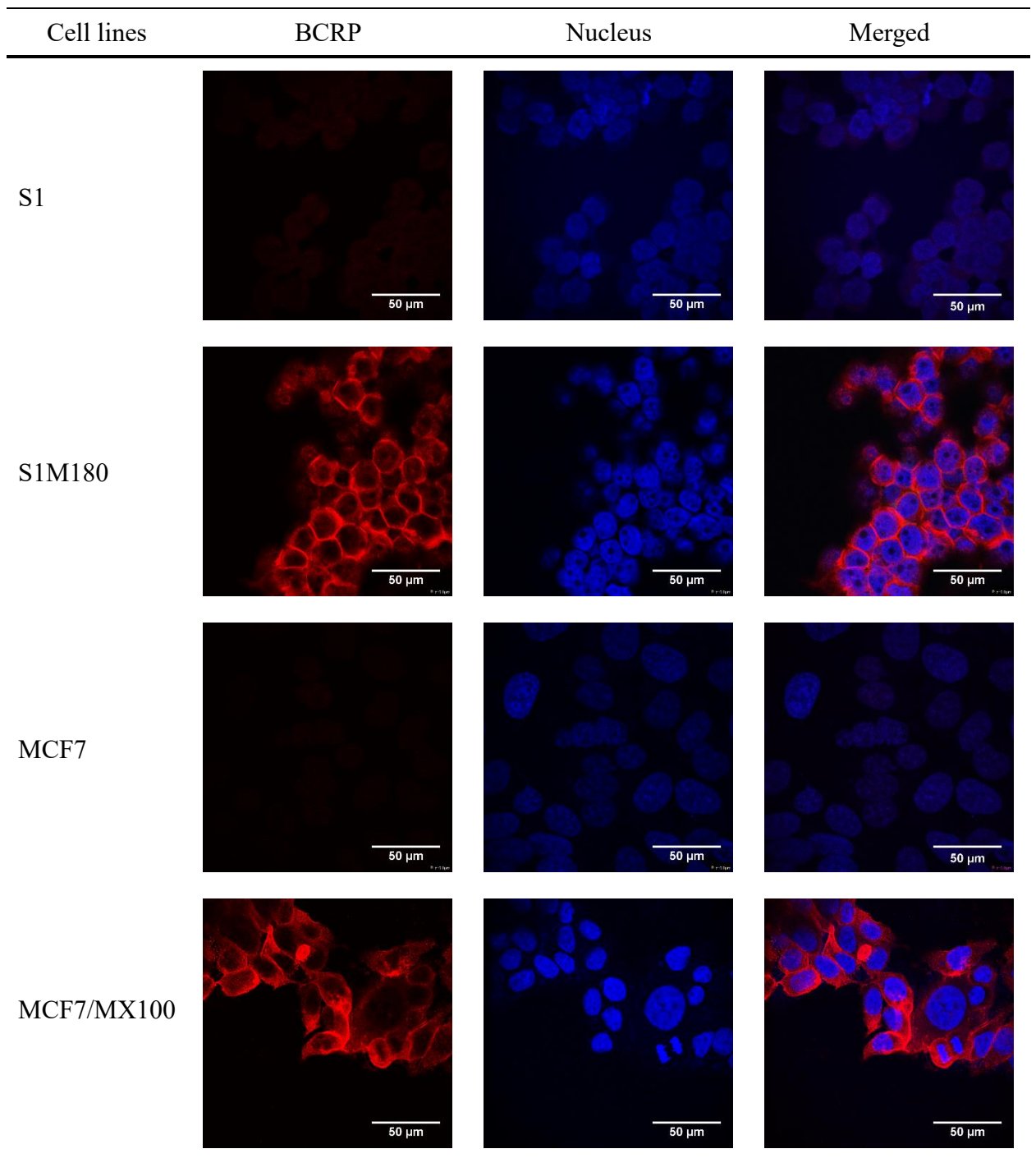


Figure 3.3. Confocal images of BCRP.

Cell lines S1, S1M180, MCF7 and MCF7/MX100 were stained with BXP21 antibody for BCRP detection and Hoechst 33342 for nucleus detection. BCRP was shown in red, the Hoechst 33342 was shown in blue.

3.4 Topotecan and doxorubicin resistance of S1 and S1M180

Topotecan and doxorubicin sensitivities were tested in S1 and S1M180 cell lines. The IC_{50} of topotecan for S1 and S1M180 were $0.51\pm 0.26 \mu\text{M}$ and $20.30\pm 7.22 \mu\text{M}$ while IC_{50} of doxorubicin for S1 and S1M180 were $0.15\pm 0.05 \mu\text{M}$ and $9.65\pm 1.37 \mu\text{M}$ respectively (Table 4). S1M180 was 40- and 65-fold more resistant to topotecan and doxorubicin than S1 respectively.

Table 4. S1 and S1M180 sensitivity to topotecan and doxorubicin.

Cell lines	IC_{50} of topotecan, μM	IC_{50} of doxorubicin, μM
S1	0.51 ± 0.26	0.15 ± 0.05
S1M180	20.30 ± 7.22	9.65 ± 1.37

The table indicated the IC_{50} s of topotecan and doxorubicin in S1 and S1M180 cell lines. The data are shown as mean \pm s.d. (n=3).

3.5 Screening for BCRP modulators

BCRP modulating activity of click flavonoid dimers were first screened by using a single concentration. Potent compounds were further selected for EC₅₀ determination.

3.5.1 Screening of BCRP modulators at high topotecan

concentration

S1M180 cells were treated with 0.2 μM of flavonoid dimers from our library and 10 μM of topotecan. Percentage of survival is shown in **Figure 3.4**. Lower survival means high reversal activity. Among the 52 flavonoid compounds screened, the most potent flavonoid dimers were Ac3Az1, Ac3Az11, Ac12Az4, Ac12Az9, Ac13Az5, Ac13Az8, Ac13Az9 and FD 15_8 with percentage of growth inhibition being 75.6%, 100%, 93.8%, 100%, 99.5%, 73.4%, 87.7% and 80.1% respectively. They were further characterized in the next section.

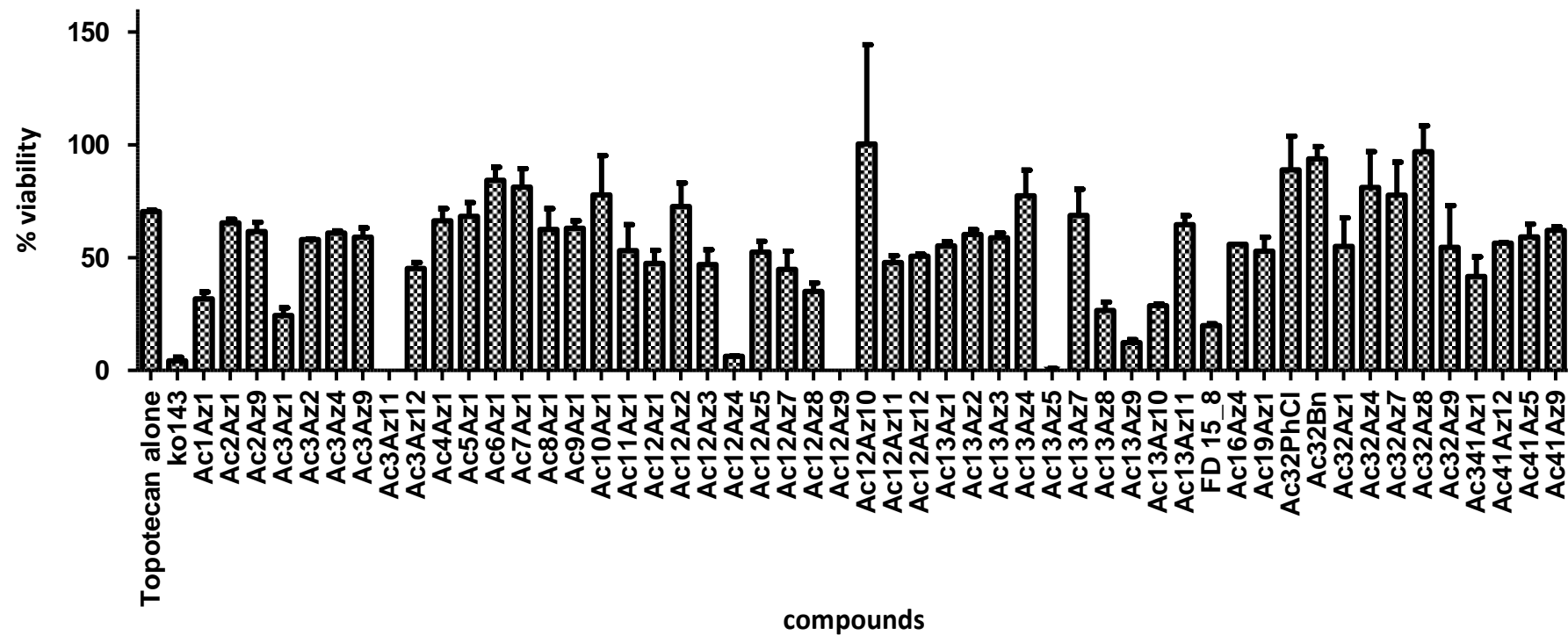


Figure 3.4. Primary screening of BCRP modulators using S1M180.

S1M180 was co-incubated with 10 μ M topotecan and various BCRP inhibitor candidate compounds at 0.2 μ M for 3 days at 37°C with 5%CO₂. Lower percentage survivor means better BCRP modulation. The percentage of survivor was compared to S1M180 in the absence of topotecan. Ac3Az1, Ac3Az11, Ac12Az4, Ac12Az9, Ac13Az5, Ac13Az8, Ac13Az9 and FD 15_8 were found to be effectively reduced cancer cell survival. Ko143 was the positive control.

3.5.2 Screening of BCRP modulator on the basis of potency

(EC₅₀)

Effective concentration 50 (EC₅₀) of the most potent compounds identified in the primary screening (**Figure 3.4**) were determined. These most potent BCRP modulators **FD 15_8**, Ac3Az11 and Ac15Az9 with EC₅₀s of 70.4±17.1nM, 53.6±23.3nM and 81.5±43.7nM respectively (**Table 5**). All 3 BCRP modulators were non-toxic to mouse fibroblast cell line L929 with IC₅₀ greater than 100 µM (**Table 6**). **FD 15_8** and Ac15Az9 were specific to BCRP-mediated resistance whereas Ac3Az11, in addition to reversing BCRP, can also reverse P-gp-and MRP1-mediated drug resistance (**Table 6**). Monospecific **FD 15_8** and Ac15Az9 were preferred. **FD 15_8** and Ac15Az9 shared similar structures and activities. **FD 15_8** has a lower molecular weight of 1213 Da. Therefore **FD 15_8** was chosen for further investigation. Its mechanism in reversing BCRP-mediated multidrug resistance, pharmacokinetic study and its *in vivo* toxicity and efficacy in reversing BCRP-mediated resistance were investigated in the next chapter.

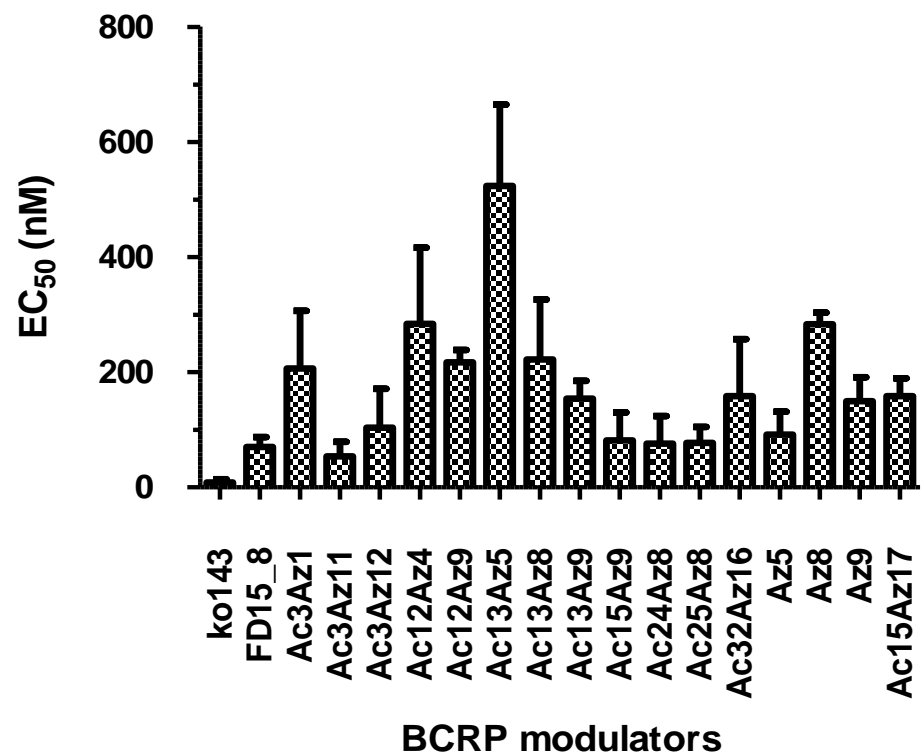


Figure 3.5. EC₅₀s of BCRP modulators in revering topotecan resistance in S1M180.

The figure shows the EC₅₀s of various BCRP modulator candidates (n=3-9). BCRP modulators at different concentrations were co-incubated with various concentrations of topotecan for 3 days at 37°C with 5% CO₂. Dose-response curves were fitted using Sigmoidal dose-response curve in GraphPad Prism 5 for determining EC₅₀s. **FD 15_8**, Ac15Az9 and Ac3Az11 were the most potent BCRP modulators with the lowest EC₅₀. Ko143 was the positive control.

Table 5. EC₅₀ of BCRP modulators in reversing topotecan resistance in S1M180 and MCF7/MX100.

Compounds	EC ₅₀ (nM)	
	S1M180	MCF7/MX100
ko143	8.7 ± 5.3	9.0 ± 1.5
FD15_8	70.4 ± 17.1	1.3 ± 0.7
Ac3Az1	206.7 ± 99.9	17.5 ± 8.1
Ac3Az11	53.6 ± 25.2	Not determined
Ac3Az12	103.7 ± 67.5	Not determined
Ac12Az4	284.2 ± 132.3	Not determined
Ac12Az9	217.3 ± 21.5	1.4 ± 0.6
Ac13Az5	523.4 ± 141.2	Not determined
Ac13Az8	222.0 ± 104.2	6.0
Ac13Az9	154.2 ± 30.6	2.0 ± 0.7
Ac15Az9	81.5 ± 48.9	2.0 ± 0.6
Ac24Az8	76.0 ± 48.0	2.0 ± 0.5
Ac25Az8	77.3 ± 27.9	1.2 ± 0.2
Ac32Az16	158.4 ± 99.4	Not determined
Az5	91.5 ± 39.7	Not determined
Az8	283.6 ± 20.0	120.0
Az9	150.0 ± 41.6	10.2 ± 1.6

EC₅₀s of compounds were tested in S1M180 cell line in combination with topotecan (n=1-9). The EC₅₀ is the effective concentration of tested compounds to reduce the IC₅₀ of topotecan by half. The data represented mean ± SD.

Table 6. Cytotoxicity of BCRP modulators to L929 fibroblast and cross reactivity with P-gp and MRP1 mediated drug resistant cell lines.

Compounds	IC ₅₀ (μM)	EC ₅₀ (nM)	
	L929	Paclitaxel resistance of LCC6/MDR	Doxorubicin resistance of 2008/MRP1
FD 15_8	>100	>3000	457.5±7.5
Ac15Az9	>100	>3000	441.7±8.3
Ac3Az11	>100	68.7±11.8	53.0±1.5

Cytotoxicity of BCRP modulators was measured as IC₅₀ towards a mouse fibroblast cell line L929. Cross reactivity of BCRP modulators was measured as EC₅₀ in reversing P-gp-mediated paclitaxel resistance in LCC6/MDR cell line and reversing BCRP-mediated doxorubicin resistance in 2008/MRP1 cell line. The data represented mean ± s.d. (n=3).

3.5.3 FD 15_8 as a potent BCRP modulator

FD 15_8 reversed BCRP-mediated topotecan resistance in a dose-dependent manner (Figure 3.6). Five hundred nM of FD 15_8 was supplied to sensitize S1M180 back to the parental level of S1 towards topotecan and doxorubicin.

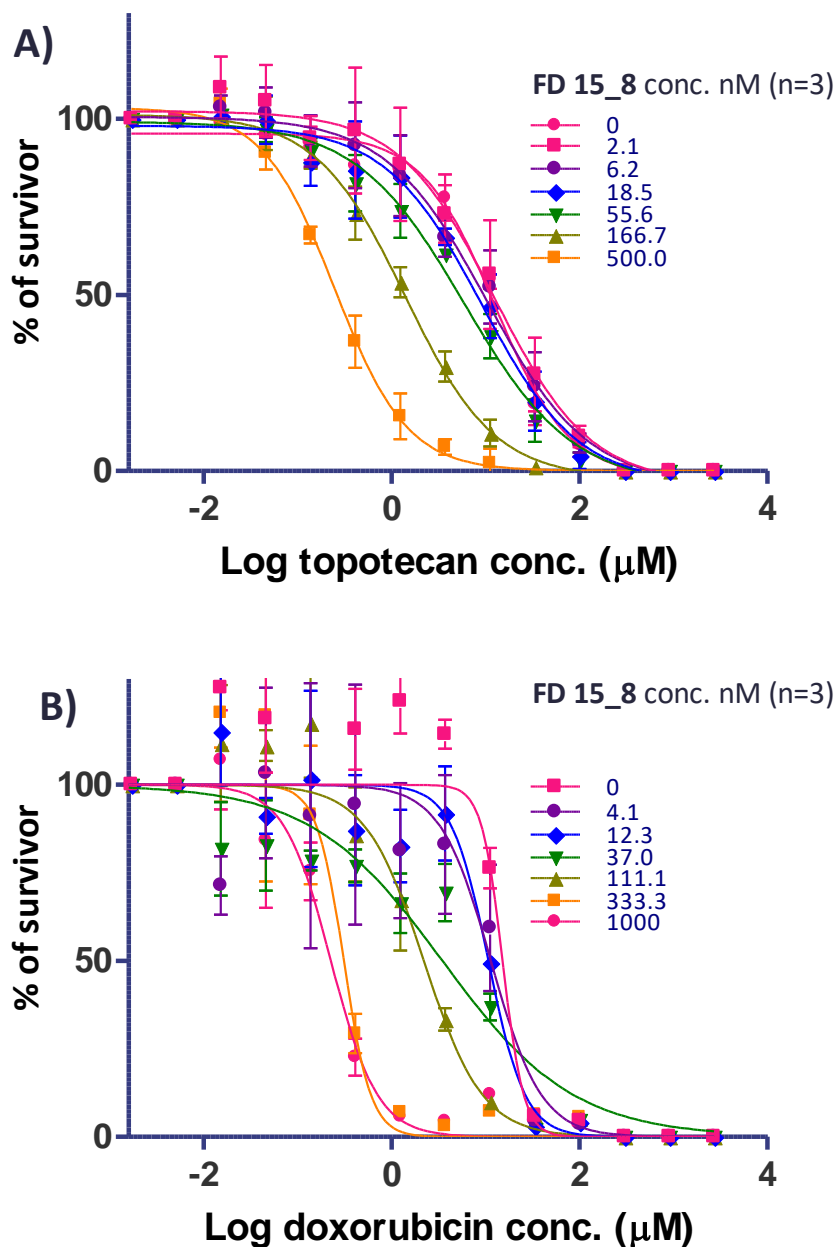


Figure 3.6. Dose dependence of FD15_8 in reversing topotecan and doxorubicin resistance in S1M180 cells.

S1M180 cells were treated with various concentrations of FD 15_8 and topotecan (A) or doxorubicin (B) for 3 days. A dose-dependent effect was observed for FD 15_8 in reversing topotecan or doxorubicin resistance in S1M180. EC_{50} were found to be 70.4 ± 17.1 nM and 56.1 ± 8.2 nM respectively. Data were shown as mean \pm s.d.(n=3).

3.5.4 Summary

Two pair of cell lines were used (S1 and S1M180; MCF7 and MCF7/MX100). The overexpression of BCRP and their plasma membrane localization was confirmed. The potency of newly synthesized click flavonoid dimers in reversing BCRP-mediated topotecan resistance was measured. **FD 15_8** was identified as the most potent BCRP modulator with EC_{50} of 1.3 ± 0.7 nM and 70.4 ± 17.1 nM for topotecan in MCF7/MX100 and S1M180 respectively. **FD 15_8** was able to restore the topotecan sensitivity of resistant cell line to the level of the sensitive cell line *in vitro*. As far as we know, this is the most potent BCRP modulator in the library.

4. MECHANISM OF FD 15_8 for REVERSING BCRP-MEDIATED MDR

4.1 Introduction

FD 15_8 can reverse BCRP-mediated topotecan resistance *in vitro* in S1M180 and MCF7/MX100 cell lines (Table 5). To elucidate how **FD 15_8** reverses BCRP-mediated drug resistance, several mechanisms were investigated, including accumulation assays, monitoring of BCRP expression level and vanadate-inhibitable ATPase activity assays. These experiments aim to determine how **FD 15_8** inhibits BCRP.

4.2 FD 15_8 accumulation and efflux assay

To evaluate if **FD 15_8** is a substrate of BCRP, **FD 15_8** accumulation and efflux in BCRP overexpressing and non-BCRP-overexpressing cell line were studied. Accumulation assay showed that intracellular concentration of **FD 15_8** increased gradually in both cell lines (Figure 4.1A). The uptake rate of **FD 15_8** in BCRP overexpressing cell line, S1M180, was higher than that in non-BCRP overexpressing cell line S1. At 120 minutes, the **FD 15_8** levels reached equilibrium in both cell lines and the intracellular **FD 15_8** levels at equilibrium were similar in both cell lines. The **FD 15_8** level increased for 2.3-fold in both cell lines compared to that at 10 minutes. Intracellular level of BCRP substrate should be lower in the BCRP-overexpressing cell line compared to non BCRP-overexpressing one. Comparable intracellular levels of **FD 15_8** in both cell lines suggested that **FD 15_8** is not a substrate of BCRP. It was observed that S1M180 had a higher uptake rate of **FD 15_8** than S1. S1M180 overexpressed BCRP which may favor **FD 15_8** binding. From the efflux experiment, **FD 15_8** might leave the cells by simple diffusion. BCRP might help to retain **FD 15_8** within the cells. Therefore S1M180 has a higher uptake rate than S1.

Efflux assay (**Figure 4.1.B**) showed that **FD 15_8** level decreased in both S1 and S1M180 cell lines. At 120 minutes, 77.5% of **FD 15_8** were retained in S1 and 51.8% in S1M180. Although the level of **FD 15_8** was lower in S1M180, the difference was not statistically significant ($p=0.311$) in t-test. If **FD 15_8** was a BCRP substrate, its intracellular level should have decreased more rapidly in ABCG2-overexpressing cell line S1M180 than non-ABCG2 overexpressing cell line S1. As the efflux rates were similar, that result suggested that **FD 15_8** was not a BCRP substrate, or that **FD 15_8** was a weak substrate. The decrease in **FD 15_8** could possibly be due to simple diffusion.

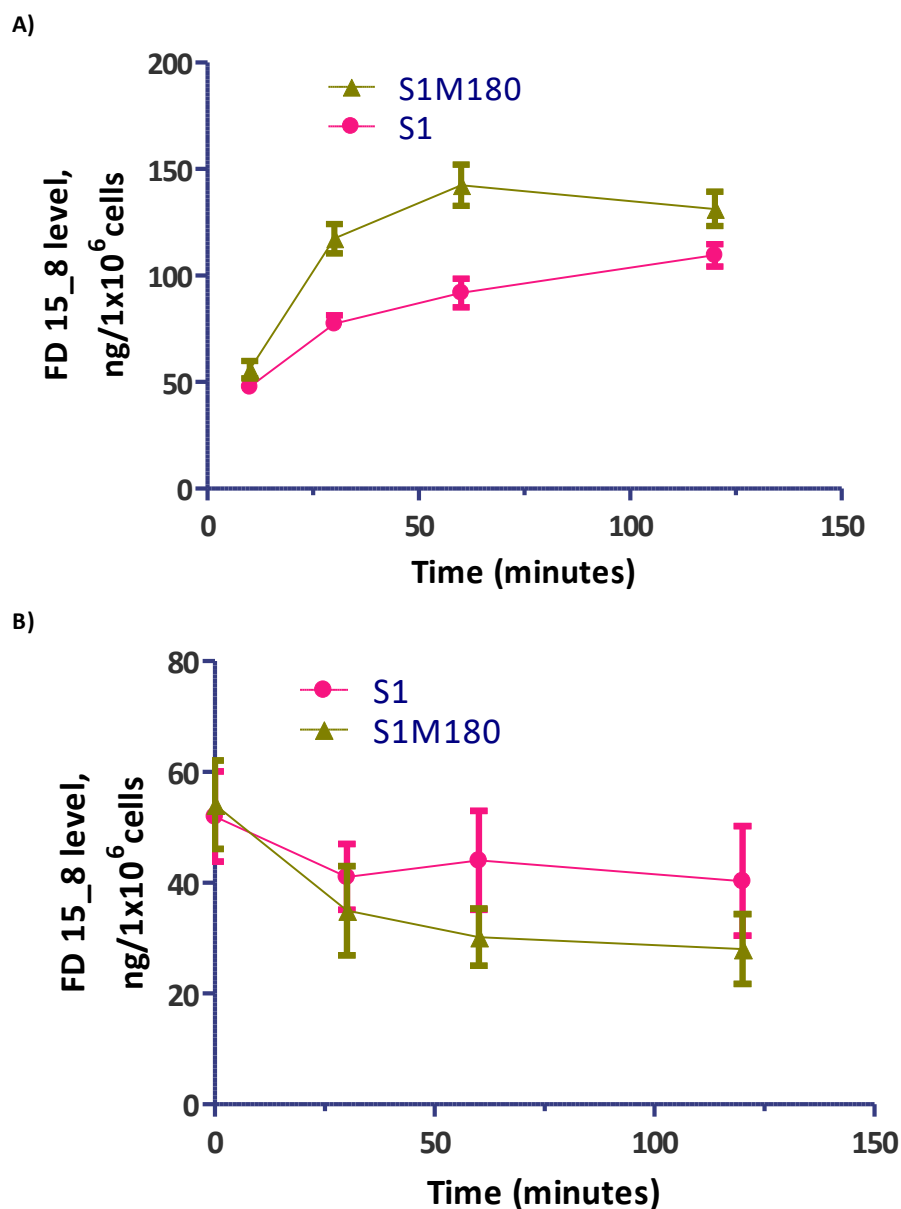


Figure 4.1. FD 15_8 accumulation and efflux assays.

For the accumulation assay A), 1 μM FD 15_8 was added to 1×10^7 S1 and S1M180 cells respectively. The cells were incubated at 37°C with shaking at 180rpm. The cells were put on ice and centrifuged. At 10, 30, 60 and 120 minutes, the cells were washed with ice cold PBS. Acetonitrile was added to lyse the cells and the supernatant was analyzed by LCMSMS (triplicate). For efflux assay B), 10 μM FD 15_8 was added to 1×10^7 S1 and S1M180 cells respectively and incubated for 2 hours at 37°C with shaking at 180rpm. The cells were put on ice and centrifuged. The cells were washed with ice-cold PBS and precipitated. The cells were re-suspended in FD 15_8 free medium. At 0, 30, 60 and 120 minutes, the cells were washed with ice cold PBS. Acetonitrile was added to lyse the cells and the supernatant was analyzed by UPLC-MSMS (triplicate). Each point represents mean \pm SEM.

4.3 Effect of FD 15_8 on BCRP protein expression level

BCRP downregulation could be triggered by some chemicals. According to Blazquez et al, acetaminophen could down-regulate BCRP expression in human choriocarcinoma cells (Blazquez et al., 2014). Another research group also found that xanthines could also down-regulate ABCG2 expression (Ding et al., 2012) in human breast cancer and choriocarcinoma cells. Xanthines down-regulate BCRP by inducing BCRP translocation and lysosomal degradation. Here the effect of **FD 15_8** on BCRP expression was investigated. As shown in **Figure 4.2**, BCRP protein level did not change after the treatment with 1 μ M **FD 15_8** for 24 hours. Therefore, **FD 15_8** did not induce degradation of BCRP and exerted no effect on BCRP expression.

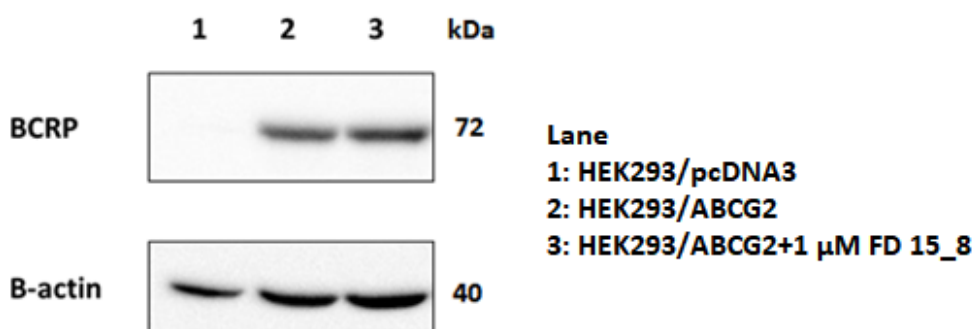


Figure 4.2. Effect of FD 15_8 on BCRP expression.

The HEK293/BCRP was treated in the presence or absence of 1 μ M **FD 15_8** for 24 hours. The cells were washed and lysed. The lysate was separated by SDS-PAGE and then transferred to PVDF membrane. BXP-21 antibody was used to probe BCRP. β -actin was the loading control. BCRP expression level did not change after treatment with 1 μ M **FD 15_8**.

4.4 Effect of FD 15_8 on BCRP intracellular localization

BCRP is a membrane protein and mediates drug efflux across the cell membrane. The level of BCRP-mediated multidrug resistance could be lowered if the BCRP did not localize on the cell membrane. As mentioned previously, xanthines could induce BCRP translocation (Ding et al., 2012). In addition, BCRP internalization could be triggered by the binding of antibody 5D3 (Studzian et al., 2015). To investigate whether **FD 15_8** affected the localization of BCRP, immunostaining was used. S1M180 cells were treated with 1 μ M or 10 μ M of **FD 15_8** for 24hours, the cells were then stained with BXP-21 antibody for detection of BCRP and DAPI stained for the nucleus.

Intracellular level of BCRP was the same in FD15_8 treatment group and DMSO control group (**Figure 4.3**). Most of the BCRP were localized on the cell membrane. Incubation of **FD 15_8** did not alter the localization of BCRP. BCRP did not translocate to the cytoplasm or the nucleus upon treatment with **FD 15_8**. No internalization of BCRP was observed. **FD 15_8** exerted no effect on BCRP localization.

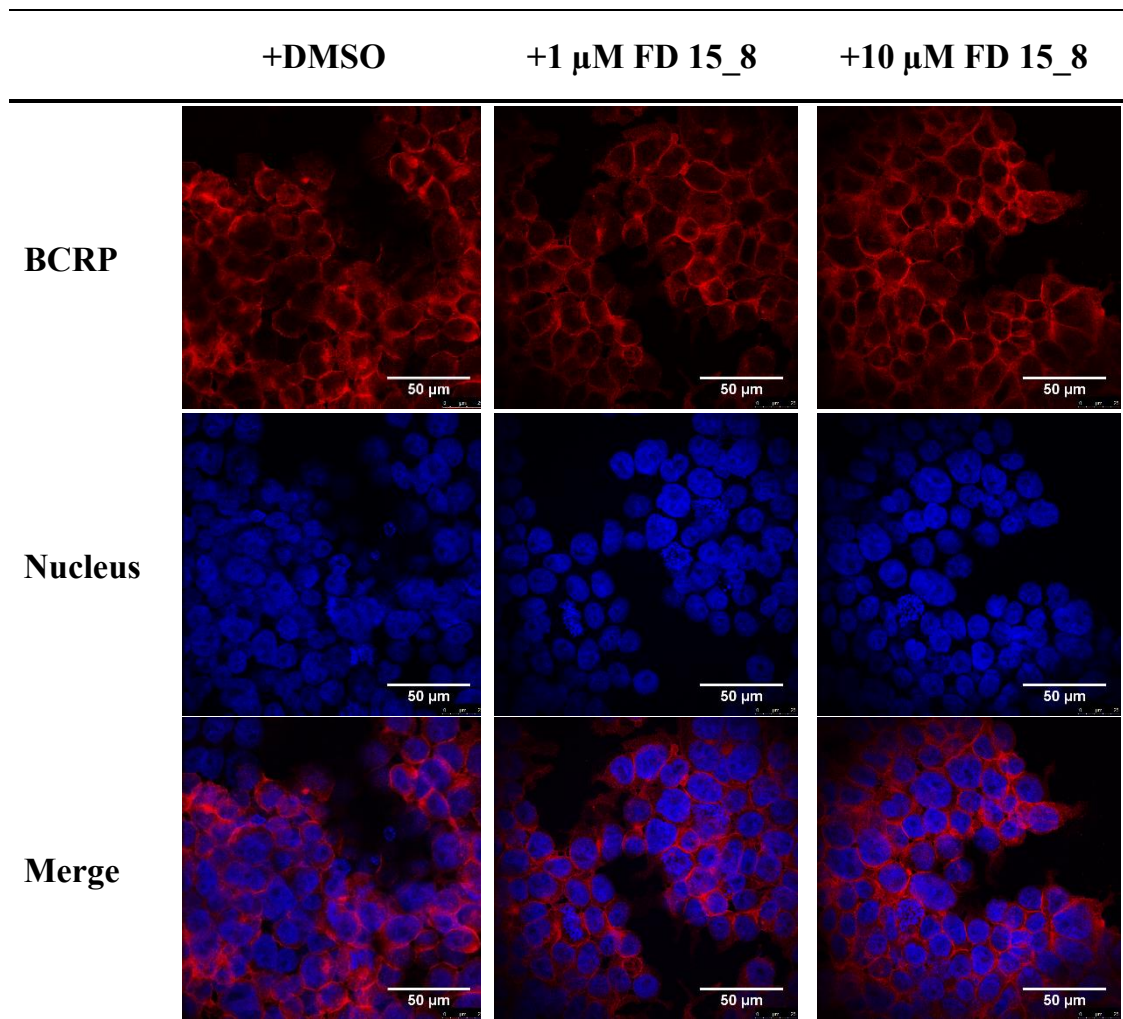


Figure 4.3. Effect of FD 15_8 on BCRP localization.

Subcellular BCRP localization after **FD 15_8** treatment was visualized by confocal microscopy. S1M180 cells were incubated with DMSO, 1 μ M **FD 15_8** or 10 μ M **FD 15_8** for 24hours. BCRP was stained by BXP-21 antibody, followed by Alex Fluo 594 anti-mouse antibody. DAPI was used to stain the nucleus.

4.5 Effect of FD 15_8 on intracellular topotecan and doxorubicin accumulation

Topotecan and doxorubicin are known substrates of BCRP and they are pumped out by BCRP. As **FD 15_8** could potentiate the cytotoxicity effect of these anticancer drugs *in vitro*, it was hypothesized that **FD 15_8** could increase substrates accumulation in BCRP-overexpressing cells.

Figure 4.4 shows that in the control group, topotecan accumulated in S1M180 cells was $29.8 \pm 14.2\%$ of S1 cells. This demonstrated that topotecan was a BCRP substrate and it was pumped out by BCRP. **FD 15_8** has no effect on the accumulation of topotecan in S1 cells. Incubation of DMSO control, 100 nM and 1000nM of **FD 15_8** in S1 cells resulted in similar intracellular level of topotecan; they were $100.0 \pm 13.5\%$, $102.3 \pm 14.3\%$ and $103.0 \pm 11.3\%$ respectively. In contrast, topotecan level in S1M180 treated with 100 nM **FD 15_8** or 1000 nM **FD 15_8** were $53.4 \pm 16.7\%$ and $124.3 \pm 46.1\%$ respectively. The higher concentration of **FD 15_8** used, the more topotecan retained within the cells. This result suggested that **FD 15_8** inhibited the BCRP-mediated efflux of topotecan in a dose-dependent manner.

FD 15_8 did not affect doxorubicin accumulation in S1 cell. Doxorubicin level in S1 cells treated with DMSO, 100 nM or 1000 nM of **FD 15_8** were $100 \pm 22.8\%$, $96.3 \pm 20.2\%$ and $102.3 \pm 13.4\%$. On the other hand, doxorubicin concentration in S1M180 cells treated with DMSO, 100 nM or 1000 nM **FD 15_8** were $32.0 \pm 16.1\%$, $69.3 \pm 15.6\%$ and $90.3 \pm 29.8\%$ respectively. This result suggested that **FD 15_8** effectively inhibited the BCRP-mediated efflux of doxorubicin in a dose-dependent manner.

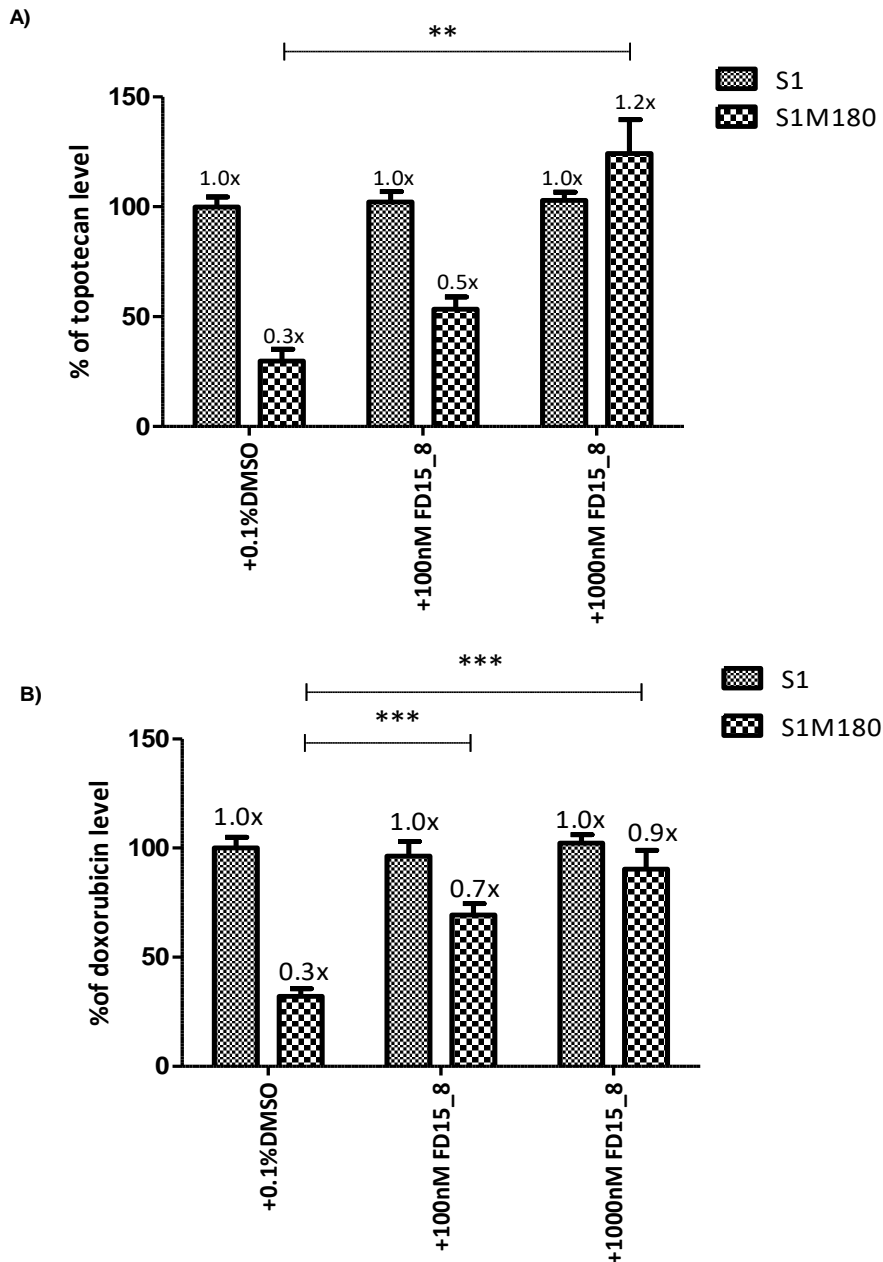


Figure 4.4. Effect of FD 15_8 on topotecan (A) and doxorubicin (B) accumulation.

For the topotecan accumulation assay A), DMSO, 100nM of **FD 15_8** or 1 μ M of **FD 15_8** were added to S1 and S1M180 respectively and incubated for 2 hours. Fifty micromolar topotecan were then added. After 60 minutes, cells were chilled on ice for 5 minutes. The cells collected were washed with ice-cold PBS and they were lysed by absolute ethanol. The supernatant was analyzed by fluorescence detection (n=3). For doxorubicin accumulation assay B), DMSO or 1 μ M of **FD 15_8** were added to S1 and S1M180 respectively and incubated for 2 hours. Twenty micromolar doxorubicin were then added. After 60 minutes, cells were chilled in ice for 5 minutes. The cells were washed with ice-cold PBS and they were lysed by doxorubicin analyzing buffer. The supernatant was analyzed by fluorescence detection (n=4-7). Student's t-test was used (** for $p \leq 0.01$, *** for $p \leq 0.001$). The data were shown as mean \pm SEM. Topotecan and doxorubicin levels were normalized to level of topotecan and doxorubicin in S1 treated with DMSO of assay A) and B) respectively.

4.6 Relationship between FD 15_8 and BCRP substrate doxorubicin

FD 15_8 can increase the intracellular concentration of the BCRP substrate doxorubicin by inhibiting BCRP. To find out the mode of action, double reciprocal plot was performed. Lineweaver-Burk plot showed that K_m was not affected (40.0 μ M) while V_{max} was reduced when FD 15_8 concentration increased, suggesting a non-competitive inhibition relationship between FD 15_8 and doxorubicin for BCRP (Figure 4.5). This result suggested that FD 15_8 and doxorubicin may bind to different sites of BCRP. Dixon plot allows a more accurate determination of K_i . Dixon plot in Figure 4.6 showed that K_i for FD 15_8 was 230 nM, which was close to the EC_{50} (56.1 \pm 8.2 nM) in S1M180. It suggested that at the concentration range from 56 to 230 nM, FD 15_8 reversed the resistance by non-competitive inhibition of BCRP.

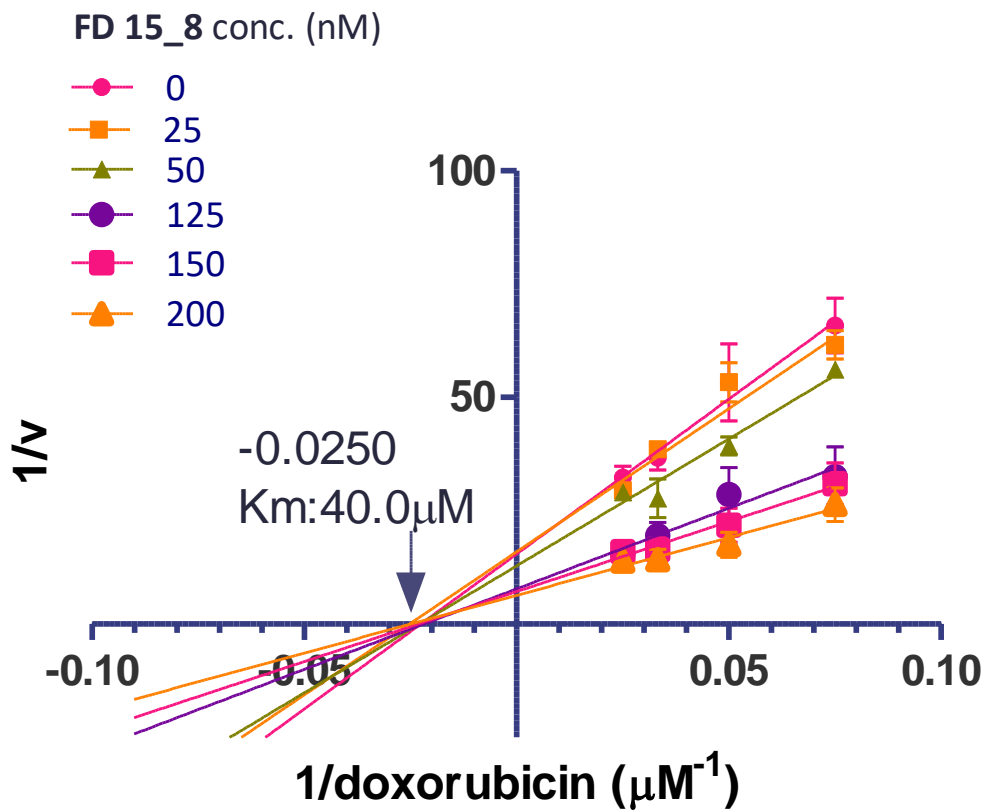


Figure 4.5. Lineweaver-Burk plot for FD 15_8 at different concentrations with doxorubicin.

S1M180 cells were incubated with various concentrations of FD 15_8 and doxorubicin (n=3-9). The cells were incubated with FD 15_8 for 2 hours prior to incubation with doxorubicin. After one hour, the cells were pelleted and washed with ice-cold PBS before analysis for doxorubicin. V was doxorubicin retention rate ($\mu\text{M}/\text{min}/500000$ cells). The curve was plotted with $1/v$ against $1/\text{doxorubicin}$ concentration added to the cells. The curves met at the X-axis. The K_m for the doxorubicin to BCRP found was $40.0 \mu\text{M}$. Each data point presented as mean \pm SEM.

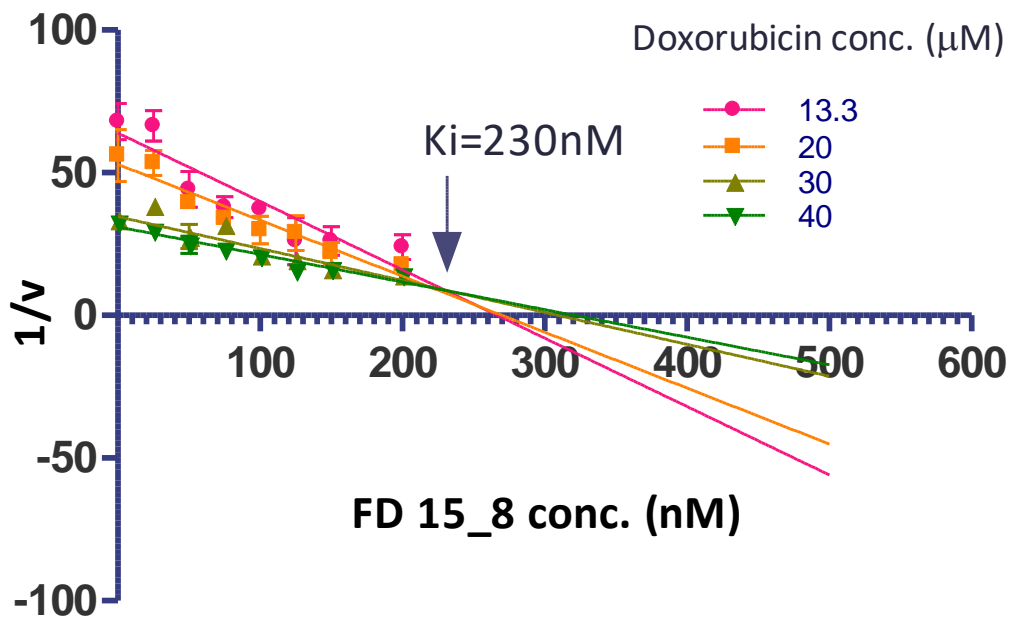


Figure 4.6. Dixon plot for FD 15_8 with at different concentrations with doxorubicin.

S1M180 cells were first incubated with FD 15_8 for two hours and then followed by doxorubicin. The cells were collected after one hour of adding doxorubicin. The cells were pelleted and washed with ice-cold PBS before lysis and analysis for doxorubicin concentration ($n=3-15$). V was doxorubicin retention rate ($\mu\text{M}/\text{min}/500000$ cells). The graph was plotted by $1/v$ against concentration of FD 15_8 added to the cells. The K_m was 230nM for FD 15_8 to doxorubicin. Each data point presented as mean \pm SEM.

4.7 Effect of FD 15_8 on doxorubicin accumulation as demonstrated by confocal microscopy

The effect of **FD 15_8** on the intracellular distribution of doxorubicin was investigated. Doxorubicin intercalates DNA and therefore it has to be inside the nucleus to work. **Figure 4.7** shows that S1 accumulate more doxorubicin than S1M180. Upon incubation with 10 μ M of **FD 15_8**, doxorubicin level was increased in S1M180. This result suggested that **FD 15_8** increased the intracellular level of doxorubicin in the BCRP-overexpressing cell line but does not affect the non-BCRP overexpressing cell line.

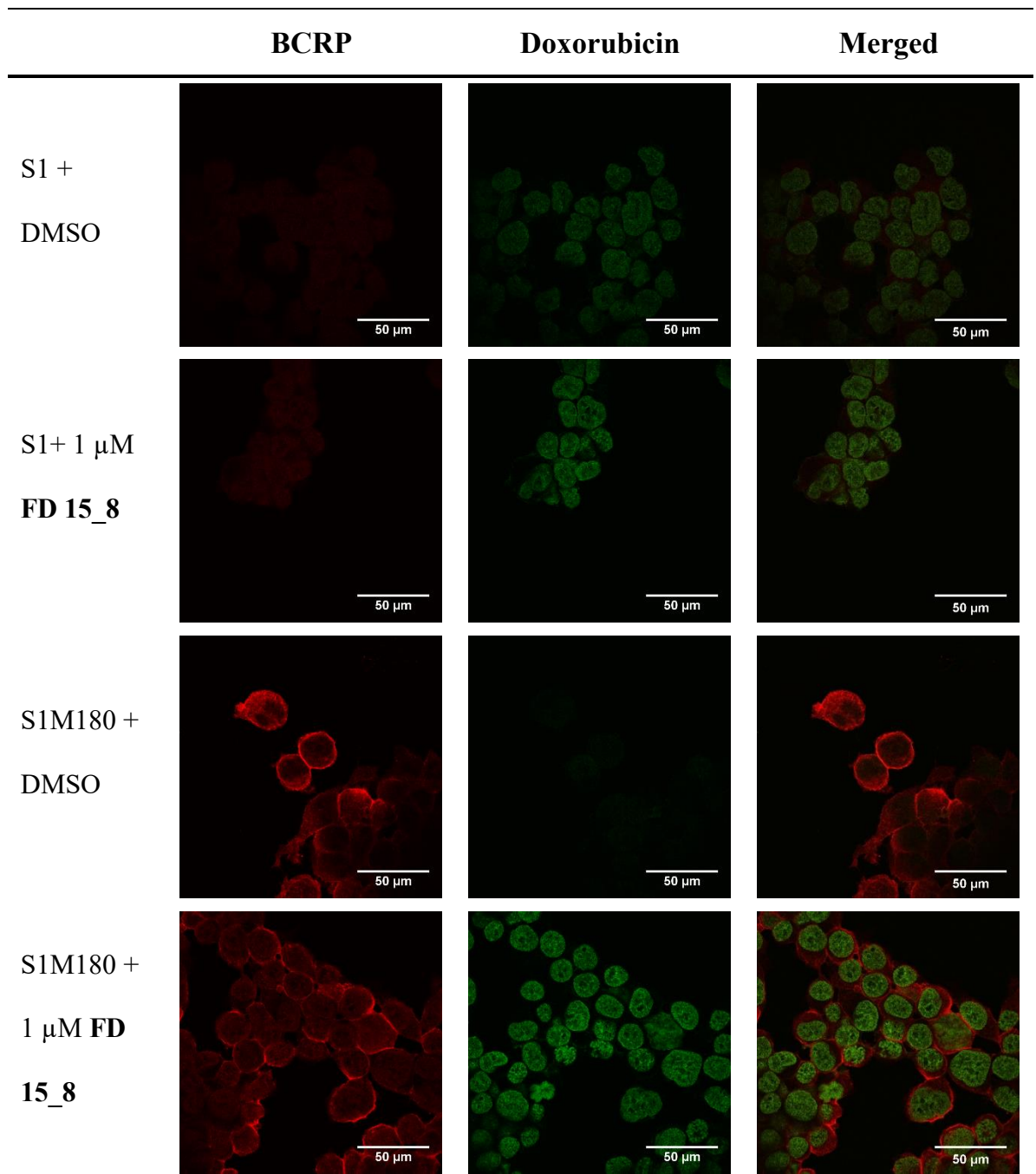


Figure 4.7. Doxorubicin accumulation in S1 and S1M180 cell lines as observed by confocal microscopy.

S1 and S1M180 were incubated with doxorubicin and DMSO or 1 μM **FD 15_8** for 24 hours. Cells were washed with ice-cold PBS and fixed with paraformaldehyde. The cells were later stained with BXP-21 for BCRP. Doxorubicin fluorescence was recorded at 488 nm excitation and 549 nm-591 nm for emission.

4.8 Effect of FD 15_8 on vanadate-inhibitable ATPase activity of BCRP

All ABC proteins have a nucleotide binding domain which has a vanadate-inhibitable ATPase activity. ATPase activity is required for an ABC protein to function. One of the possible mechanism by which **FD 15_8** inhibits BCRP is through inhibition of the vanadate-inhibitable ATPase of BCRP. It was found that **FD 15_8** inhibited BCRP vanadate-inhibitable ATPase, similar to another BCRP inhibitor ko143 (Gallus et al., 2014) (**Figure 4.8**). The IC_{50s} of both ko143 and **FD 15_8** for inhibiting ATPase were 6.5 nM and 7.5 nM respectively. **FD 15_8** inhibited ATPase activity in a dose-dependent manner. On the other hand, Az8, the monomer of **FD 15_8**, stimulated ATPase activity. This result suggested that the binding sites of **FD 15_8** is different from its monomer Az8. Another BCRP substrate mitoxantrone also stimulated BCRP ATPase activity as expected. The linker Ac15 had no effect on ATPase. It was inferred that the triazole ring in the linker was not involved in BCRP binding. All these results suggested that **FD 15_8** inhibited BCRP by inhibiting the ATPase function.

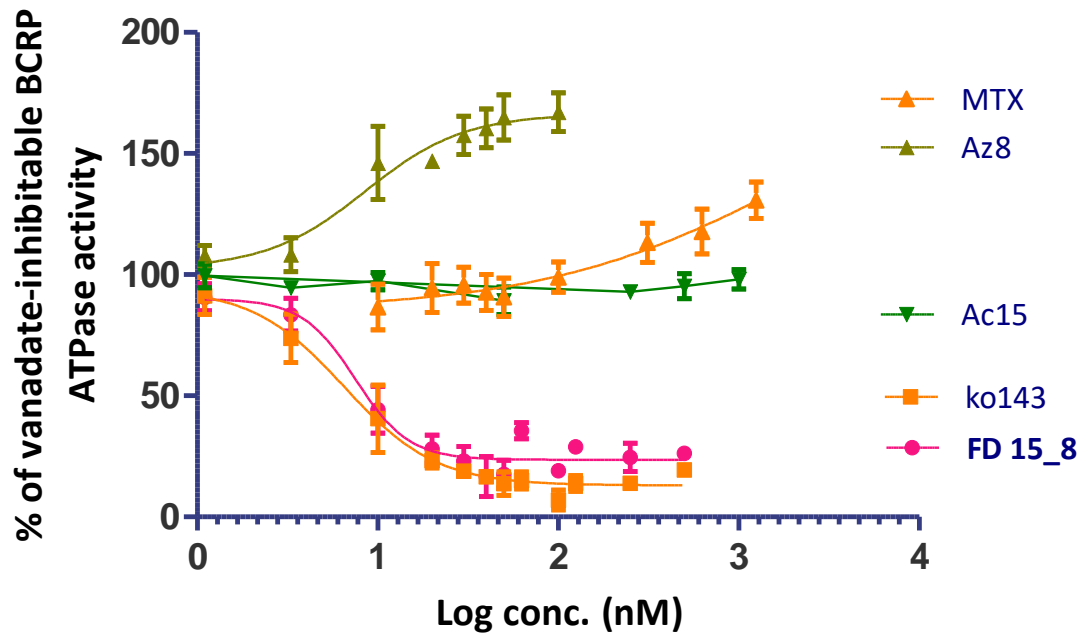


Figure 4.8. Effect of FD 15_8 on vanadate-inhibitable BCRP ATPase activity.

S1M180 cells were collected and lysed by sonication. The lysate was first centrifuged to remove cell debris followed by ultracentrifugation to obtain the membrane fraction. The membrane fraction was reconstituted in assay buffer to form microsome fraction. Assay contained ouabain (Na^+/K^+ -ATPase inhibitor) and sodium azide to inhibit non-ABC transporter ATPase activities. Compounds to be tested including mitoxantrone, ko143, **FD 15_8**, Az8 and Ac15, were added to the microsome and preincubated at 37°C for 30 minutes. ATP was added and incubated for 1 hour. After reaction was stopped, phosphate level was determined using colorimetry method ($n=3-4$). The data were shown as mean \pm SEM.

4.9 Evaluation of FD 15_8 binding to nucleotide binding site through docking

Molecular docking was performed to predict the binding site of **FD 15_8**. BCRP cryo-EM structure (Taylor et al., 2017b) (PDB ID:5nj3) was used as the receptor. As water molecules are less likely to be involved in the hydrophobic drug binding, they are removed to reduce the interference and make it easier to determine the drug-protein binding. Hydrogen atoms were added to protein to compute Gasteiger charges for AutoDock calculating drug-protein interaction. Three dimensional structures of ko143, **FD 15_8** and ATP were generated by ChemDraw Ultra 12.0. Pdbqt files were generated by AutoDock Tools (Morris et al., 2009) version 1.5.6. Autodock vina version 1.1.2 (Trott and Olson, 2010) was used for docking.

ko143, **FD 15_8** and ATP was docked to nucleotide binding site of 5nj3 (**Figure 4.9**). The xyz dimensions were 21.84 x 25.88 x 23.53Å³ and the grid box parameters were x center: 117.628, y center: 114.075 and z center: 169.667and spacing 1Å. The exhaustiveness was 15.

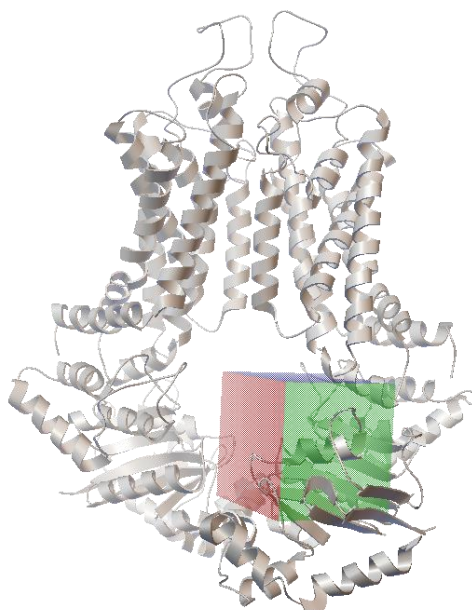


Figure 4.9. BCRP cryo-EM structure with grid box at the nucleotide binding domain.
The BCRP cryo-EM structure and a grid box was demonstrated. The location of grid box was enclosing nucleotide binding domain.

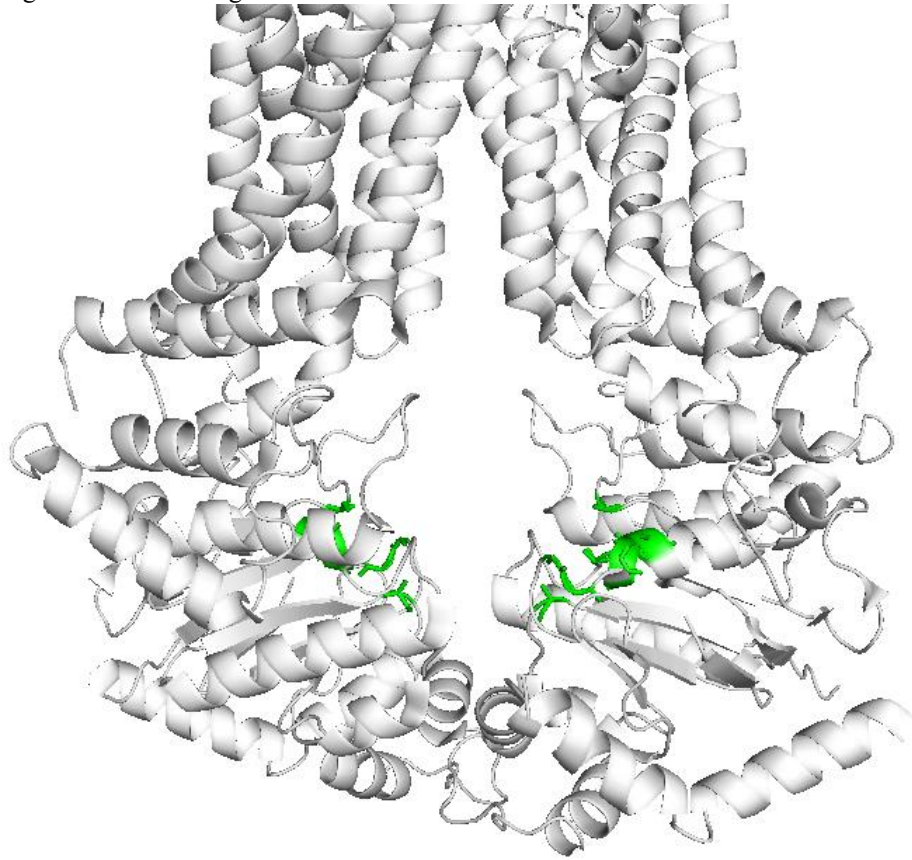


Figure 4.10. BCRP cryo-EM structure and walker A and walker B highlighted green.
The walker A and walker B of BCRP were highlighted green. They were within the grid box for docking.

The binding energy for ko143, **FD 15_8** and ATP were -7.3 kcal, -7.2 kcal and -6.4 kcal respectively. This might suggest that ko143 and **FD 15_8** had a higher affinity to nucleotide binding site than that of ATP. Based on these data, it was hypothesized that **FD 15_8** could compete with ATP for the nucleotide binding site and inhibited ATPase activity.

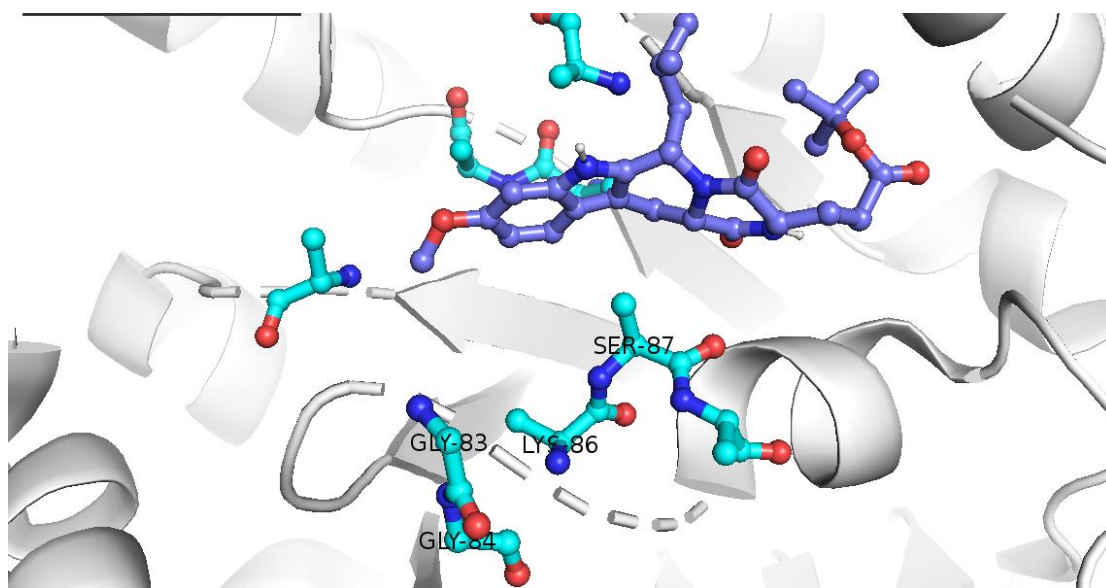


Figure 4.11. Ko143 docked to nucleotide binding domain of BCRP model.
The binding energy of ko143 was -7.3 kcal/mol. The deep blue color was the ko143.

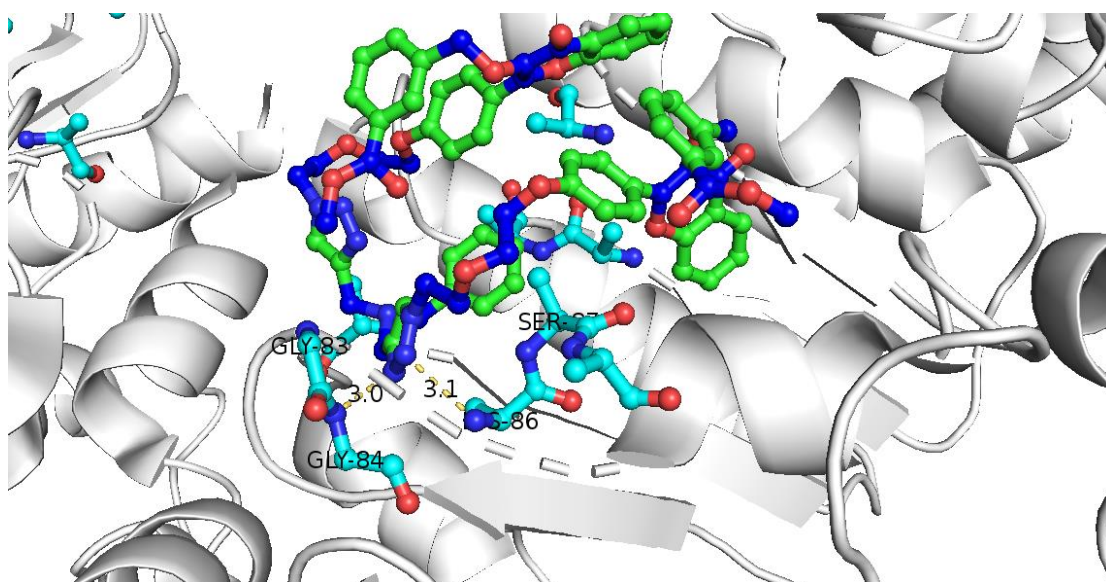


Figure 4.12. FD 15_8 docked to nucleotide binding domain of BCRP model.
The binding energy of **FD 15_8** was -7.2 kcal/mol. The green color was the structure of **FD 15_8**. The yellow dots were the possible polar contacts with Gly-84, Lys-86 of 3.0 Å and 3.1 Å respectively.

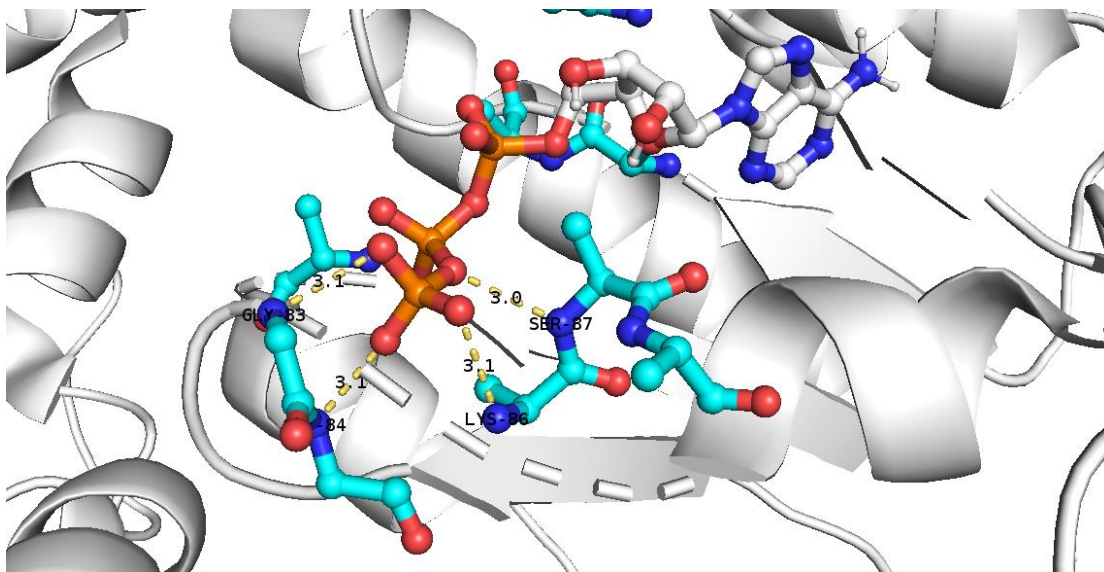


Figure 4.13. ATP docked to nucleotide binding domain of BCRP model.

The binding energy for ATP was -6.4 kcal/mol. The orange and grey color was the ATP. The yellow dots were the possible polar contacts with Gly-83, Gly-84, Lys-86 and Ser-87 of 3.0, 3.0, 3.0 and 3.1 Å respectively.

4.10 Summary

This chapter studied the mechanism by which **FD15_8** inhibits BCRP. **FD 15_8** may reverse BCRP by inhibiting its ATPase activity, thereby inhibiting substrates efflux, resulting in an increase in intracellular level of topotecan and doxorubicin. **FD 15_8** did not change BCRP protein level, nor does it change the intracellular localization of BCRP. The Lineweaver-Burk plot in **Figure 4.5** showed that **FD 15_8** was a non-competitive inhibitor to BCRP with doxorubicin. The Dixon plot in **Figure 4.6** showed that **FD 15_8** was in a mixed type mode of inhibition. The **FD 15_8** efflux assay in **Figure 4.1** showed that **FD 15_8** did not act as a BCRP substrate. **FD 15_8** was more likely to bind to the nucleotide binding site of the BCRP than the substrate binding site. While its monomer Az8 stimulated ATPase activity, suggesting that Az8 has a different binding site to BCRP when compared to **FD 15_8**. Az8 was able to reverse topotecan resistance in S1M180 with EC_{50} of 283.6 ± 20.0 nM (**Table 5**). Therefore, although **FD 15_8** and Az8 shared the similar structure, dimerization resulted in a different mechanism of inhibition of BCRP.

5. PHARMACOKINETIC STUDIES AND TOXICITY STUDIES OF FD 15_8

5.1 Introduction

The pharmacokinetic study of **FD 15_8** was investigated prior to the efficacy experiment. The purpose was to understand if **FD 15_8** is bioavailable in rodents, such as rat and mice. The routes of administration used result in different level of bioavailability. Plasma concentration and half-life of **FD 15_8** could provide a hint for designing dosage regimen in subsequent efficacy experiment. In addition, pharmacokinetic study could reveal potential drug-drug interaction between **FD 15_8** and topotecan.

Toxicity study was also performed to investigate if **FD 15_8** with topotecan was toxic to mice.

5.2 Pharmacokinetic study of FD 15_8

Pharmacokinetic study of **FD 15_8** was performed in both rats and mice. **FD 15_8** was administered to rats via intraperitoneal, intravenous and oral route. Plasma concentration of **FD 15_8** was shown in **Figure 5.1** and detailed pharmacokinetic parameters are shown in **Table 7**.

Figure 5.1 showed that intraperitoneal administration of **FD 15_8** yielded a C_{max} of 805 ng/ml. It took 8 hours to reach the C_{max} , the absorption was slow. The elimination phase half-life was 254 minutes. Administration of **FD 15_8** through intraperitoneal route allowed plasma level of topotecan to stay above its EC_{50} 70.4 ± 17.1 nM for 13 hours. Intraperitoneal administration allowed **FD 15_8** to be supplied to blood continuously and slowly, which was similar to infusion, resulting in a long-lasting plasma concentration of **FD 15_8**. The bioavailability of **FD 15_8** through intraperitoneal administration was 40.5% and the area under curve (0-infinity) normalized to administration dose was 25118 ng-min/ml.

Intravenous administration of **FD 15_8** resulted elimination half-life of 94 minutes, which was shorter than that of intraperitoneal administration. The area under curve (0-infinity) normalized to administration dose was 61969 ng-min/ml. It was 2.4-fold higher than that of intraperitoneal administration. The time for **FD 15_8** above its EC_{50} was less than 6 hours through intravenous administration, which was much shorter than by intraperitoneal administration.

Oral administration of **FD 15_8** resulted in less than 10 ng/ml plasma concentration. **FD 15_8** may not be able to get through the gastrointestinal tract, or it was eliminated during first-pass metabolism. Carboxylesterases are found in the liver. Carboxylesterases could metabolize ester groups of drugs. The structure of **FD 15_8** contains ester groups which could be hydrolyzed by carboxylesterases. **FD 15_8** could

be metabolized as soon as it underwent first pass metabolism. This might explain the low bioavailability of **FD 15_8** when it was orally administrated.

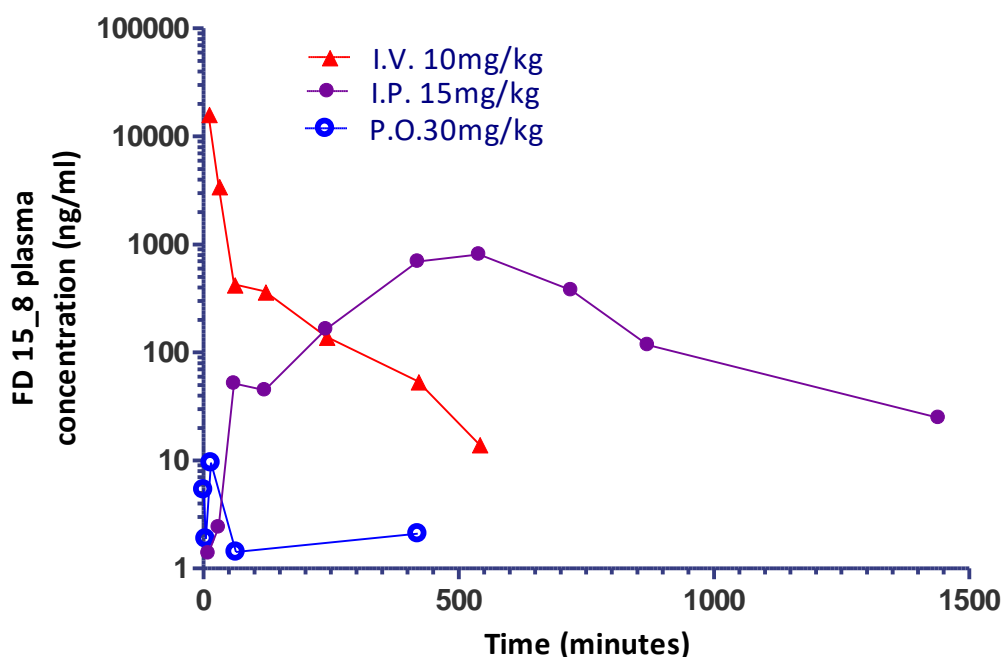


Figure 5.1. Pharmacokinetics of FD 15_8 in rat.

Rats received jugular vein cannulation prior to **FD 15_8** administration. **FD 15_8** was administrated to rats through oral (30mg/kg), intraperitoneal (15mg/kg) or intravenous (10mg/kg) route. Blood was drawn from cannula at the indicated time points and **FD 15_8** plasma concentrations were determined by LC-MSMS after extraction.

Table 7. Pharmacokinetic parameters of FD 15_8 in rats.

Parameters			
Dose of FD 15_8 (mg/kg)	10	15	30
Route of administration	IV	IP	P.O.
C_{max} (ng/ml)	16141	805	9.5
T_{max} (min)	-	540	15
$AUC_{(0-inf)}$ (ng-min/ml)	619691	376765	-
$AUC_{(0-inf)}/Dose$	61969	25118	-
Half-life(E-phase) (min)	94	254	-
$V_d(area)$ (ml)	2189	14643	-
$CL(area)$ (ml/min)	16	39	-
Bioavailability	-	40.5%	-

Detailed pharmacokinetic parameters of **FD 15_8** in rats. Data was from **Figure 5.1**. PK solutions was used to calculate the pharmacokinetic data.

Pharmacokinetic study was also studied in mice. **Figure 5.2** showed that intraperitoneal administration of **FD 15_8** with a C_{max} of 15718 ng/ml and T_{max} at 180 minutes. The elimination phase half-life was 637 minutes. The time of **FD 15_8** above its EC_{50} was more than 24 hours. The bioavailability of **FD 15_8** through intraperitoneal administration was 829% and the area under curve (0-infinity) normalized to administration dose was 111383 ng-min/ml.

Intravenous administration of **FD 15_8** resulted elimination half-life of 114 minutes. It was shorter than that of intraperitoneal administration. The area under curve (0-infinity) normalized to administration dose was 13433 ng-min/ml. The time for **FD 15_8** above its EC_{50} was 193 minutes by intravenous administration, which was far shorter than that of intraperitoneal administration.

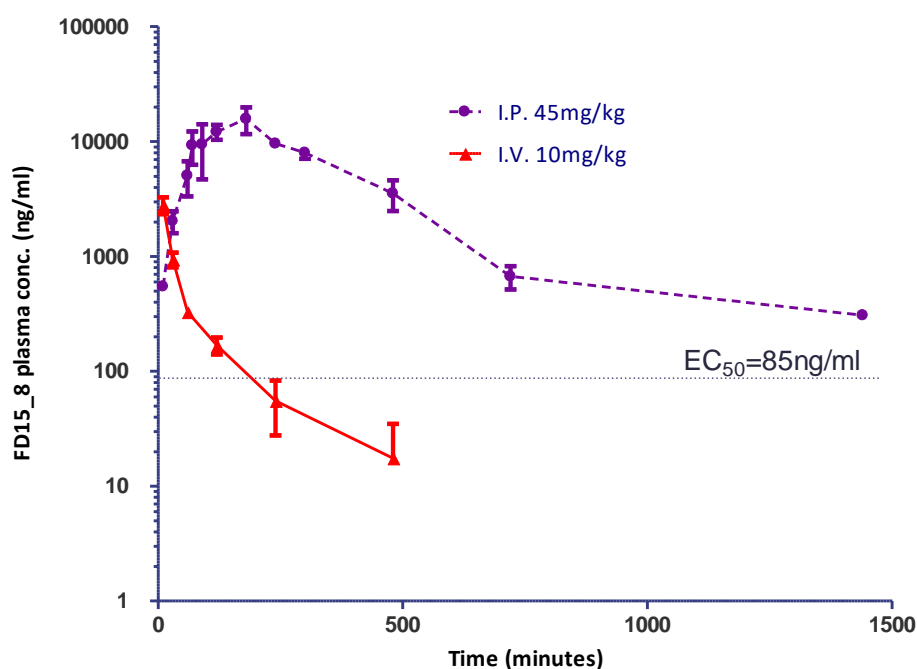


Figure 5.2. Pharmacokinetic study of FD 15_8 at mice.

FD 15_8 was administrated to mice through intraperitoneal administration (45mg/kg) or intravenously injection (10mg/kg) (three animals each group). Plasma extraction and quantification of **FD 15_8** was performed as in **Figure 5.1**.

Table 8. Pharmacokinetic parameters of FD 15_8 in mice.

Parameters		
Dose of FD 15_8 (mg/kg)	10	45
Route of administration	IV	IP
C _{max} (ng/ml)	2800	15718
T _{max} (min)	-	180
AUC _(0-inf) (ng-min/ml)	134332	5012270
AUC _(0-inf) /Dose	13433	111383
Half-life(E-phase) (min)	114	637
V _d (area) (ml)	12234	8258
CL(area) (ml/min)	74	9
Bioavailability	-	829%

Detailed pharmacokinetic parameters of **FD 15_8** in mice. Data was from **Figure 5.2**. PK solutions was used to calculate the pharmacokinetic data.

5.3 Pharmacokinetic study of topotecan

Topotecan pharmacokinetic study was performed in mice. Mice were administrated with topotecan with or without co-administration of **FD 15_8** (**Figure 5.3**). The aim was to find out whether **FD 15_8** affected topotecan pharmacokinetics.

Solvent control group and **FD 15_8** treatment group resulted in similar trend of topotecan distribution in plasma. The T_{max} of both groups were at 60th minute. At 2mg/kg of topotecan administration, **FD 15_8** increase the AUC by one-fold when compared to solvent control. It was implied that **FD 15_8** had a small but significant effect on topotecan pharmacokinetics by prolonging the residence time of topotecan in the plasma.

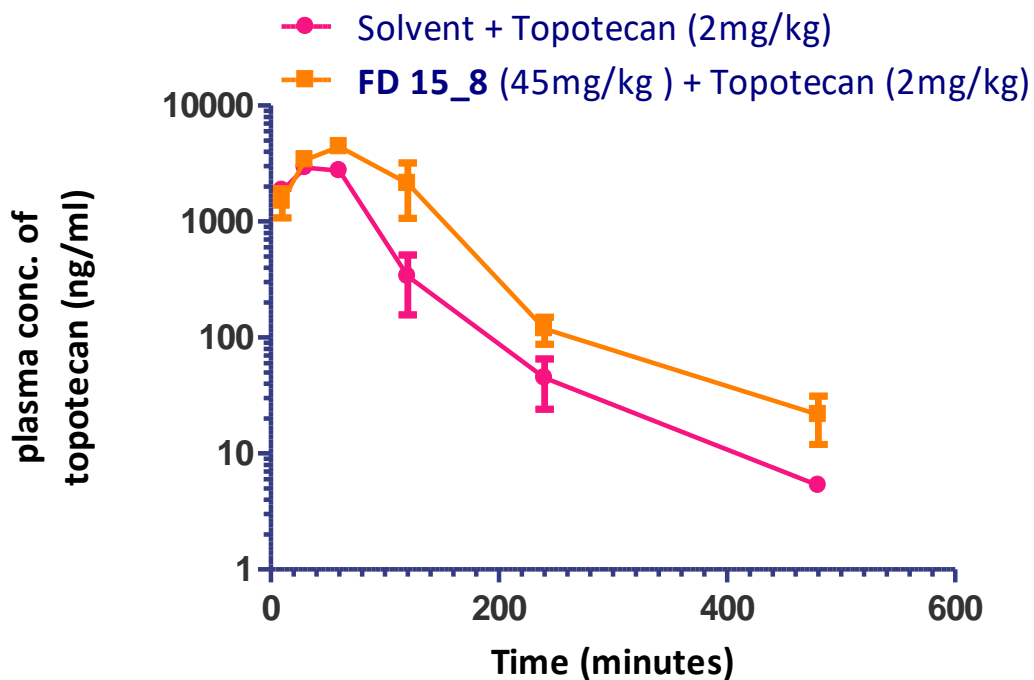


Figure 5.3. Effect of FD 15_8 on pharmacokinetics of topotecan in mice.

Mice were administrated with 2mg/kg topotecan with or without 45mg/kg **FD 15_8**. **FD 15_8** or solvent was administrated 1 hour prior to topotecan injection. Both **FD 15_8** and topotecan were administrated through intraperitoneal administration. Solvent used was were 10% NMP, 10%, Cremophor-EL and 80% water. Data presented as mean \pm SEM. Each data point consisted of 2-3 mice (n=2-3). Blood was collected at the above timepoints. Plasma concentration of topotecan was analyzed by LC-MSMS after extraction.

Table 9. Effect of FD 15_8 on pharmacokinetic parameters of in mice.

Parameters		
Dose of topotecan (mg/kg)	2	2
Dose of FD 15_8 (mg/kg)	-	45
Route of administration	IP	IP
C_{max}, ng/ml	2907	4413
t_{max}, min	30	60
AUC(0-inf), ng-min/ml	263178	524973
AUC(0-inf)/Dose	131589	262487
Half-life, min	78	98
Vd(area), ml	856	536
CL(area), ml/min	8	4

Detailed pharmacokinetic parameters of topotecan in mice. Data was from **Figure 5.3**.

PK solutions was used to calculate the pharmacokinetic data

5.4 Toxicity studies for FD 15_8 and topotecan in combination

Toxicity studies of combination treatment of **FD 15_8** and topotecan were carried out in BALB/c mice. BALB/c mice were treated with topotecan at 3, 6, 9, 12 or 15 mg/kg combined with 15 or 45 mg/kg **FD 15_8** with topotecan at 15 mg/kg. **FD 15_8** was administered 1 hour prior to topotecan administration. Both were injected intraperitoneally. The mice received treatment every four days. A total of four rounds of treatments were given. Results showed that there was no significant body weight loss in the mice (**Figure 5.4**). The greatest weight loss was 2.7% in the group receiving 45mg/kg **FD 15_8** and 15mg/kg topotecan after the first round of treatment. Generally, there were slight weight losses after each round of treatment. However, mice recovered during the resting period of 4 days. Two days after the last round of treatments, the mice regained their weights to equal to or higher than the original weights before treatments. **FD 15_8** combined with topotecan was safe in BALB/c mice. Furthermore, increasing **FD 15_8** from 15 mg/kg to 45 mg/kg in combination with 15mg/kg topotecan did not result in further weight loss. Seven days after the end of all treatments, no incidence of mice death was observed. It was suggested that **FD 15_8** was safe to the mice at the above dose. These drugs combinations at different dosages provided references for dosing in subsequent *in vivo* efficacy experiment.

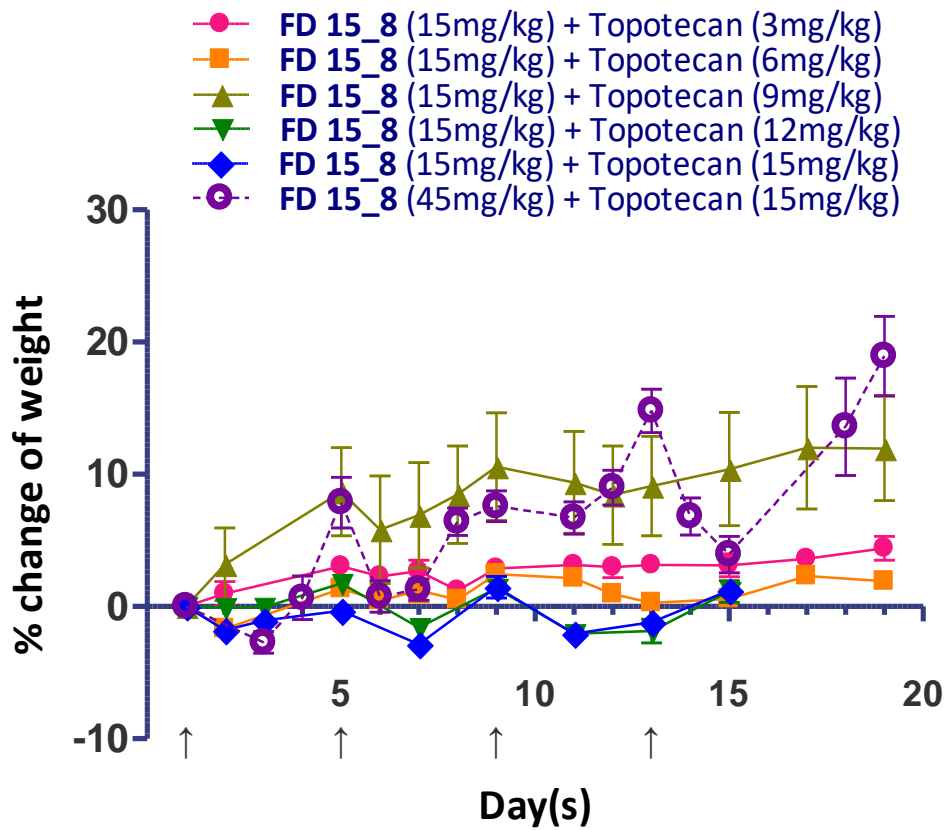


Figure 5.4. Body weight change of BALB/c mice after receiving FD 15_8 and or topotecan.

BALB/c mice received 15mg/kg FD 15_8 and various dosages (3, 6, 9, 12 and 15mg/kg) of topotecan treatment (each group with 5 animals). Another group of mice received 45mg/kg FD 15_8 with 15mg/kg topotecan. FD 15_8 was intraperitoneally injected 1 hour prior to topotecan intraperitoneal injection. Total 4 rounds of treatments. Each data point was mean \pm SEM. Upward arrow (\uparrow) indicated drug administration day.

6. *IN VIVO* EFFICACY OF FD 15_8 IN REVERSING BCRP-MEDIATED DRUG RESISTANCE

6.1 Introduction

Efficacy of **FD 15_8** in reversing BCRP-mediated topotecan resistance was tested on an BCRP-overexpressing xenograft model in BALB/c nude mice. Mice received treatments of topotecan with or without **FD 15_8**.

6.2 *In vivo* efficacy of FD 15_8 in modulating BCRP-mediated drug resistance

FD 15_8 was administrated at 45mg/kg intraperitoneally one hour before topotecan at 2mg/kg intraperitoneally. According to the results from a separate *in vitro* experiment, preincubating **FD 15_8** one hour before adding topotecan resulted in a higher intracellular level of topotecan in accumulation assay. Therefore this dosing sequence was adopted. Treatments were administrated once every two days.

S1 xenograft was found to be sensitive to topotecan treatment as shown in **Figure 6.1 (A)**. After 4 times of topotecan administration, S1 tumor volume was significantly smaller than the group receiving solvent. Mice receiving topotecan alone or combination treatment were sacrificed on day 11 because of serious weight loss (**Figure 6.2 (A)**).

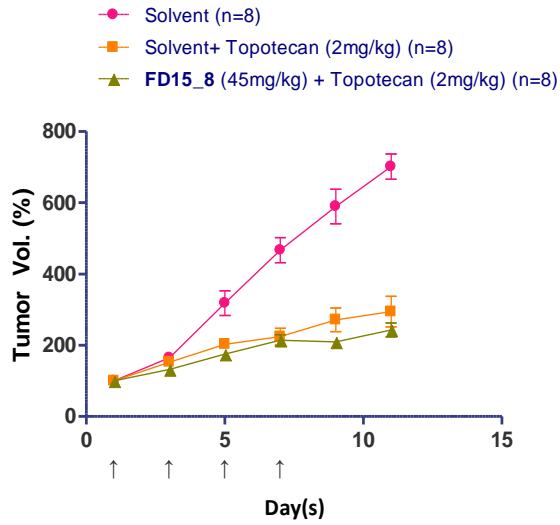
On the contrary, S1M180 xenograft was more resistant to topotecan treatment as shown in **Figure 6.1 (B)**. Topotecan alone at 2mg/kg could slow down tumor growth of S1M180 compared to solvent control. However, combination treatment of **FD 15_8** and topotecan significantly reduced tumor growth ($p < 0.0001$), resulting in a 40.3% growth inhibition when compared to topotecan alone. The combination of **FD 15_8** and

topotecan also reduced the tumor doubling time from 9.5 ± 0.5 days (solvent control group) and 12.3 ± 0.7 days (topotecan group) to 14.1 ± 0.6 days (**Table 10**). Excised tumor weight of combination group was also significantly reduced compared with topotecan alone (**Figure 6.3**). These results suggest that **FD 15_8** potentiated the anti-tumor effect of topotecan. This was only observed in the BCRP-overexpressing S1M180 xenograft but not in the S1 xenograft. It was likely that **FD 15_8** can reverse the topotecan resistance by modulating the efflux action of BCRP in S1M180 xenograft. **FD 15_8** was tested for its effect on S1M180 xenograft. Intraperitoneally administration of 45mg/kg **FD 15_8** did not inhibit tumor growth (**Figure 6.4**) and it did not cause weight loss of S1M180-bearing mice.

S1 xenograft grew faster than S1M180. Tumour volume in control group S1 has already reached 600mm^3 while that of S1M180 was only 400mm^3 . This might explain why S1-bearing mice have a more severe body weight loss.

In addition, 15mg/kg topotecan with 15mg/kg **FD 15_8** was found to be toxic to the BALB/c nude mice. One out of two animals was dead and both of them had weight loss over 20% (**Figure 6.5**). This result was different from toxicity data found in BALB/c mice, which did not result in any no animal death and significant weight loss.

A)



B)

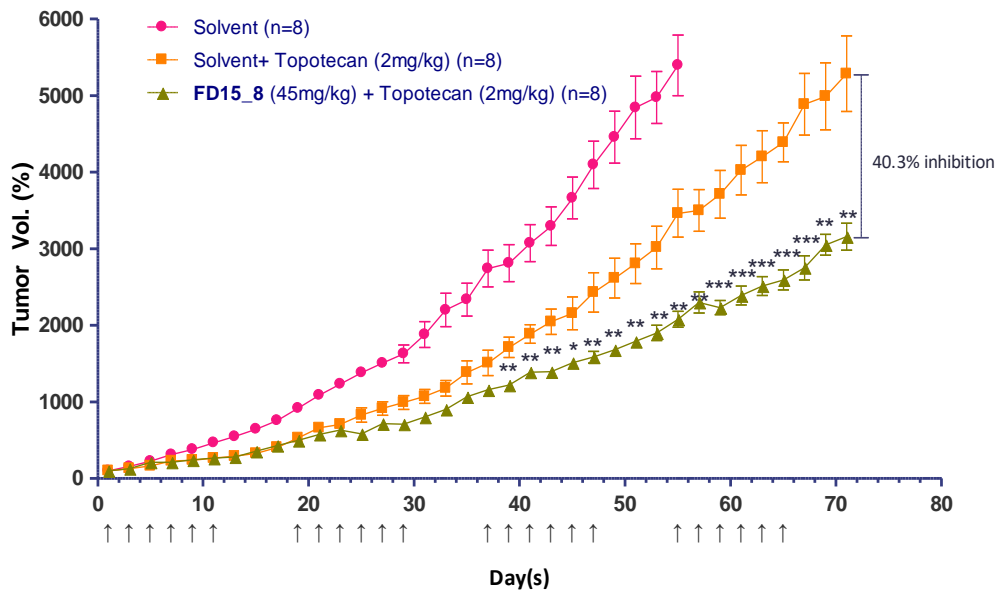


Figure 6.1. Effect of topotecan with or without FD 15_8 on S1 and S1M180 xenograft.

S1 or S1M180 were inoculated into BALB/c nude mice subcutaneously. S1 (n=8 animals) (A) and S1M180 (n=7 animals) (B) tumor bearing mice were treated with solvent control, 2mg/kg topotecan, combination of 45mg/kg **FD 15_8** and 2mg/kg topotecan. In additions, S1M180 bearing mice received 45mg/kg **FD 15_8**. Treatments were made as indicated on the x-axis. S1 bearing mice only received 4 times of treatment because of serious weight loss. S1M180 bearing mice received 24 treatments except that solvent group received 18 treatments as the tumor burden is too large and they were sacrificed on day 55. Student's t-test was used to compare combination group (**FD 15_8** + topotecan) and topotecan alone. * for $p \leq 0.05$, ** for $p \leq 0.01$, *** for $p \leq 0.001$.

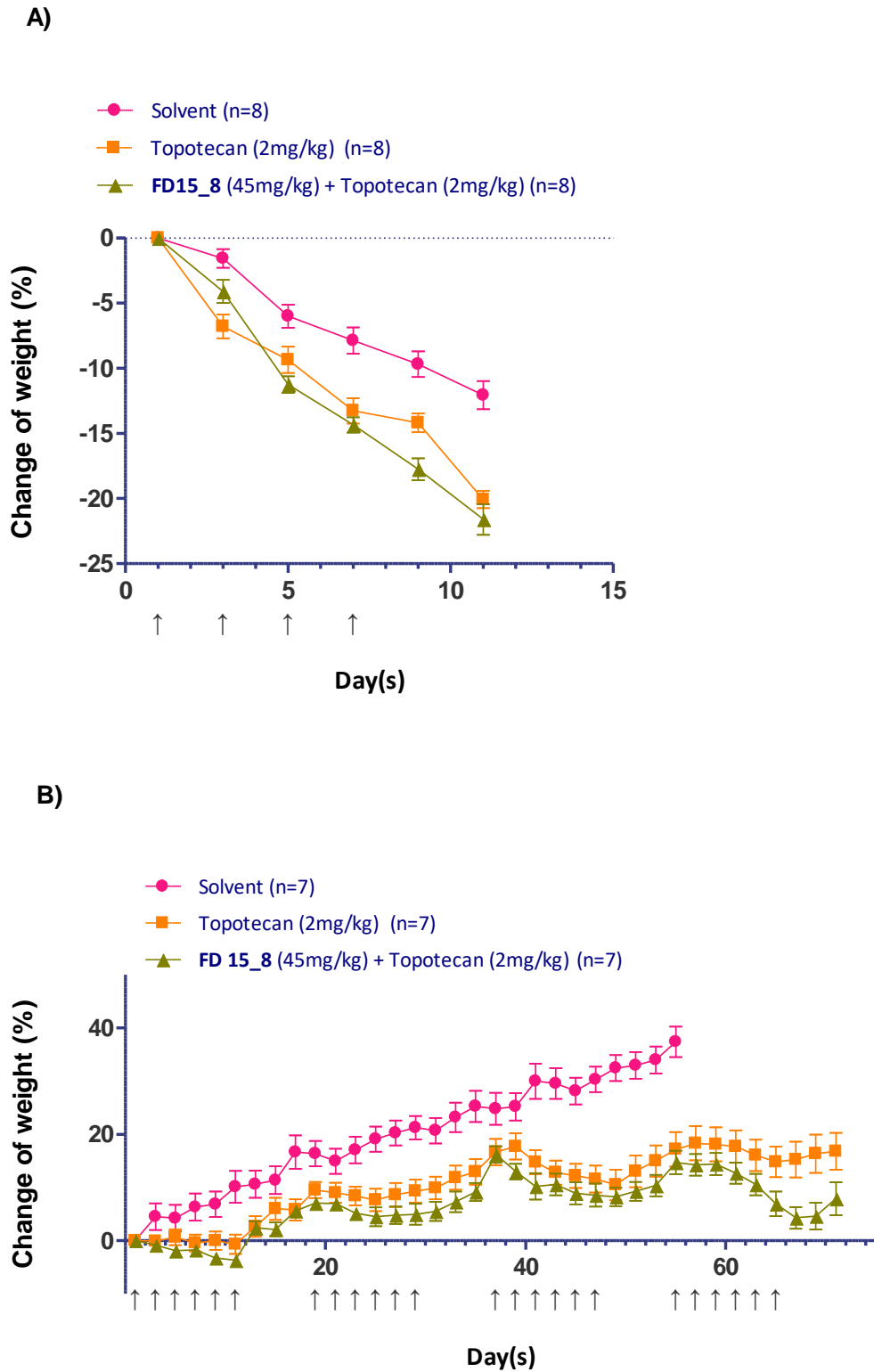


Figure 6.2. Effect of topotecan with or without FD 15_8 on the body weight of S1 or S1M180-bearing BALB/c nude mice.
 A) S1 (n=8) or B) S1M180 (n=7) xenograft were treated with solvent, topotecan or topotecan with **FD 15_8**. Their body weight was monitored and plotted. Upward arrow (↑) indicated drug administration day.

Table 10. Effect of topotecan with or without FD 15_8 on tumor volume and tumor doubling time of BCRP-overexpressing S1M180 xenograft

Excised S1M180 tumor	Treatment	Ave. % change to tumor volume	Ave. tumor doubling time (days)
	FD 15_8 solvent+ Topotecan solvent	Day 55: 5397±1049	9.5±0.5
	FD 15_8 solvent+ Topotecan (2mg/kg)	Day 55: 3464±825 Day 71: 5287±1303	12.3±0.7
	FD 15_8 (45mg/kg) + Topotecan (2mg/kg)	Day 55: 2080±273 Day 71: 3157±464	14.1±0.6

S1M180 xenograft were treated with FD 15_8 solvent+ topotecan solvent, FD 15_8 solvent+ Topotecan (2mg/kg) or **FD 15_8** (45mg/kg) + Topotecan (2mg/kg). At the end of experiment as indicated (either day 55 or 71), tumors were excised and their volume measured. Percentage change of tumor volume and tumor doubling time are shown.

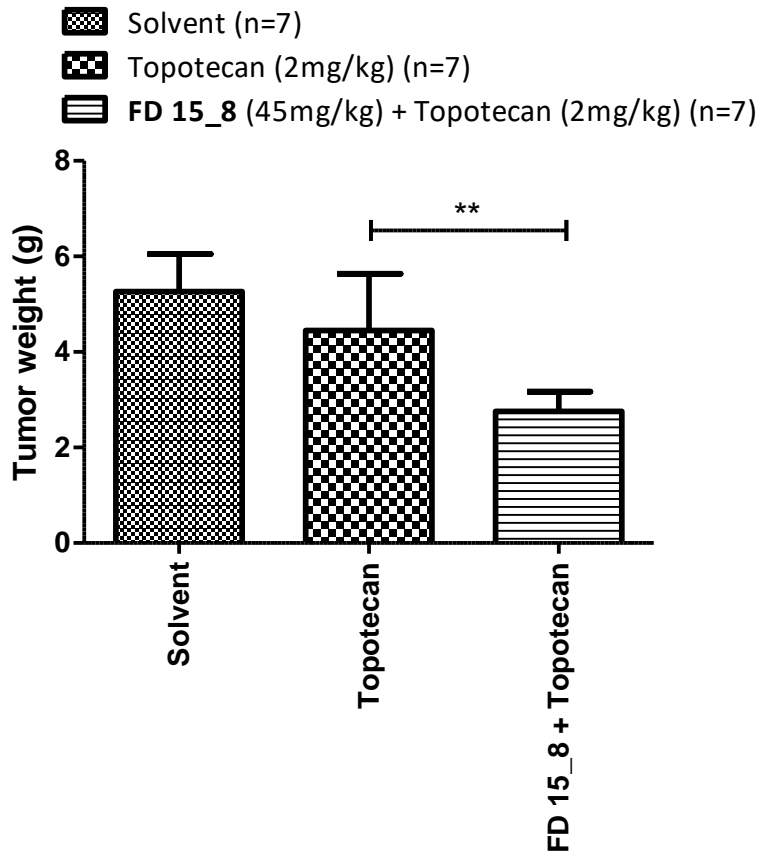


Figure 6.3. Effect of topotecan with or without FD 15_8 on tumor weight of S1M180 xenograft.

S1M180 xenograft was treated with FD 15_8 solvent + topotecan solvent, FD 15_8 solvent + topotecan (2mg/kg) or **FD15_8** (45mg/kg) + topotecan (2mg/kg). At the end of experiment, tumor was excised and the tumor weight was measured. Tumor of solvent group were excised on day 55, topotecan and FD 15_8 and topotecan combination group were from day 71. Student's t-test was used to compare topotecan with **FD15_8** plus topotecan (* for $p \leq 0.05$, ** for $p \leq 0.01$, *** for $p \leq 0.001$).

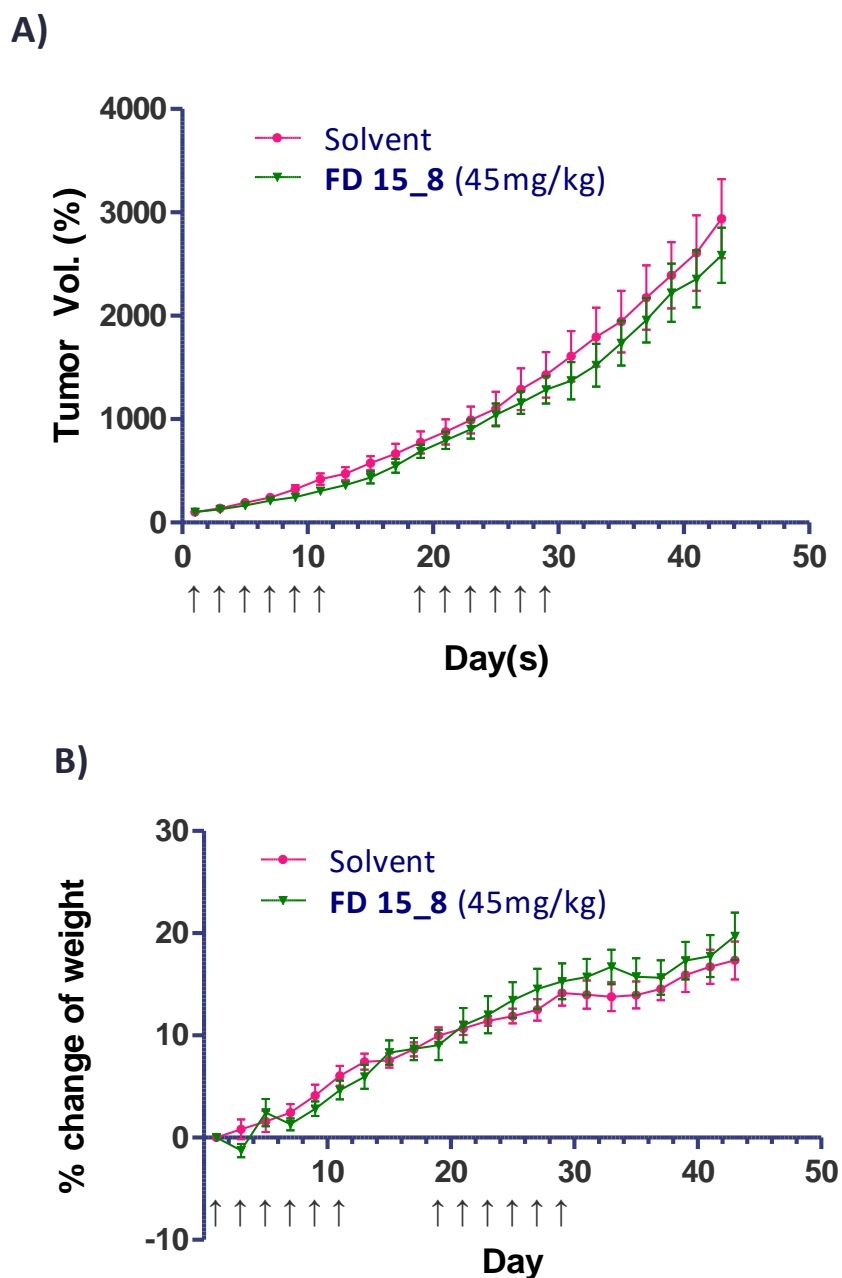


Figure 6.4. Effect of FD 15_8 on tumor volume of S1M180 xenograft and its body weight. Nude mice bearing S1M180 xenograft were treated with solvent (10 animals) or **FD 15_8** (9 animals). Tumor volume was shown in (A) and body weight change was shown in (B). Solvent or **FD 15_8** were administrated intraperitoneally, once every two days for 6 times. Treatment was stopped for 7 days. A second cycle was repeated with a total treatment of 12 times. Each point represented mean \pm SEM.

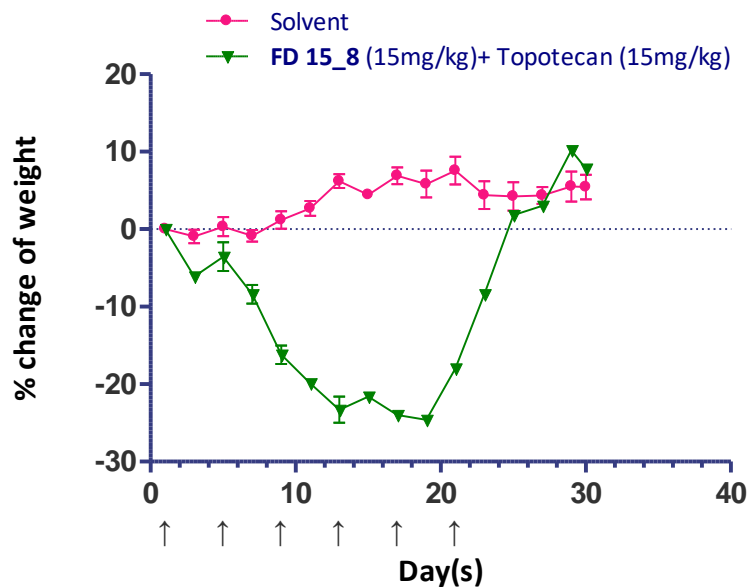


Figure 6.5. Effect of 15mg/kg topotecan on body weight of S1M180 bearing BALB/c nude mice. BALB/c nude mice bearing S1M180 received intraperitoneal administration solvent (6 animals) or 15mg/kg of **FD 15_8** and 15mg/kg topotecan (2 animals). Treatment was once every four days. Administration was made as indicates in x-axis upward arrow. One mice died on day 15 in the treatment group of **FD 15_8** with topotecan. The data points represent mean \pm SEM.

6.3 Effect of FD 15_8 on topotecan accumulation in S1M180 xenograft

As **FD 15_8** can potentiate topotecan in reducing tumor volume of S1M180, it is likely that **FD 15_8** can inhibit BCRP in S1M180 xenograft. Here, the effect of **FD 15_8** on the accumulation of topotecan in S1M180 was investigated. S1M180 tumor bearing mice were injected intraperitoneally with 45mg/kg **FD 15_8**, followed by 6 mg/kg of topotecan one hour later. Mice were sacrificed 5 hours after injection with topotecan. Plasma and tumors were collected. Topotecan levels in plasma and tumor were determined (**Figure 6.6**). The topotecan level in plasma was increased when **FD 15_8** was administrated but the increase was not significant (from 75.7 ± 20.6 ng/ml to 103.2 ± 28.8 ng/ml). On the contrary, **FD 15_8** increased the topotecan level in S1M180 xenograft significantly ($p=0.0036$). The topotecan level in the **FD 15_8**-treated group (145.8 ± 41.5 ng/g tumor) was two-fold higher than that in the solvent-topotecan group (73.2 ± 22.3 ng/g tumor). **FD 15_8** increased the topotecan level in S1M180 xenograft but did not interfere with the plasma topotecan level. **FD 15_8** also accumulated at S1M180 tumor (102.2 ± 71.4 ng/g). This result suggests that **FD 15_8** can accumulate in tumor, inhibit activity of BCRP, increase topotecan level in the tumor and finally inhibiting the growth rate of S1M180 xenograft.

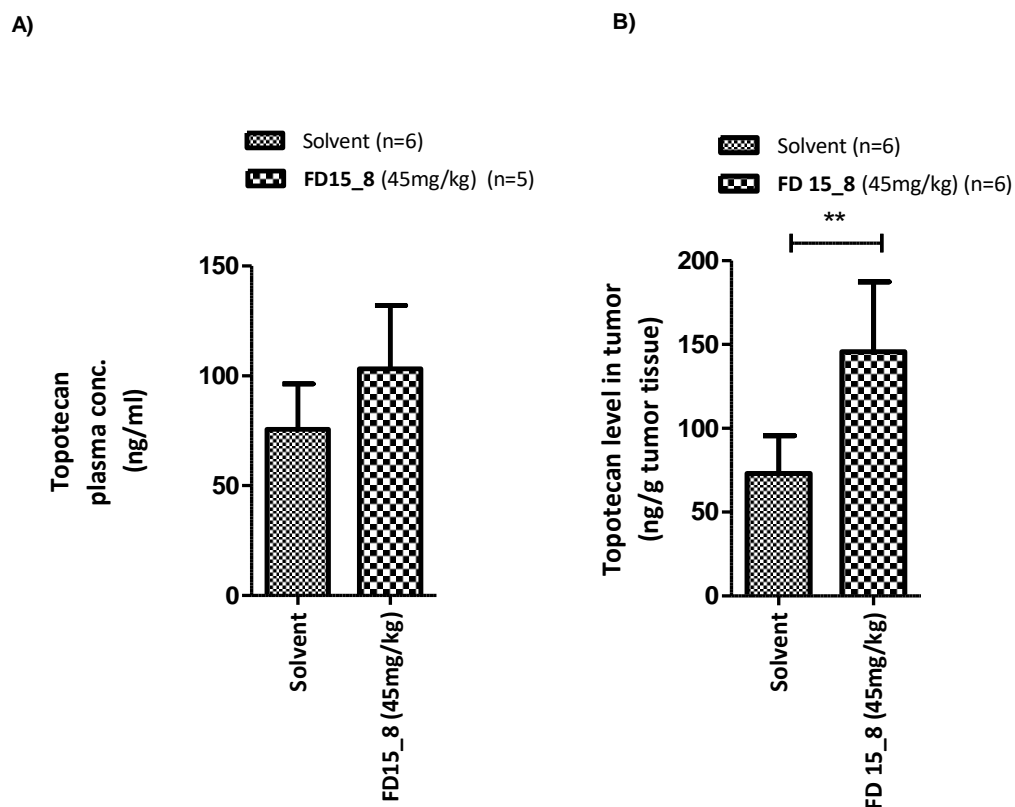


Figure 6.6. Effect of FD 15_8 on the accumulation of topotecan in plasma and S1M180 xenograft. S1M180 tumor bearing mice were administrated with 45mg/kg of FD 15_8 1 hour prior to topotecan (6mg/kg). Both FD 15_8 and topotecan were administrated intraperitoneally. Five hours after topotecan administration, mice were sacrificed and the plasma and tumors were collected and analyzed for topotecan level using LCMSMS. There were no significant differences of plasma level of topotecan between FD 15_8 treatment and the solvent control. There was a significant increase in topotecan level in tumor when the mice were treated with FD 15_8 (N=6). Student's t-test was used (* for $p \leq 0.05$, ** for $p \leq 0.01$, *** for $p \leq 0.001$).

7. GENERAL DISCUSSION

Multidrug resistance in cancer is one of the major obstacles in chemotherapy. Since the first demonstration of a correlation between ABC transporters and MDR, there was a hope that inhibition of ABC transporters can reverse MDR. MDR was first demonstrated to be associated with P-gp, followed by MRP1 and BCRP. A safe and potent BCRP inhibitor is needed for clinical use. However, very few BCRP inhibitors have been developed. Success of developing flavonoid dimers to reverse ABCB1-mediated MDR suggest that flavonoid dimers may also reverse BCRP-mediated MDR. However, to produce a diverse compound library, traditional synthesis methods required many steps and it is time consuming. In order to develop a flavonoid dimer library to screen for BCRP inhibitors, click chemistry approach was used. Click chemistry enables rapid synthesis of diverse combinations of flavonoid dimers, both homodimers and heterodimers. These flavonoid dimers can form a compound library for the screening of potent BCRP inhibitors.

After screening for their inhibitory activities towards P-gp, MRP1 and BCRP, flavonoid dimers were classified into two types: multi-selective inhibitor and mono-specific inhibitor. Multi-selective inhibitors inhibit two or more ABC transporters, while mono-specific inhibitors target only one type of ABC transporter. **FD 15_8** was one of the potent mono-specific inhibitors that solely modulated BCRP with a high potency with $EC_{50} = 1.3 \pm 0.7$ nM in BCRP overexpressing cell line MCF7/MX100 and $EC_{50} = 70.4 \pm 17.1$ nM in S1M180 to reverse topotecan resistance (**Table 5**). **FD 15_8** can fully reverse topotecan and doxorubicin to that of parental cell lines (**Table 4** and **Figure 3.6**). For examples, when S1M180 was treated with 500nM of **FD 15_8**, IC_{50} of topotecan was reduced to as low as 0.2 μ M, which was similar to that of sensitive cell line S1.

The mechanism of **FD 15_8** to reverse BCRP-mediated MDR was studied. **FD 15_8** increased the substrate levels including topotecan and doxorubicin, in BCRP overexpressing cell line (**Figure 4.4**). **FD 15_8** inhibited topotecan and doxorubicin efflux mediated by BCRP. Substrates level was restored to that of parental cell line after treatment with **FD 15_8** (**Figure 4.4** and **Figure 4.7**). To investigate how **FD 15_8** inhibited BCRP, the BCRP expression level was examined after treating the HEK293/BCRP cell line with **FD 15_8**. Incubation of 1 μ M **FD 15_8** did not down-regulate BCRP expression. **FD 15_8** did not trigger degradation of BCRP or inhibit BCRP synthesis (**Figure 4.2**). BCRP expression level was similar when S1M180 was treated with **FD 15_8**. Treatment of **FD 15_8** did not alter the intracellular localization of BCRP. Most BCRP remained at cell membrane and did not internalize (**Figure 4.3**). Furthermore, effect of **FD 15_8** on ATPase activity of BCRP was investigated (**Figure 4.8**). BCRP-ATPase was found to be inhibited by **FD 15_8** resulting in the inhibition of BCRP-mediated drug efflux. From the Lineweaver-Burk plot (**Figure 4.5**) and the Dixon plot (**Figure 4.6**), **FD 15_8** was suggested to be a non-competitive inhibitor of doxorubicin for BCRP or it was a mixed type of inhibition mode. Together with the observation that **FD 15_8** inhibits ATPase of BCRP, it was suggested that **FD 15_8** may bind to the nucleotide binding site instead of the substrate binding site of BCRP. **FD 15_8** might not compete with doxorubicin to bind to the substrate binding site of BCRP. These results support the notion that **FD 15_8** is a non-competitive inhibitor towards BCRP. Furthermore, by computer simulation, **FD 15_8** has a higher affinity (-7.2kcal, **Figure 4.12**) to the nucleotide binding domain of BCRP than ATP (-6.4 kcal, **Figure 4.13**), which might suggest that **FD 15_8** inhibited ATPase activity by competing with ATP for the nucleotide binding sites.

It was previously observed that dimerizing flavonoids enhanced the potency in

reversing P-gp-mediated MDR (Chan et al., 2006). In this thesis, it was found that **FD 15_8** (**Figure 1.7**), a dimer of Az8 (**Figure 1.6**), was 4-fold more potent (**Table 5**). However, the mechanisms of Az8 and **FD 15_8** to reverse BCRP-mediated resistance was different. While Az8 monomer stimulated ATPase activity of BCRP, **FD 15_8** inhibited it. Dimerization of flavonoid monomers could change the binding sites of the compounds.

From the pharmacokinetics study, it was shown that **FD 15_8** has a low oral bioavailability (**Figure 5.1**). On the other hand, **FD 15_8** was well absorbed by intraperitoneal administration with a slow release of **FD 15_8**. Intraperitoneal administration of 45mg/kg **FD 15_8** can achieve a plasma concentration above EC_{50} for more than 600 minutes (**Figure 5.2**). The duration could be sufficient for **FD 15_8** to inhibit BCRP in xenograft. **FD 15_8** increased the AUC of plasma topotecan by 1-fold when compared to solvent control. **FD 15_8** could affect the topotecan pharmacokinetics to some extent. The high value of calculated LogP of **FD 15_8** (9.23 ± 1.43) suggests that **FD 15_8** was hydrophobic with low solubility. **FD 15_8** did not dissolve in water. However, the low water solubility could increase the residence time of **FD 15_8** in circulatory system as it was less likely to be excreted. The high hydrophobicity could also be beneficial to a membrane protein modulator. Hydrophobic drugs could access the hydrophobic plasma membrane more readily.

FD 15_8 was found to be safe when co-administrated with topotecan in BALB/c mice. No behavioral changes, severe weight loss (**Figure 6.2**) or animal deaths were observed when mice were treated with **FD 15_8**. Treating mice with **FD 15_8** alone at 45mg/kg did not cause weight loss (**Figure 6.4.B**). Increasing dosage of **FD 15_8** from 15mg/kg to 45mg/kg did not increase toxicity of topotecan (**Figure 5.4**). However, when immunocompromised mice BALB/c nude mice were used, severe weight loss was

observed (**Figure 6.5**), suggesting that the genetic background difference between BALB/c and BALB/c nude mice might cause the different response.

Combination of **FD 15_8** and topotecan slowed down the tumor growth rate when compared to the topotecan alone treatment group (**Table 10**). It was found that **FD 15_8** increased the topotecan level in tumor. It is in agreement with effect of **FD 15_8** on increasing topotecan accumulation in cancer cell *in vitro*. Besides, **FD 15_8** was found in the tumor sample at the level of about 100ng/g tumor (**Figure 6.6**). Therefore, **FD 15_8** could be delivered to tumor through the intraperitoneal administration. This suggested that **FD 15_8** inhibited the efflux of BCRP in xenograft tumor, increased topotecan level and finally decreased the growth rate of tumor.

Other than S1 and S1M180, another pair of cell lines MCF7 and MCF7/MX100 were tried to establish a xenograft model. When they were subcutaneously injected to BALB/c nude mice, there was no tumor formation. Even after implanting mice with estrogen pellet for a week prior to cancer cell injection, and the inclusion of Matrigel during implantation, only a small tumor was formed. Since the growth rate of these tumor was very slow even after two months of growing, they were not used in this thesis.

In conclusion, **FD 15_8** is a safe and potent BCRP modulator. It can enhance the topotecan efficacy to treat BCRP-mediated drug resistant tumor model *in vivo*. The **FD 15_8** did not alter the expression level of BCRP and its localization *in vitro*. **FD 15_8** modulated BCRP by inhibition of the ATPase of the BCRP, thus depleting the energy supply and stopped drugs efflux by BCRP.

8. FURTHER STUDIES

Structure-activity relationships of other flavonoid dimers can be used to study the structural requirement of flavonoid dimers in inhibiting BCRP. By doing so, it could be possible to identify the pharmacophores. This information allows further optimization of the flavonoid dimers. It is possible to generate a series of more potent and specific compounds to reverse BCRP-mediated multidrug resistance. Flavonoid dimers of the series of Az8 and Az9 were relatively potent when compared to other Az series. The ester group of the Az8 and Az9 flavonoid dimers might be the important functional group for inhibiting BCRP. Addition of ester group to other compounds in the Az might further increase their BCRP modulating activities.

9. APPENDIX: SUPPLEMENTARY FIGURES

FIGURES

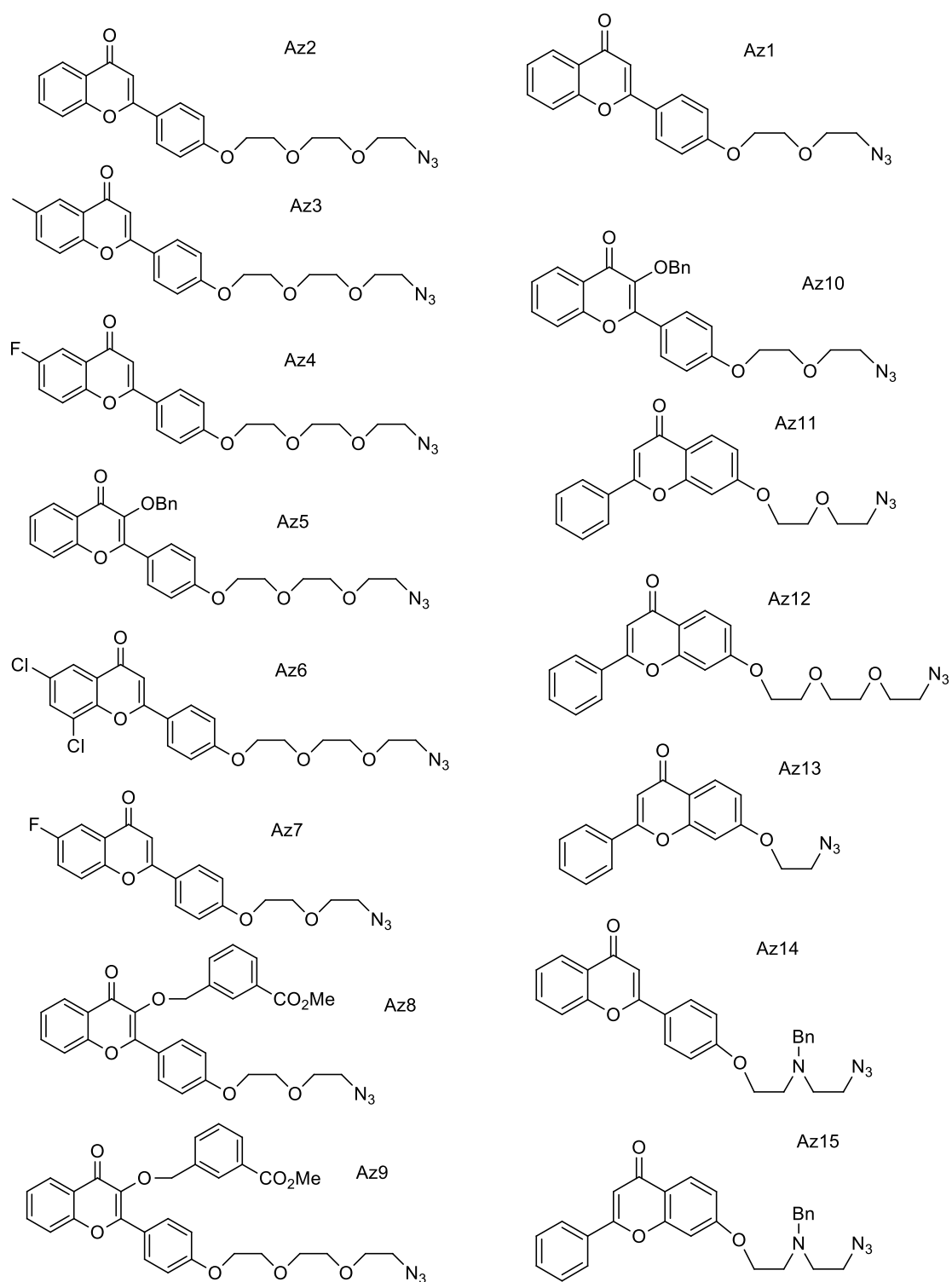


Figure 9.1. Structures of Az monomers.

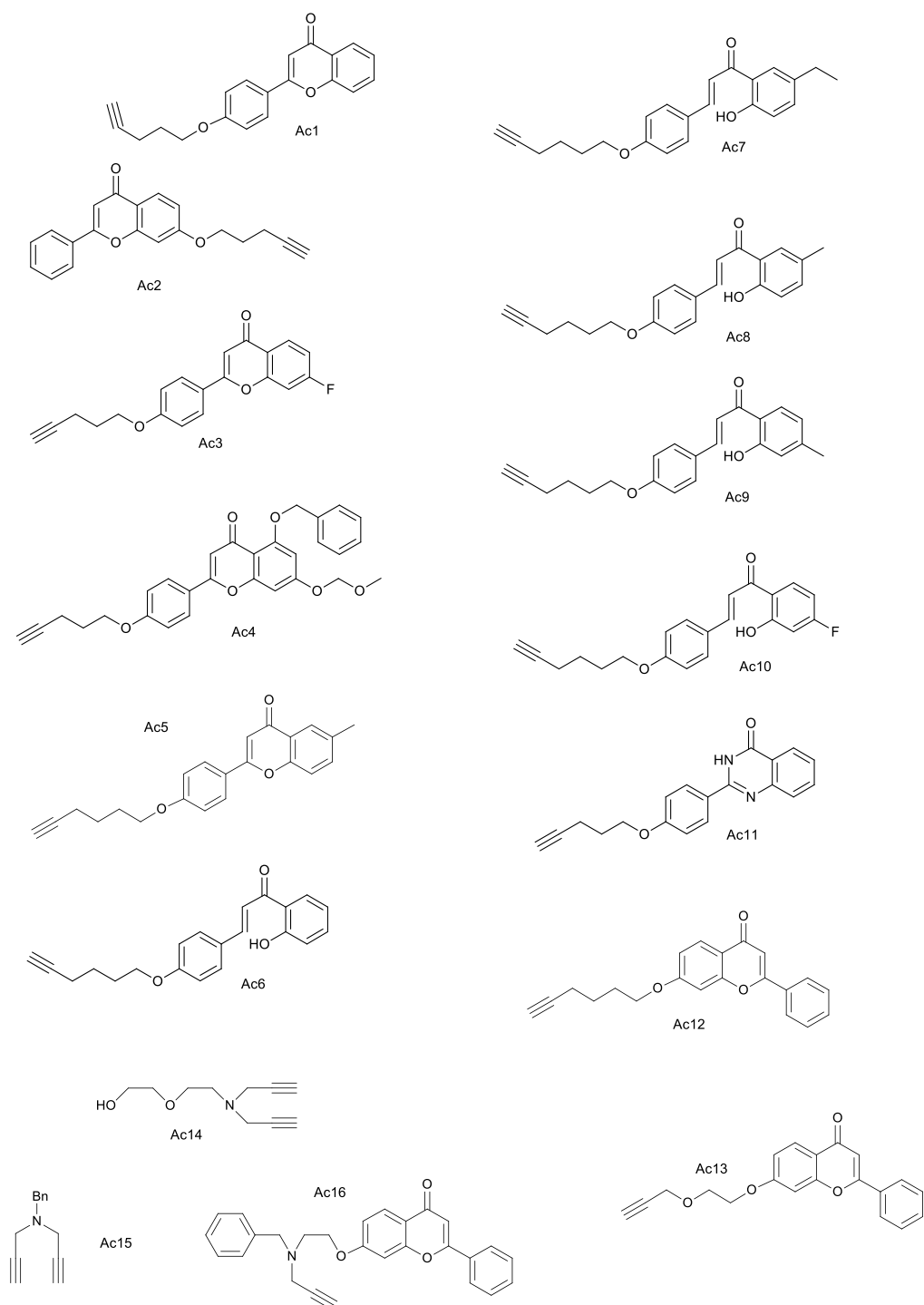
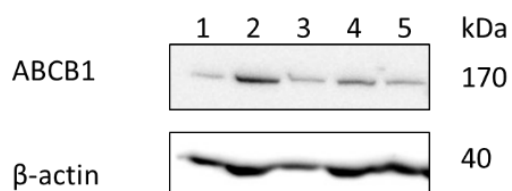


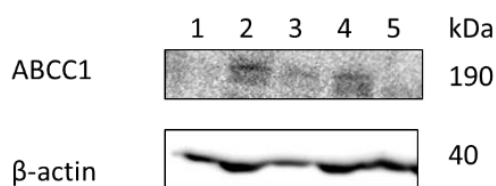
Figure 9.2. Structures of Ac monomers.



Lane
 1:HEK293/pcDNA3.1
 2:S1
 3:HEK293/R2
 4:S1M180
 5:MCF7/MX100

Figure 9.3 ABCB1 expression level in different cell lines.

Ten micrograms protein was loaded in each lane. Lane 1: HEK293/pcDNA3.1, lane 2: S1, lane 3: HEK293/R2, lane 4: S1M180 and lane 5: MCF7/MX100 cell lysates were separated by SDS-PAGE, transferred to PVDF membrane and ABCB1 was detected by Mdr-1 antibody (D-11). Beta-actin acted as loading control and was detected by mouse anti- β -actin antibody C4. ABCB1 is expected to have 170 kDa.



Lane
 1:HEK293/pcDNA3.1
 2:S1
 3:HEK293/R2
 4:S1M180
 5:MCF7/MX100

Figure 9.4 ABCC1 expression level in different cell lines.

Ten micrograms protein was loaded in each lane. Lane 1: HEK293/pcDNA3.1, lane 2: S1, lane 3: HEK293/R2, lane 4: S1M180 and lane 5: MCF7/MX100 cell lysates were separated by SDS-PAGE, transferred to PVDF membrane and ABCC1 was detected by MRP1 antibody(QCRL-1). Beta-actin acted as loading control and was detected by mouse anti- β -actin antibody C4. ABCC1 is expected to have 190 kDa.

10. LIST OF REFERENCES

Alam, C., Whyte-Allman, S.-K., Omeragic, A., And Bendayan, R. (2016). Role And Modulation Of Drug Transporters In HIV-1 Therapy. *Advanced Drug Delivery Reviews* 103, 121-143.

Alizadeh, A.M., Shiri, S., And Farsinejad, S. (2014). Metastasis Review: From Bench To Bedside. *Tumor Biology* 35, 8483-8523.

Basseville, A., Hall, M.D., Chau, C.H., Robey, R.W., Gottesman, M., Figg, W.D., And Bates, S.E. (2016). The ABCG2 Multidrug Transporter. In *ABC Transporters-40 Years On* (Springer), Pp. 195-226.

Blazquez, A.G., Briz, O., Gonzalez-Sanchez, E., Perez, M.J., Ghanem, C.I., And Marin, J.J. (2014). The Effect Of Acetaminophen On The Expression Of BCRP In Trophoblast Cells Impairs The Placental Barrier To Bile Acids During Maternal Cholestasis. *Toxicology And Applied Pharmacology* 277, 77-85.

Cancerresearchuk Worldwide Cancer Statistics| Cancer Research UK.

Chan, K.-F., Zhao, Y., Burkett, B.A., Wong, I.L., Chow, L.M., And Chan, T.H. (2006). Flavonoid Dimers As Bivalent Modulators For P-Glycoprotein-Based Multidrug Resistance: Synthetic Apigenin Homodimers Linked With Defined-Length Poly (Ethylene Glycol) Spacers Increase Drug Retention And Enhance Chemosensitivity In Resistant Cancer Cells. *Journal Of Medicinal Chemistry* 49, 6742-6759.

Chipuk, J.E., Kuwana, T., Bouchier-Hayes, L., Droin, N.M., Newmeyer, D.D., Schuler, M., And Green, D.R. (2004). Direct Activation Of Bax By P53 Mediates Mitochondrial Membrane Permeabilization And Apoptosis. *Science* 303, 1010-1014.

Creemers, G., Bolis, G., Gore, M., Scarfone, G., Lacave, A., Guastalla, J., Despax, R., Favalli, G., Kreinberg, R., And Van Belle, S. (1996). Topotecan, An Active Drug In The Second-Line Treatment Of Epithelial Ovarian Cancer: Results Of A Large European Phase II Study. *Journal Of Clinical Oncology* 14, 3056-3061.

Dai, C.-L., Tiwari, A.K., Wu, C.-P., Su, X.-D., Wang, S.-R., Liu, D.-G., Ashby, C.R., Huang, Y., Robey, R.W., And Liang, Y.-J. (2008). Lapatinib (Tykerb, GW572016) Reverses Multidrug Resistance In Cancer Cells By Inhibiting The Activity Of ATP-Binding Cassette Subfamily B Member 1 And G Member 2. *Cancer Research* 68, 7905-7914.

Dash, R.P., Babu, R.J., And Srinivas, N.R. (2017). Therapeutic Potential And Utility Of Elacridar With Respect To P-Glycoprotein Inhibition: An Insight From The Published In Vitro, Preclinical And Clinical Studies. *European Journal Of Drug Metabolism And Pharmacokinetics*, 1-19.

Dezi, M., Fribourg, P.-F., Di Cicco, A., Arnaud, O., Marco, S., Falson, P., Di Pietro, A., And Lévy, D. (2010). The Multidrug Resistance Half-Transporter ABCG2 Is Purified As A Tetramer Upon Selective Extraction From Membranes. *Biochimica Et Biophysica*

Acta (BBA)-Biomembranes 1798, 2094-2101.

Ding, R., Shi, J., Pabon, K., And Scotto, K.W. (2012). Xanthines Down-Regulate The Drug Transporter ABCG2 And Reverse Multidrug Resistance. *Molecular Pharmacology* 81, 328-337.

Diop, N.K., And Hrycyna, C.A. (2005). N-Linked Glycosylation Of The Human ABC Transporter ABCG2 On Asparagine 596 Is Not Essential For Expression, Transport Activity, Or Trafficking To The Plasma Membrane. *Biochemistry* 44, 5420-5429.

Doyle, L.A., Yang, W., Abruzzo, L.V., Krogmann, T., Gao, Y., Rishi, A.K., And Ross, D.D. (1998). A Multidrug Resistance Transporter From Human MCF-7 Breast Cancer Cells. *Proceedings Of The National Academy Of Sciences* 95, 15665-15670.

Eadie, L., Hughes, T., And White, D. (2014). Interaction Of The Efflux Transporters ABCB1 And ABCG2 With Imatinib, Nilotinib, And Dasatinib. *Clin Pharmacol Ther* 95, 294-306.

Ee, P.L.R., Kamalakaran, S., Tonetti, D., He, X., Ross, D.D., And Beck, W.T. (2004). Identification Of A Novel Estrogen Response Element In The Breast Cancer Resistance Protein (ABCG2) Gene. *Cancer Research* 64, 1247-1251.

Gallus, J., Juvale, K., And Wiese, M. (2014). Characterization Of 3-Methoxy Flavones For Their Interaction With ABCG2 As Suggested By Atpase Activity. *Biochimica Et Biophysica Acta (BBA)-Biomembranes* 1838, 2929-2938.

Galmarini, C., Mackey, J., And Dumontet, C. (2001). Nucleoside Analogues: Mechanisms Of Drug Resistance And Reversal Strategies. *Leukemia* 15, 875.

Gottesman, M.M., And Ling, V. (2006). The Molecular Basis Of Multidrug Resistance In Cancer: The Early Years Of P-Glycoprotein Research. *FEBS Letters* 580, 998-1009.

Hertog, M.G., Kromhout, D., Aravanis, C., Blackburn, H., Buzina, R., Fidanza, F., Giampaoli, S., Jansen, A., Menotti, A., And Nedeljkovic, S. (1995). Flavonoid Intake And Long-Term Risk Of Coronary Heart Disease And Cancer In The Seven Countries Study. *Archives Of Internal Medicine* 155, 381-386.

Holohan, C., Van Schaeybroeck, S., Longley, D.B., And Johnston, P.G. (2013). Cancer Drug Resistance: An Evolving Paradigm. *Nature Reviews Cancer* 13, 714-726.

Honjo, Y., Hrycyna, C.A., Yan, Q.-W., Medina-Pérez, W.Y., Robey, R.W., Van De Laar, A., Litman, T., Dean, M., And Bates, S.E. (2001). Acquired Mutations In The MXR/BCRP/ABCP Gene Alter Substrate Specificity In MXR/BCRP/ABCP-Overexpressing Cells. *Cancer Research* 61, 6635-6639.

Housman, G., Byler, S., Heerboth, S., Lapinska, K., Longacre, M., Snyder, N., And Sarkar, S. (2014). Drug Resistance In Cancer: An Overview. *Cancers* 6, 1769-1792.

Imai, Y., Asada, S., Tsukahara, S., Ishikawa, E., Tsuruo, T., And Sugimoto, Y. (2003). Breast Cancer Resistance Protein Exports Sulfated Estrogens But Not Free Estrogens. *Molecular Pharmacology* 64, 610-618.

Jonker, J.W., Buitelaar, M., Wagenaar, E., Van Der Valk, M.A., Scheffer, G.L., Scheper, R.J., Plösch, T., Kuipers, F., Elferink, R.P.O., And Rosing, H. (2002). The Breast Cancer Resistance Protein Protects Against A Major Chlorophyll-Derived Dietary Phototoxin And Protoporphyrin. *Proceedings Of The National Academy Of Sciences* 99, 15649-15654.

Jonker, J.W., Merino, G., Musters, S., Van Herwaarden, A.E., Bolscher, E., Wagenaar, E., Mesman, E., Dale, T.C., And Schinkel, A.H. (2005). The Breast Cancer Resistance Protein BCRP (ABCG2) Concentrates Drugs And Carcinogenic Xenotoxins Into Milk. *Nature Medicine* 11, 127-129.

Jordan, C.T., Guzman, M.L., And Noble, M. (2006). Cancer Stem Cells. *New England Journal Of Medicine* 355, 1253-1261.

Jouyban, A., Fakhree, M.A.A., And Shayanfar, A. (2010). Review Of Pharmaceutical Applications Of N-Methyl-2-Pyrrolidone. *Journal Of Pharmacy & Pharmaceutical Sciences* 13, 524-535.

Kathawala, R.J., Chen, J.-J., Zhang, Y.-K., Wang, Y.-J., Patel, A., Wang, D.-S., Talele, T.T., Ashby, C.R., And Chen, Z.-S. (2014). Masitinib Antagonizes ATP-Binding Cassette Subfamily G Member 2-Mediated Multidrug Resistance. *International Journal Of Oncology* 44, 1634-1642.

Kolb, H.C., And Sharpless, K.B. (2003). The Growing Impact Of Click Chemistry On Drug Discovery. *Drug Discovery Today* 8, 1128-1137.

Kondo, C., Suzuki, H., Itoda, M., Ozawa, S., Sawada, J.-I., Kobayashi, D., Ieiri, I., Mine, K., Ohtsubo, K., And Sugiyama, Y. (2004). Functional Analysis Of Snps Variants Of BCRP/ABCG2. *Pharmaceutical Research* 21, 1895-1903.

Krishnamurthy, P., Ross, D.D., Nakanishi, T., Bailey-Dell, K., Zhou, S., Mercer, K.E., Sarkadi, B., Sorrentino, B.P., And Schuetz, J.D. (2004). The Stem Cell Marker Bcrp/ABCG2 Enhances Hypoxic Cell Survival Through Interactions With Heme. *Journal Of Biological Chemistry* 279, 24218-24225.

Lemos, C., Jansen, G., And Peters, G. (2008). Drug Transporters: Recent Advances Concerning BCRP And Tyrosine Kinase Inhibitors. *British Journal Of Cancer* 98, 857-862.

Levine, A.J. (1997). P53, The Cellular Gatekeeper For Growth And Division. *Cell* 88, 323-331.

Lin, Y., Shi, R., Wang, X., And Shen, H.-M. (2008). Luteolin, A Flavonoid With Potential For Cancer Prevention And Therapy. *Current Cancer Drug Targets* 8, 634-646.

Litman, T., Jensen, U., Hansen, A., Covitz, K.-M., Zhan, Z., Fetsch, P., Abati, A., Hansen, P.R., Horn, T., And Skovsgaard, T. (2002). Use Of Peptide Antibodies To Probe For The Mitoxantrone Resistance-Associated Protein MXR/BCRP/ABCP/ABCG2. *Biochimica Et Biophysica Acta (BBA)-Biomembranes* 1565, 6-16.

Liu, L., Zuo, L.F., And Guo, J.W. (2014). ABCG2 Gene Amplification And Expression

In Esophageal Cancer Cells With Acquired Adriamycin Resistance. *Molecular Medicine Reports* 9, 1299-1304.

Ma, C., Wei, S., And Song, Y. (2011). T790M And Acquired Resistance Of EGFR TKI: A Literature Review Of Clinical Reports. *Journal Of Thoracic Disease* 3, 10.

Mahringer, A., And Fricker, G. (2010). BCRP At The Blood– Brain Barrier: Genomic Regulation By 17 β -Estradiol. *Molecular Pharmaceutics* 7, 1835-1847.

Mao, Q., And Unadkat, J.D. (2015). Role Of The Breast Cancer Resistance Protein (BCRP/ABCG2) In Drug Transport—An Update. *The AAPS Journal* 17, 65-82.

Marchetti, S., De Vries, N.A., Buckle, T., Bolijn, M.J., Van Eijndhoven, M.A., Beijnen, J.H., Mazzanti, R., Van Tellingen, O., And Schellens, J.H. (2008). Effect Of The ATP-Binding Cassette Drug Transporters ABCB1, ABCG2, And ABCC2 On Erlotinib Hydrochloride (Tarceva) Disposition In In Vitro And In Vivo Pharmacokinetic Studies Employing *Bcrp1^{-/-}/Mdr1a/1b^{-/-}* (Triple-Knockout) And Wild-Type Mice. *Molecular Cancer Therapeutics* 7, 2280-2287.

Martin, C.M., Ferdous, A., Gallardo, T., Humphries, C., Sadek, H., Caprioli, A., Garcia, J.A., Szweda, L.I., Garry, M.G., And Garry, D.J. (2008). Hypoxia-Inducible Factor-2 α Transactivates *Abcg2* And Promotes Cytoprotection In Cardiac Side Population Cells. *Circulation Research* 102, 1075-1081.

Mcdevitt, C.A., Collins, R., Kerr, I.D., And Callaghan, R. (2009). Purification And Structural Analyses Of ABCG2. *Advanced Drug Delivery Reviews* 61, 57-65.

Miller, K.D., Siegel, R.L., Lin, C.C., Mariotto, A.B., Kramer, J.L., Rowland, J.H., Stein, K.D., Alteri, R., And Jemal, A. (2016). Cancer Treatment And Survivorship Statistics, 2016. *CA: A Cancer Journal For Clinicians* 66, 271-289.

Mizuarai, S., Aozasa, N., And Kotani, H. (2004). Single Nucleotide Polymorphisms Result In Impaired Membrane Localization And Reduced Atpase Activity In Multidrug Transporter ABCG2. *International Journal Of Cancer* 109, 238-246.

Morris, G.M., Huey, R., Lindstrom, W., Sanner, M.F., Belew, R.K., Goodsell, D.S., And Olson, A.J. (2009). Autodock4 And Autodocktools4: Automated Docking With Selective Receptor Flexibility. *Journal Of Computational Chemistry* 30, 2785-2791.

Nishida, N., Yano, H., Nishida, T., Kamura, T., And Kojiro, M. (2006). Angiogenesis In Cancer. *Vascular Health And Risk Management* 2, 213.

Noguchi, K., Katayama, K., And Sugimoto, Y. (2014). Human ABC Transporter ABCG2/BCRP Expression In Chemoresistance: Basic And Clinical Perspectives For Molecular Cancer Therapeutics. *Pharmgenomics Pers Med* 7, 53-64.

Ohshima, H., Yoshie, Y., Auriol, S., And Gilibert, I. (1998). Antioxidant And Pro-Oxidant Actions Of Flavonoids: Effects On DNA Damage Induced By Nitric Oxide, Peroxynitrite And Nitroxyl Anion. *Free Radical Biology And Medicine* 25, 1057-1065.

Ozaki, T., And Nakagawara, A. (2011). Role Of P53 In Cell Death And Human Cancers. *Cancers* 3, 994-1013.

Patrawala, L., Calhoun, T., Schneider-Broussard, R., Zhou, J., Claypool, K., And Tang, D.G. (2005). Side Population Is Enriched In Tumorigenic, Stem-Like Cancer Cells, Whereas ABCG2+ And ABCG2- Cancer Cells Are Similarly Tumorigenic. *Cancer Research* 65, 6207-6219.

Rabindran, S.K., Ross, D.D., Doyle, L.A., Yang, W., And Greenberger, L.M. (2000). Fumitremorgin C Reverses Multidrug Resistance In Cells Transfected With The Breast Cancer Resistance Protein. *Cancer Research* 60, 47-50.

Robert, N., Leyland-Jones, B., Asmar, L., Belt, R., Ilegbodu, D., Loesch, D., Raju, R., Cobleigh, M., Albain, K., And Slamom, D. (2004). Randomized Phase III Study Of Trastuzumab, Paclitaxel, And Carboplatin Versus Trastuzumab And Paclitaxel In Women With HER-2 Overexpressing Metastatic Breast Cancer: An Update Including Survival. *Journal Of Clinical Oncology* 22, 573-573.

Saison, C., Helias, V., Ballif, B.A., Peyrard, T., Puy, H., Miyazaki, T., Perrot, S., Vayssier-Taussat, M., Waldner, M., And Le Penec, P.-Y. (2012). Null Alleles Of ABCG2 Encoding The Breast Cancer Resistance Protein Define The New Blood Group System Junior. *Nature Genetics* 44, 174-177.

Sarkadi, B., Özvegy-Laczka, C., Németh, K., And Váradi, A. (2004). ABCG2-A Transporter For All Seasons. *FEBS Letters* 567, 116-120.

Scambia, G., Ranelletti, F., Panici, P.B., De Vincenzo, R., Bonanno, G., Ferrandina, G., Piantelli, M., Bussa, S., Rumi, C., And Cianfriglia, M. (1994). Quercetin Potentiates The Effect Of Adriamycin In A Multidrug-Resistant MCF-7 Human Breast-Cancer Cell Line: P-Glycoprotein As A Possible Target. *Cancer Chemotherapy And Pharmacology* 34, 459-464.

Scheffzek, K., Ahmadian, M.R., Kabsch, W., Wiesmüller, L., Lautwein, A., Schmitz, F., And Wittinghofer, A. (1997). The Ras-Rasgap Complex: Structural Basis For Gtpase Activation And Its Loss In Oncogenic Ras Mutants. *Science* 277, 333-339.

Sever, R., And Brugge, J.S. (2015). Signal Transduction In Cancer. *Cold Spring Harbor Perspectives In Medicine* 5, A006098.

Sodani, K., Patel, A., Anreddy, N., Singh, S., Yang, D.-H., Kathawala, R.J., Kumar, P., Talele, T.T., And Chen, Z.-S. (2014). Telatinib Reverses Chemotherapeutic Multidrug Resistance Mediated By ABCG2 Efflux Transporter In Vitro And In Vivo. *Biochemical Pharmacology* 89, 52-61.

Studzian, M., Bartosz, G., And Pulaski, L. (2015). Endocytosis Of ABCG2 Drug Transporter Caused By Binding Of 5D3 Antibody: Trafficking Mechanisms And Intracellular Fate. *Biochimica Et Biophysica Acta (BBA)-Molecular Cell Research* 1853, 1759-1771.

Takimoto, C., And Arbuck, S. (1997). Clinical Status And Optimal Use Of Topotecan. *Oncology (Williston Park, NY)* 11, 1635-1646; Discussion 1649-1651, 1655-1637.

Taylor, N.M., Manolaridis, I., Jackson, S.M., Kowal, J., Stahlberg, H., And Locher, K.P. (2017a). Structure Of The Human Multidrug Transporter ABCG2. *Nature*.

Taylor, N.M., Manolaridis, I., Jackson, S.M., Kowal, J., Stahlberg, H., And Locher, K.P. (2017b). Structure Of The Human Multidrug Transporter ABCG2. *Nature* 546, 504.

Tew, K.D. (2016). Glutathione-Associated Enzymes In Anticancer Drug Resistance. *Cancer Research* 76, 7-9.

Tiwari, A.K., Sodani, K., Dai, C.-L., Abuznait, A.H., Singh, S., Xiao, Z.-J., Patel, A., Talele, T.T., Fu, L., And Kaddoumi, A. (2013). Nilotinib Potentiates Anticancer Drug Sensitivity In Murine ABCB1-, ABCG2-, And ABCC10-Multidrug Resistance Xenograft Models. *Cancer Letters* 328, 307-317.

Trott, O., And Olson, A.J. (2010). Autodock Vina: Improving The Speed And Accuracy Of Docking With A New Scoring Function, Efficient Optimization, And Multithreading. *Journal Of Computational Chemistry* 31, 455-461.

Van Den Heuvel-Eibrink, M., Wiemer, E., Prins, A., Meijerink, J., Vossebeld, P., Van Der Holt, B., Pieters, R., And Sonneveld, P. (2002). Increased Expression Of The Breast Cancer Resistance Protein (BCRP) In Relapsed Or Refractory Acute Myeloid Leukemia (AML). *Leukemia* 16, 833.

Vasiliou, V., Vasiliou, K., And Nebert, D.W. (2009). Human ATP-Binding Cassette (ABC) Transporter Family. *Human Genomics* 3, 281.

Verbrugge, S.E., Al, M., Assaraf, Y.G., Kammerer, S., Chandrupatla, D.M., Honeywell, R., Musters, R.P., Giovannetti, E., O'Toole, T., And Scheffer, G.L. (2016). Multifactorial Resistance To Aminopeptidase Inhibitor Prodrug CHR2863 In Myeloid Leukemia Cells: Down-Regulation Of Carboxylesterase 1, Drug Sequestration In Lipid Droplets And Pro-Survival Activation ERK/Akt/Mtor. *Oncotarget* 7, 5240.

Wang, H., Zhou, L., Gupta, A., Vethanayagam, R.R., Zhang, Y., Unadkat, J.D., And Mao, Q. (2006). Regulation Of BCRP/ABCG2 Expression By Progesterone And 17 β -Estradiol In Human Placental BeWo Cells. *American Journal Of Physiology-Endocrinology And Metabolism* 290, E798-E807.

Weidner, L.D., Zoghbi, S.S., Lu, S., Shukla, S., Ambudkar, S.V., Pike, V.W., Mulder, J., Gottesman, M.M., Innis, R.B., And Hall, M.D. (2015). The Inhibitor Ko143 Is Not Specific For ABCG2. *Journal Of Pharmacology And Experimental Therapeutics* 354, 384-393.

Wong, I.L., Chan, K.-F., Tsang, K.H., Lam, C.Y., Zhao, Y., Chan, T.H., And Chow, L.M.C. (2009). Modulation Of Multidrug Resistance Protein 1 (MRP1/ABCC1)-Mediated Multidrug Resistance By Bivalent Apigenin Homodimers And Their Derivatives. *Journal Of Medicinal Chemistry* 52, 5311-5322.

Woodward, O.M., Tukaye, D.N., Cui, J., Greenwell, P., Constantoulakis, L.M., Parker, B.S., Rao, A., Köttgen, M., Maloney, P.C., And Guggino, W.B. (2013). Gout-Causing Q141K Mutation In ABCG2 Leads To Instability Of The Nucleotide-Binding Domain And Can Be Corrected With Small Molecules. *Proceedings Of The National Academy Of Sciences* 110, 5223-5228.

Yan, C.S., Wong, I.L., Chan, K.-F., Kan, J.W., Chong, T.C., Law, M.C., Zhao, Y., Chan,

S.W., Chan, T.H., And Chow, L.M. (2015). A New Class Of Safe, Potent, And Specific P-Gp Modulator: Flavonoid Dimer FD18 Reverses P-Gp-Mediated Multidrug Resistance In Human Breast Xenograft In Vivo. *Molecular Pharmaceutics* 12, 3507-3517.